

# Fatigue Crack Initiation in Weldments

by

Takatoshi Nakamura

B.E. Mechanical Engineering (1987) & M.E. Mechanical Engineering (1989)  
Keio University, Tokyo, Japan

SUBMITTED TO THE DEPARTMENT OF OCEAN ENGINEERING  
AND THE DEPARTMENT OF MECHANICAL ENGINEERING  
IN PARTIAL FULFILLMENT OF THE REQUIREMENTS  
FOR THE DEGREES OF

OCEAN ENGINEER

and

MASTER OF SCIENCE IN MECHANICAL ENGINEERING

at the

MASSACHUSETTS INSTITUTE OF TECHNOLOGY  
February, 1994

© Takatoshi Nakamura, 1994. All rights reserved.

The author hereby grants to MIT permission to reproduce and to  
distribute copies of this thesis document in whole or in part.

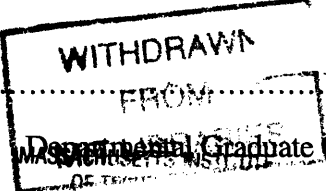
Signature of Author .....  
Department of Ocean Engineering, February, 1994

Certified by .....  
Professor Koichi Masubuchi, Thesis Supervisor  
Department of Ocean Engineering

Certified by .....  
Associate Professor Lallit Anand, Thesis Reader  
Department of Mechanical Engineering

Accepted by .....  
Professor A. Douglas Carmichael, Chairman,  
Departmental Graduate Committee, Ocean Engineering

Accepted by .....  
Professor Ain A. Sonin, Chairman,  
Departmental Graduate Committee, Mechanical Engineering



APR 15 1994

# Fatigue Crack Initiation in Weldments

by

Takatoshi Nakamura

Submitted to the Department of Ocean Engineering on September 27, 1993  
in partial fulfillment of the requirements for the Degree of  
Ocean Engineer and  
Master of Science in Mechanical Engineering.

## ABSTRACT

Since fusion welding involves melting and rapid solidification, some discontinuities including porosity, cracking, and lack of fusion are frequently formed. These discontinuities often cause fractures of welded structures. With the development of a new scanning microscope, it is now possible to examine microscopic features of the weld surface with virtually no preparation. The information generated through the observation should be useful in studying fatigue crack initiation in weldments of various materials.

Forty six new specimens made in four different materials (aluminum, titanium, stainless steel and mild steel) and by three different welding processes (gas tungsten arc welding electron beam welding, and laser beam welding) were produced to observe surface discontinuities of weldments made under similar welding conditions. The resulting surface discontinuities were classified in terms of shape and size of discontinuities and types of grains.

Using the information obtained through observation, two different kinds of fatigue tests were conducted. The combination of a confocal scanning microscope and a portable video image microscope showed very good observation capabilities. Most of the surface discontinuities did not grow, instead newly created fatigue cracks grew. Fatigue cracks in weldments occurred mostly at the craters or start-up toes. Only one crack seemed to grow and others stopped growing. Based on these findings, a newly developed test method is proposed in this thesis.

Thesis Supervisor: Professor Koichi Masubuchi

Title: Kawasaki Professor of Engineering

## Acknowledgments

I would like to express my sincere thanks to Dr. Koichi Masubuchi. His willingness to answer questions and discuss problems exemplifies his dedication as an educator and researcher. His support made this research possible. I would also like to thank Dr. Lallit Anand for giving me important advice at all times.

Mr. Shinji Koga and Mr. Toshiaki Araki were very important in that they also gave me a great deal of helpful advice as well as helping me to conduct the research experiments. I would like to thank Mr. Takahiro Ode who instructed me in the use of new equipment, especially the scanning laser microscope.

Many thanks go to Mrs. Stephanie Douglas, Mr. Philippe Tannery, Mr. Nikolaos Kafetsis, and Mr. Albert T. Supple, Jr. They cooperated with me in the part of this research and had discussion with me many times throughout the research.

Finally, I would like to extend special thanks and deep gratitude to my parents and to all the people who have helped me both in studies and private life.

# TABLE OF CONTENTS

	Pages:
ABSTRACT	2
ACKNOWLEDGMENT	3
TABLE OF CONTENTS	4
LIST OF FIGURES	7
LIST OF TABLES	10
LIST OF ACRONYMS AND ABBREVIATIONS	11
CHAPTER 1: THESIS OVERVIEW	13
CHAPTER 2: BACKGROUND	16
2.1 Short History of Research on Fatigue Fracture	16
2.2 Research on Fatigue Crack Initiation in Welds at MIT	19
CHAPTER 3: INTRODUCTION	22
3.1 Laser Microscope and Video Image Microscope	22
3.2 Surface Discontinuities	25
3.3 Weld Cracking	32
3.3.1 Hot Cracking	32
3.3.2 Cold Cracking	33
3.3.3 Stress Corrosion Cracking	34

3.3.4 Hydrogen Embrittlement	34
3.4 Fracture of Weldments	35
3.4.1 Fracture Theory	36
3.4.2 Brittle and Ductile Fractures	38
3.4.3 Fatigue Fracture	38
3.4.3.1 S-N Diagram	39
3.4.3.2 Low Cycle Fatigue and High Cycle Fatigue	40
3.4.3.3 Crack Growth	41
3.4.3.4 Fatigue Crack Initiation	42
3.5 Residual Stresses and Stress Concentrations	44
3.5.1 Residual Stresses	44
3.5.2 Stress Concentrations	45
3.6 Non-Destructive Examination of Welds	46
CHAPTER 4: OBSERVATION OF WELDED SPECIMENS	50
4.1 Objectives	50
4.2 Specimen and Equipment	52
4.3 Experimental Procedure	56
CHAPTER 5: EXPERIMENTAL RESULTS AND DISCUSSIONS FOR OBSERVATION	58
5.1 Low Carbon Steels	58
5.2 Stainless Steels	76
5.3 Aluminum Alloys	94
5.4 Titanium Alloys	112
CHAPTER 6: EXPERIMENTS ON FATIGUE CRACK INITIATION	126

6.1 Objectives	126
6.2 Specimen and Equipment	128
6.3 Experimental Procedure	132
<b>CHAPTER 7: EXPERIMENTAL RESULTS AND DISCUSSIONS FOR FATIGUE EXPERIMENT</b>	<b>135</b>
7.1 Fatigue Test I	135
7.2 Fatigue Test II	139
7.2.1 Low-Carbon Steel	139
7.2.2 Stainless Steel	140
7.2.3 Aluminum Alloy	140
7.2.4 Titanium Alloy	141
<b>CHAPTER 8: CONCLUSIONS AND RECOMMENDATIONS</b>	<b>156</b>
8.1 Conclusions	156
8.2 Practical Use of Results	158
8.3 Recommendations	159
<b>REFERENCES</b>	<b>160</b>
<b>APPENDICES</b>	<b>163</b>
A-1 Observation Data	A-2
A-2 Fatigue Test Data	A-16

## List of Figures

	Page:	
Figure 3.1.1	System configuration	24
Figure 3.2.1	Cracks in welded joints	26
Figure 3.2.2	Types of horizontal discontinuity	29
Figure 3.2.3	Types of vertical discontinuity	31
Figure 3.4.1	Transgranular and intergranular fractures	35
Figure 3.4.2	Modes of cracking	36
Figure 3.4.3	Crack in an infinite plate	37
Figure 3.4.4	Brittle-Ductile transition	38
Figure 3.4.5	S-N diagram	39
Figure 3.4.6	Relation between $da/dN$ and $\Delta K$	41
Figure 3.4.7	Wood's model for fatigue crack initiation	42
Figure 3.4.8	Example of fatigue crack initiation	43
Figure 3.5.1	Residual stresses due to welding	45
Figure 3.6.1	New Non-Destructive Examination	49
Figure 4.2.1	Specimen for observation	55

Figure 4.3.1	Location of welded specimen	57
Figure 6.2.1	Specimen for fatigue Test I	130
Figure 6.2.2	A slit on a weld	131
Figure 6.2.3	Specimen for fatigue Test II	131
Figure 7.1.1	M-2	138
Figure 7.1.2	M-2	138
Figure 7.1.3	M-2	138
Figure 7.2.1	Surface discontinuity (Type V1) at start-up toe of MT-3	143
Figure 7.2.2	Surface discontinuity (inclusion) at weld edge of MT-3	144
Figure 7.2.3	Surface features of MT-3	145
Figure 7.2.4	Surface discontinuity (inclusion) of ST-3	146
Figure 7.2.5	Surface discontinuity at crater of ST-3	147
Figure 7.2.6	Surface features of ST-3	148
Figure 7.2.7	Section of crater	141
Figure 7.2.8	Surface discontinuity at crater of AT-2	149
Figure 7.2.9	Surface discontinuity at start-up toe of AT-2	150
Figure 7.2.10	Surface features of AT-2	151
Figure 7.2.11	Fatigue fracture of AT-2	142



Figure 7.2.12	Surface discontinuity at crater of TT-2	152
Figure 7.2.13	Surface discontinuity at weld edge of TT-2	153
Figure 7.2.14	Surface features of TT-2	154
Figure 7.2.15	Grain slip after tensile strength test	155
Figure 7.2.16	Fatigue fracture of TT-2	142

## List of Tables

		Page:
Table 3.1.1	Lens magnification	23
Table 3.2.1	Degrees of grain sizes	28
Table 4.2.1	Specifications of specimens	53
Table 4.2.2	Welding conditions for EBW	53
Table 4.2.3	Welding conditions for LBW	53
Table 4.2.4	Details of specimens	54
Table 6.2.1	Details of specimens for Fatigue Test II	129
Table 6.2.2	Specifications of Materials	129
Table 7.1.1	Summarized results of Fatigue Test I	135
Table 7.1.2	Locations of fatigue crack initiation	136
Table 7.2.1	Summarized results of Fatigue Test II	139

## List of Acronyms and Abbreviations

HY	High Yielding
NDE	Non-Destructive Examination
SEM	Scanning Electron Microscope
CSLM	Confocal Scanning Laser Microscope
PVIM	Portable Video Image Microscope
TEM	Transmission Electron Microscopy
CSR	Critical Solidification Range
HAZ	Heat Affected Zone
CE	Carbon Equivalent
BCC	Body Centered Cubic
LCF	Low -Cycle Fatigue
HCF	High-Cycle Fatigue
EBW	Electron Beam Welding
LBW	Laser Beam Welding
GTAW	Gas Tungsten Arc Welding
a.s.	After Shielded

N.A.S.	Not Available See
H.C.	Hot Cracking
C.C.	Cold Cracking
GB	Grain Boundary
SGB	Sub-Grain Boundary
LBW1	Laser Beam Welding without After Shielded
LBW2	Laser Beam Welding with After Shielded
YTS	Yielding Tensile Stress
UTS	Ultimate Tensile Stress

## Chapter 1: Thesis Overview

Welding has been the most important fabrication technology to join metallic materials since World War II. This is because welding, which is used in all industries, has indispensable advantages such as water or air tightness, light weight and structural strength over fabricating techniques including riveting, forging, and casting.

Although numerous structures have been constructed using welding, a major problem associated with welded structures is related to how to minimize the occurrence of cracks and failures. Not only old structures, but also recent structures, have been reported to have fatigue fractures which have caused considerable damage. Therefore, how to detect fatigue fracture in its early stage or possibly avoid or remove it from those structures has become a primary concern. The Welding Research Group at Massachusetts Institute of Technology has been engaged in research on this problem for years, concentrating on early detection of fatigue crack initiation for different types of materials.

Many recent structures use aluminum alloys, high strength steels, titanium alloys, and stainless steels as well as low-carbon steels to reduce weight. For example, high strength HY steels have been used for Navy warships and submarines. Aluminum alloys and titanium alloys are intensively used in aerospace industries. Automobile industries are considering using aluminum alloys for ordinary cars in the future. Fatigue fracture characteristics of welds must be investigated for each material.

Four major goals being considered are as follows:

1. Verify the effectiveness and capability of a recently developed confocal scanning laser microscope (CSLM) and a portable video image microscope (PVIM) to observe welded structures and detect fatigue crack initiations.
2. Develop a new non-destructive examination (NDE) method to identify structurally dangerous discontinuities such as cracks in the early stages using a CSLM and a PVIM.
3. Establish a method of early detection of fatigue crack initiations on different materials.
4. Establish a new theory on early detection of fatigue crack initiation in weldments from the data of the above experiments.

To achieve the above goals, the two following stages of research are indispensable:

1. Because the observation of the surface of the welded specimens using a CSLM and a PVIM is new and exhaustive results have not been available yet to the public, it is important to observe and know microstructural features of the surface of materials welded under various conditions with different processes. It will be the basis of all further researches by using a CSLM and a PVIM. Especially for the research of fatigue crack initiation in welds, it is significant to observe the surface of each welded specimen and find created surface discontinuities in the welds which often may be the causes of fatigue cracks.
2. Conduct experiments of fatigue fractures on all five materials, aluminum alloys, high strength steels, titanium alloys, stainless steels and low-carbon steels.

The research presented in this thesis covers both stages. For the first stage, it is the first publication to provide microstructural information of welded structures prepared only for this purpose and observed by using a CSLM and a PVIM. For the second stage, it involves the continued work on low-carbon steels and introductory work for stainless steels, aluminum alloys, and titanium alloys.

Chapter 2 presents a brief history of research on fatigue fracture and fatigue crack initiation in welds. Chapter 3 covers the basic theories in this field. In Chapters 4 and 5, experimental work of observation by using a CSLM and a PVIM are shown with detailed data, including observation of the surface discontinuities for four different materials welded by four different welding processes. Chapters 6 and 7 include the experiments on fatigue crack initiation on stainless steels, aluminum alloys, and titanium alloys as well as low-carbon steels.

# Chapter 2: Background

## 2.1 Short History of Research on Fatigue Fracture

The research on fatigue started around 1830, and a few years later the first S-N curve was introduced. It shows the relationship between the applied stress,  $S$  and the fatigue or failure life,  $N$ . Some materials including steels show endurance limit below which stress fatigue does not occur. It is most widely used in the practical world to design structures and improve fatigue life.

Fracture mechanics theories were introduced in the 1950's. In the elastic case the stress intensity factor is a sufficient parameter to describe the whole stress field at the tip of a crack. When the size of the plastic zone at the crack tip is small compared to crack length, the stress intensity factor still gives a good expression of the stress field near the crack tip. If two different cracks have the same stress field, i.e. the same stress intensity factor, they behave in the same manner and show equal rates of crack growth. Paris, Gomez, and Anderson were the first to suggest that the fracture mechanics theory could be applied to study fatigue crack growth. The rate of fatigue crack growth per cycle,  $da/dN$ , is governed by the stress intensity factor range  $\Delta K$  in 1962 [Ref. 2, 16 and 17]:

$$\frac{da}{dN} = f(\Delta K) \quad (2.1.1)$$

Equation 2.1.1 is often assumed to be a simple power function:

$$\frac{da}{dN} = C (\Delta K)^m \quad (2.1.2)$$

where  $C$  and  $m$  are material constants. A double-logarithmic plot of  $da/dN$  versus  $\Delta K$  would then be a straight line. However, equation 2.1.2 does not



represent reality. Actual experimental data fall on an S-shaped curve. This fact infers the existence of the threshold value of  $\Delta K$  below which there is no crack growth at all. It is often difficult to verify the existence of this value,  $\Delta K_{th}$ . The fatigue crack initiation has been in question.

Wood suggested a fatigue crack initiation model in 1958 [Ref. 8]. He used the concept of intrusion and extrusion on the surface of the specimens caused by fatigue.

In 1966 McClintock and Argon claimed that a fatigue crack generally initiates from a persistent slip band [Ref. 10]. The slip band becomes more intense and develops into micro-cracks as the specimen is fatigued. The micro-cracks join together and eventually form a large crack. Welded specimens often contain defects which are not ordinarily present in the base metal. The weld may have inclusions, porosity, pits, voids, and other types of defects. Liaw, yang, and Palusamy found in 1991 that these defects, along with persistent slip bands and grain boundaries are typical fatigue crack initiation sites [Ref. 15]. Francis, Lankford, and Lyle found in 1976 that fatigue cracks in welds may also initiate from pre-existing cracks, regions with lack-of-fusion or lack-of-penetration, and sites of geometrical stress concentrations such as a weld toe and a toe of the weld reinforcement [Ref. 9].

Investigations of fracture mechanics rely largely on electron microscopy. The early electron microscopy is known as electron beam fractography, which uses replica techniques. It enabled one to observe the striations of fatigue fracture. Many researches have been conducted using electron microscopes since then.

Recently a scanning electron microscope (SEM) and a confocal scanning laser microscope (CSLM) were developed and used to observe the

microstructures of materials. They made it possible to observe specimens without replica techniques.

Fatigue crack initiation including the existence of  $\Delta K_{th}$  are still under investigation. Especially microstructural features in weldments have not yet been studied intensively. In 1991 several specimens with fatigue cracks cut from ship hulls were sent to the Welding Research Group at Massachusetts Institute of Technology. The group found interesting phenomena in the weldments by using a newly developed confocal scanning laser microscope. From those observations the group came to the conclusion that:

*There must be some relation between fatigue crack initiation and surface microstructural discontinuities in welds. Possibly certain discontinuities have more influence on the growth of fatigue cracks than others, or discontinuities themselves may grow to be fatigue cracks. If the relation will be found, the fatigue crack while it is small or microstructural features which may have some influence on fatigue cracks will be able to be detected.*

The group has been engaged in this problem since then. The next section discusses our efforts.

## 2.2 Research on Fatigue Crack Initiation in Welds at MIT

There have been several studies on fatigue crack initiation in welds conducted by the Welding Research Group at Massachusetts Institute of Technology prior to the work presented in this thesis.

As the first effort in 1992, Stephanie A. Douglas carried on the introductory series of observation on welds in 1992 in cooperation with the author [Ref. 6 and 14] in order to determine the effects on the formation of microscopic surface formations and microcracks in an attempt to classify the possible sensitivity to fracture in service. This was the first attempt to observe the weld surface without any preparation such as polishing the surface or removing surface oxides, which was enabled by using a confocal scanning laser microscope developed by Lasertec Corporation. The materials investigated include low-carbon steel, aluminum, 304 stainless steel, titanium, and high strength steels. The welding processes considered include electron beam welding (EBW), gas tungsten welding (GTAW), gas metal arc welding (GMAW), and laser beam welding (LBW). It was found that heat input per unit length seemed to play an important role in affecting the type of microstructure produced during the solidification process. However, more exhaustive and complete observation work was suggested to be conducted in the future to use the information obtained through observation, because the study was limited in the amount of specimens and their quality of welds.

John M. Cushing Jr. conducted in 1992 a number of fatigue tests on welded low-carbon steel specimens to investigate changes in the surface microstructure caused by fatigue [Ref. 3]. The microstructures were examined using a scanning microscope and a scanning laser microscope. He proposed a replica technique, because of its usefulness to be used to record surface microstructures as a part of a

new NDE in his research. By this technique, the surface records for even large structures such as ship hulls or airplane shells can be taken to the laboratory to be investigated more completely. He found that fatigue cracks causing final failure initiated in the center of the weld crater and in the heat affected zone at the start-up toe of the weld bead. He also found that "while the laser microscope is limited in its range of magnification, its high contrast image makes it a better microscope for detecting micro-cracks than a scanning electron microscope (SEM)." Through his research he discovered that the presence of micro-cracks before service does not necessarily mean a problem area.

Philippe Tannery succeeded to Cushing's work with the author in 1993 [Ref. 4]. Our work also included extensive low-cycle fatigue tests on welded low-carbon steel specimens using both a CSLM and a portable video image microscope (PVIM). The combination of those two microscopes was found quite effective to detect small fatigue crack initiation. Fatigue crack did not always occur at the parts such as the center of a crater or HAZ at start-up toe of weld where Cushing found most likely fatigue cracks happened in his research. Instead, our welded specimens showed that the fatigue cracks initiated from the microcracks in the other parts of welds. These microcracks did or did not exist before testing. Consequently, the early fatigue crack detection was found difficult. Because of the lack of experimental data, the study was not conclusive. Tannery suggested more experimental works to have general conclusions.

In 1993, Edward Olsen carried out an experimental work on high strength steel (HY-80 and HY-100) specimens to observe microcrack initiation and growth of overmatched and undermatched butt welded high strength steel samples using globally elastic low cycle fatigue testing [Ref. 5]. All specimens had a crack initiator slit machined in the test section. He also used both a CSLM and a PVIM for his research. In the HY 80 tests, the undermatched specimens failed with less

cycles than the overmatched ones. In the HY the difference between the undermatched and the overmatched specimens was small. He suggested that more experiments would be necessary to allow a meaningful statistical treatment of the data.

In 1993, Nikolaos Kafetsis and the author finished the observation of the welded materials. This result was the first exhaustive attempt and provided the base of the research of fatigue crack initiations on various materials including low-carbon steels, stainless steels, aluminum alloys, and titanium alloys. This result is presented in Chapter 4 and 5 of this thesis.

Research on the fatigue crack initiations in weldments for low-carbon steels has been continued by the author. This part of the work is included in Chapters 6 and 7. Two year experimental works and discussions with Dr. Masubuchi and the group members led to remarkable findings. They are summarized as follows:

1. Only one fatigue crack grew to failure after it became observable by using the PVIM for most of the specimens.
2. Microstructural surface discontinuities themselves did not grow. Instead, a crack newly created by fatigue grew.
3. Consequently, it is difficult to detect and specify the microstructural features which may have some influence on fatigue crack initiations. However, microstructural surface discontinuities seemed to affect the initiation of the fatigue cracks due to stress concentrations around them.

Although the work done by the Welding Research Group at MIT has not been sufficient yet to arrive at a general conclusion, detailed experimental work in the future will assure the findings we obtained to date.

## Chapter 3: Introduction

### 3.1 Laser Microscope and Video Image Microscope

Investigation of fracture mechanisms had been borne largely on electron microscopy until recently. This technique was known and called electron beam fractography. Since electrons can be transmitted through only a few hundreds to a thousand angstroms of material, a fracture surface could not be examined directly by transmission of electron microscopy (TEM). Then replication technique was used to take the surface record. The study of fracture mechanisms also requires the examination of metal structures by means of electron microscopy. In order to accomplish this, metal is made into very thin foil by an electron polishing technique.

Scanning electron microscopy (SEM) was introduced recently and it enabled us to observe the fracture surface directly. Both have advantages and limitations. SEM can show more depth and TEM shows more details. However, a specimen must be small enough to be placed in the vacuum chamber and it takes a few minutes to make the chamber vacuum. Furthermore, it is not easy to take whole equipment to the site of examination.

Recently a confocal scanning laser microscope was developed by Lasertec Corporation and kindly donated to the Welding Systems Laboratory at Massachusetts Institute of Technology. The CSLM system uses a He-Ne laser and includes a confocal imaging system and an image processing unit. The CSLM focuses limited height of layers of specimens and integrates those images into one full picture. This feature makes the system distinctive and enables the study

of welds of which the surface is not usually flat. The optical microscope of the system is a Nikon model 1LM11. Five objective lenses can be put on the objective turret with the available range of 1X to 200X. The Welding Systems Laboratory at MIT has the lens of 5X, 10X, 20X, 40X, and 100X. The image displayed on the 12 inch video monitor is further magnified by a factor of 60X.

A portable video image microscope (PVIM) system was introduced recently (1993) to the Welding Systems Laboratory at MIT. This is the Hi-Scope System Model KH-2200 manufactured by Hirox Co. in Japan. The system uses ordinary visible light. Lens 250 was used in the research.

Both systems share the 12 inch monitor and are connected to a video recorder and a video image printer as shown in Figure 3.1.1. The video image printer, made by Sony corporation in Japan, prints out full color pictures.

The magnifications of the pictures both on the monitor and the printed paper are shown in Table 3.1.1.

	Monitor	Printed Picture
PVIM 250	220X	84X
CSLM Lens 5	300X	113X
CSLM Lens 10	600X	225X
CSLM Lens 20	1200X	450X
CSLM Lens 40	2400X	900X
CSLM Lens 100	6000X	2260X

Table 3.1.1. Lens magnification

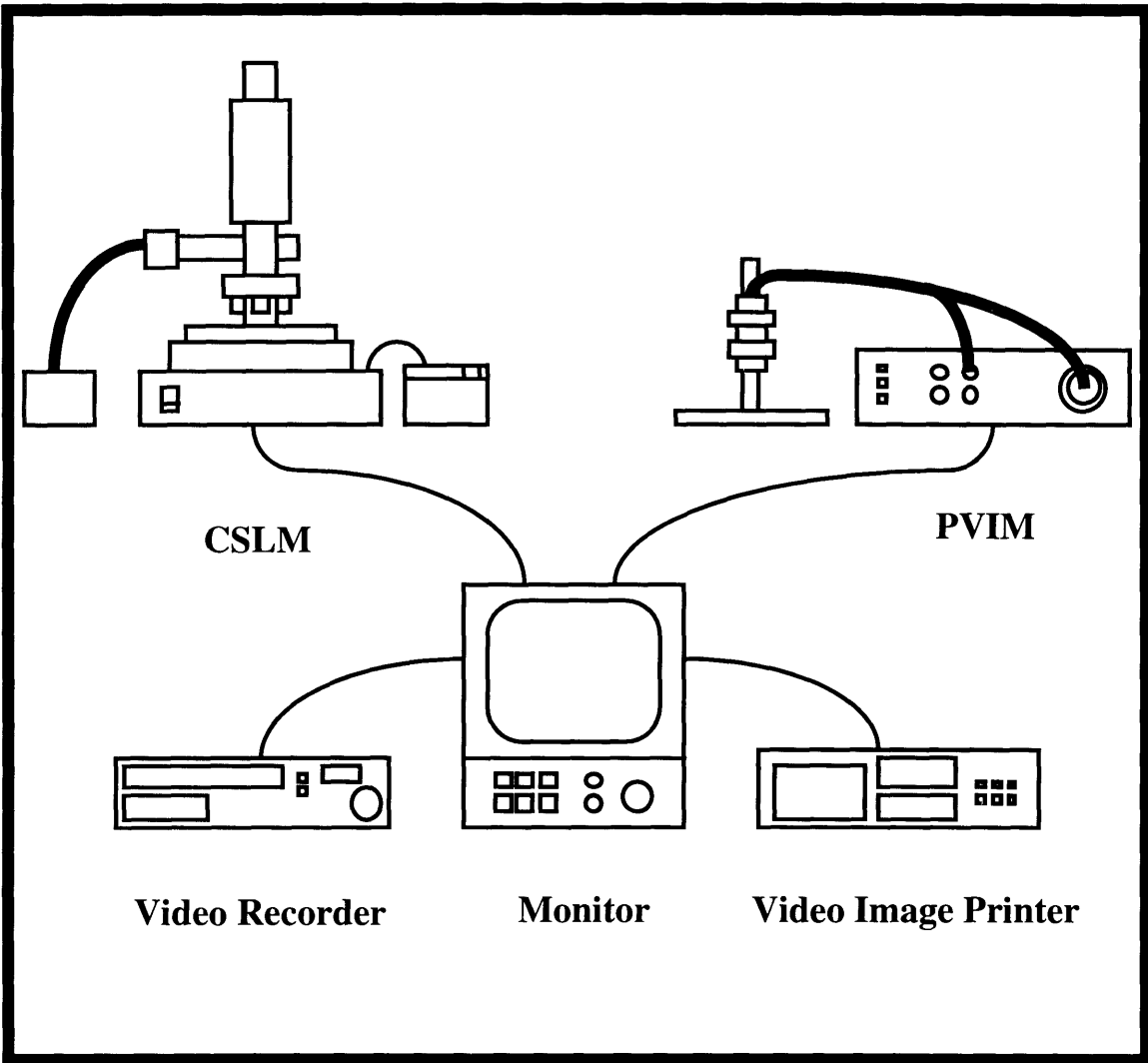


Figure 3.1.1. System configuration



## 3.2 Surface Discontinuities

Surface discontinuities can be the initiation of fatigue fracture. They result from cracks, grain boundaries, undercuts, inclusions, arc strikes, and craters to name a few. There are a number of different types of surface discontinuities on welded structures. They need to be classified into several categories to make further analysis and develop a NDE of crack initiations.

It is important to classify them in terms of appearance and location, especially for future development of NDE. The classic theory used three categories to classify cracks as follows: [Ref. 1]

### 1. Transverse weld metal cracks (C1)

These cracks are perpendicular to the axis of the weld and in some cases have been observed to extend beyond the weld metal into the base metal.

### 2. Longitudinal weld metal cracks (C2)

These cracks are predominantly within the weld metal and are usually confined to the center of the weld. The direction of this type of cracks is parallel to the axis of the weld.

### 3. Crater cracks (C3)

Whenever the welding operation is interrupted, there is a tendency for the formation of cracks in the crater. These cracks are usually star-shaped and proceed only to the edge of the crater.

Figure 3.1.1 shows the three categories.

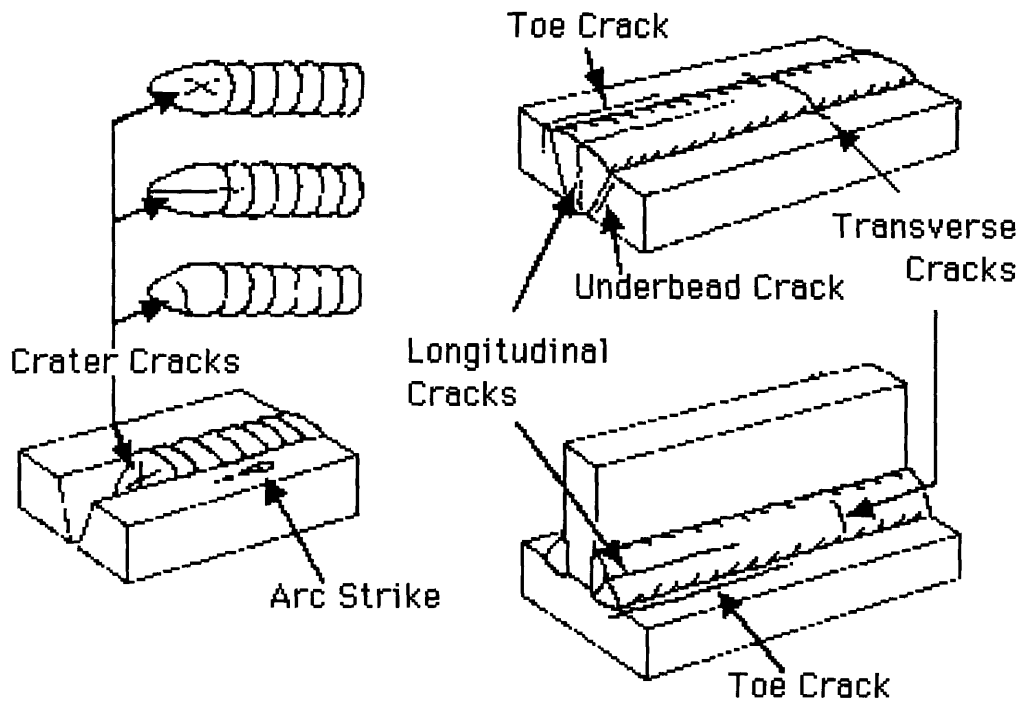


Figure 3.2.1. Cracks in welded joints [Ref. 1]

Although this classification was sufficient to visible cracks, a new classification standard is necessary to make classification of micro surface discontinuities of the weld surface. The new standard refers to shape, direction, and depth or height. First, two major categories, horizontal discontinuities and vertical discontinuities are suggested. Horizontal discontinuities are the horizontal openings, which are usually deep and called cracks. They are classified into three subcategories by their appearance and direction. Figure 3.2.2 shows those three types. They are as follows:

1. Longitudinal weld metal cracks (H1)

These cracks are parallel to the axis of the weld and equivalent to C2.

2. Transverse weld metal cracks (H2)

These cracks are perpendicular to the axis of the weld and equivalent to C1.

### 3. Mixed longitudinal and transverse weld metal cracks (H3)

There are many of cracks connecting each other and forming rather circular patterns. These types of cracks were categorized into one as mixed longitudinal and transverse weld metal cracks.

Vertical discontinuities are vertical irregularities like mountains and valleys on the surface. They are classified into five subcategories by their appearance and consisting parts. Figure 3.2.3 shows types of vertical discontinuity. They are as follows:

#### 1. One line (V1)

Two relatively flat parts face each other on one line. One part is relatively higher than the other.

#### 2. Two crossed lines (V2.1 and V2.2)

Two relatively flat parts face each other on two crossed lines. One part is relatively higher than the other. There are two kinds in this subcategory. If the smaller part which has a small angle is higher, then it is a type V2.1.

Conversely if the larger part which has a larger angle is higher, then it is a type V2.2.

#### 3. Two parallel lines (V3.1 and V3.2)

Two parts face each other sandwiching a relatively lower (or higher) narrow slip. This category is different from cracks (horizontal discontinuity), because the narrow slip is not very deep or high. It is a type V3.1 if the narrow slip is low and a type V3.2 if high.

4. Two ovals (GB1 and GB2)

These are the types relating to type V3.1 and V3.2. The ends of parallel lines connect the other ends and form two circular patterns. If the part surrounded by the ovals is relatively higher, it is a type GB1 and if lower, it is a type GB2.

5. Three crossed lines (V4)

Three relatively flat parts face one another forming vertical irregularity. The boundary usually becomes three crossed lines.

Additionally Grains or subgrains are frequently observed on the surface of welded structures, thus the degrees of grain sizes are suggested to describe their density by the numbers as shown in Table 3.2.1.

0	no grains can be observed at all
1	a few grains can be observed
2	some grains can be observed
3	50% grains can be observed
4	75% grains can be observed all over the area
5	100% grains can be observed all over the area

Table 3.2.1. Degrees of grain sizes

This standard, newly suggested and used in the observation work in Chapter 4, was found quite convenient and sufficient for observation of microstructures.

1. Longitudinal weld metal cracks



2. Transverse weld metal cracks



3. Mixed longitudinal and transverse weld metal cracks

(Type H3)

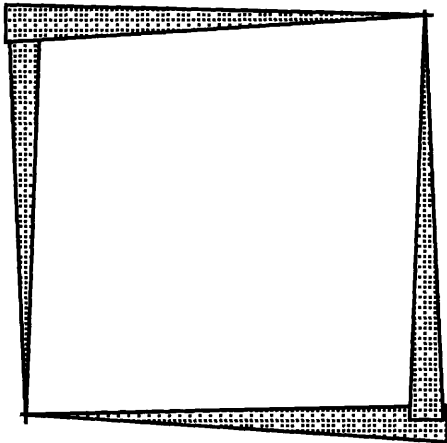
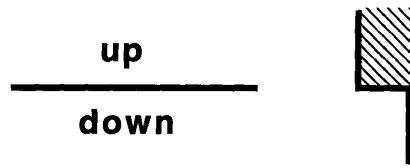


Figure 3.2.2. Types of horizontal discontinuity

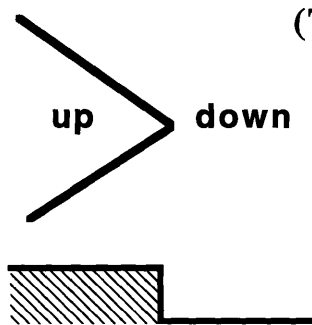
1. One line

(Type V1)

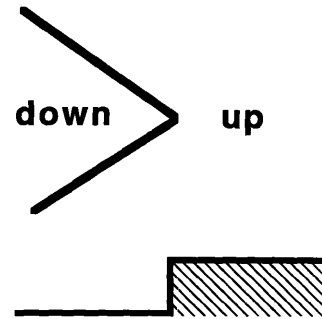


2. Two crossed lines

(Type V2.1)

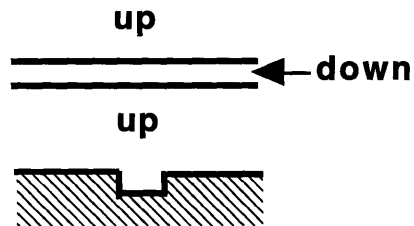


(Type V2.2)

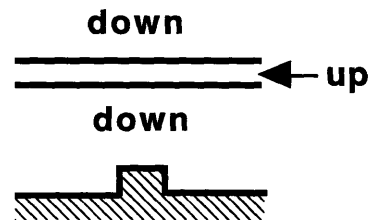


3. Two parallel lines

(Type V3.1)

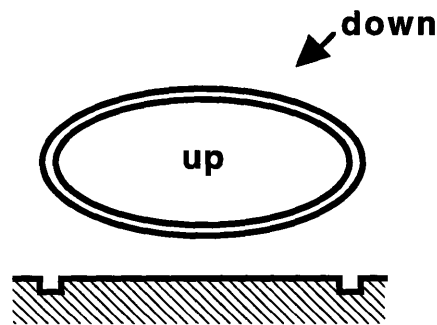


(Type V3.2)

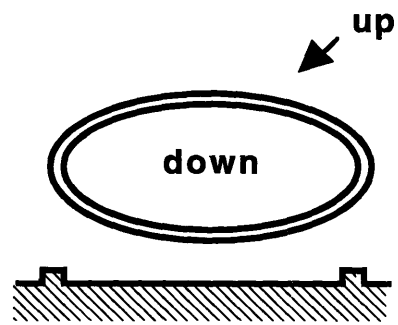


4. Two ovals

(Type GB1)



(Type GB2)



## 5. Three crossed lines

(Type V4)

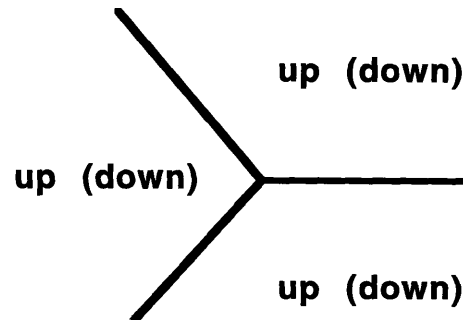


Figure 3.2.3. Types of vertical discontinuity

## 3.3 Cracking

Weld cracks can be classified into two categories in terms of condition of formation.[Ref. 1] They are hot cracks and cold cracks. Cracks formed near the bulk solidus temperatures are hot cracks. Cracks formed at a much lower temperature generally below about 400°F are called cold cracks.

Welded structures are often exposed to environments which cause material embrittlement. There are two well-known types of the environment induced cracks, stress corrosion cracking and hydrogen embrittlement.

### 3.3.1 Hot Cracking

Hot cracking occurs at temperatures near the melting point during or immediately after welding. An alloy which has a long freezing range resulting in a high shrinkage rate is susceptible to hot cracking and segregation under the high shrinkage stresses generated by the contracting mass of metal. It is an intergranular crack. Kammer et al. [Ref. 7] introduced a generalized theory of hot cracking, consisting of four stages.

1. *Primary dendrite formation.* The solid phases are dispersed in the liquid, with both phases capable of relative movement.
2. *Dendrite interlocking.* Both liquid and solid phases are continuous, but only the liquid is capable of relative movement. The liquid can move freely between the dendrites.



3. *Grain-boundary development.* The solid crystals are in an advanced stage of development and the movement of the liquid is restricted; relative movement of the two phases is impossible.

4. *Solidification.* The remaining liquid has solidified.

Stage 3 is the significant stage in cracking and is called the critical solidification range (CSR).

The base metal melts partially in the heat affected zone (HAZ) outside the fusion zone where the peak temperatures during welding fall between the solidus and liquidus temperatures. These cracks are usually small, extending for only one to several grains.

### 3.3.2 Cold Cracking

Cold cracks are generally transgranular and divided into two types, short-time and delayed. Short-time cracks are initiated during cooling to room temperature after welding or after a short time at room temperature. Delayed cracks are initiated after some time, weeks or months at room temperature. They are generally transgranular and occur both in weld metals and HAZ. Hydrogen is known to be responsible for cold cracking in steels.

It is important to know the chemical composition to determine if the material is susceptible or not. Carbon equivalent is usually used to determine the cold cracking sensitivity of a steel plate. The equation is as follows:

$$CE = C + \frac{Mn}{6} + \frac{Ni}{20} + \frac{Cr}{10} + \frac{Cu}{40} - \frac{Mo}{50} - \frac{V}{10} \quad (3.3.1)$$

When CE exceeds 40, underbead cracking may occur.

### 3.3.3 Stress Corrosion Cracking

Stress corrosion cracking occurs in materials under static or slowly increasing load in the presence of certain corrosive environments. This is due to the combined action of stress and corrosion. The surface direction of the cracks is perpendicular to the direction of the load. Alloys have less resistance to stress corrosion cracking than pure metals.

### 3.3.4 Hydrogen Embrittlement

Hydrogen embrittlement, one of the causes of cold cracking and occurs in certain materials containing hydrogen and is one of the most common and serious types of time-dependent fracture. It is on materials which have a body centered cubic (BCC) crystal structure such as steels, titanium, zirconium, and their alloys. Hydrogen is often introduced into these materials during processing, cleaning and electroplating operations. Steels generally tend to become more susceptible to hydrogen cracking as the strength levels increase.

### 3.4 Fracture of Weldments

Fracture means the separation of body into several parts. It is affected by several factors such as material, applied stress, and temperature. Weld fractures are often initiated at weld defects, such as surface discontinuities, sharp notches, or cracks. In terms of its way of propagation, fracture is classified into two types, transgranular and intergranular fractures as shown in Figure 3.4.1.

Transgranular fracture has a cleavage mode and a shear mode depending on the crystal structures of materials.

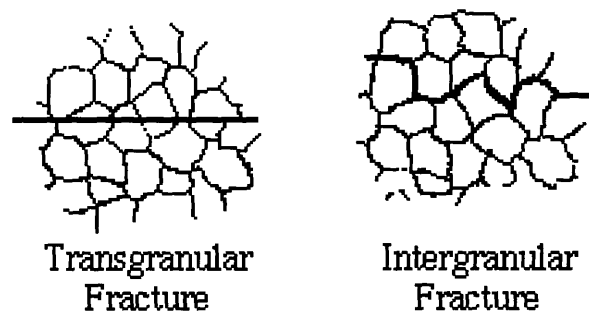


Figure 3.4.1. Transgranular and intergranular fractures

Fracture which occurs under the single application of a continuously increasing load can be either brittle cleavage fracture or fracture associated with plastic deformation, ductile fracture. The other important fracture is called fatigue fracture which occurs after numbers of cyclic loadings. All three fractures are transgranular.

### 3.4.1 Basic Fracture Mechanics Theory

There are three modes of cracking as shown in Figure 3.4.2. Normal stresses cause the opening mode (Mode I), in-plane shear stresses give the sliding mode (Mode II) and out-of-plane shear stresses make tearing mode (Mode III). Although the superposition of all three modes describes the general case of loading, Mode I is the most important for fracture mechanics theory.

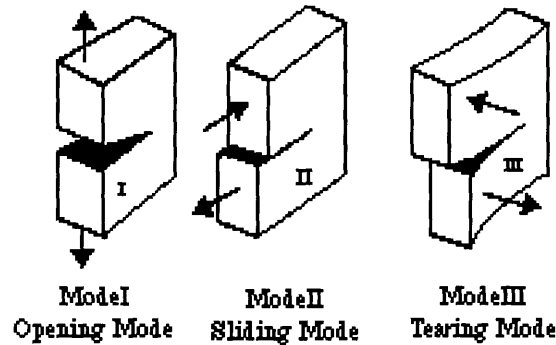


Figure 3.4.2. Modes of cracking

Consider a simple case which is a through-the thickness Mode I crack of arbitrary size,  $2a$ , in an infinite plate as shown in Figure 3.4.3. The crack tip stresses can be written as

$$\sigma_x = \frac{K}{\sqrt{2\pi r}} \cos\frac{\theta}{2} \left[ 1 - \sin\frac{\theta}{2} \sin\frac{3\theta}{2} \right] \quad (3.4.1)$$

$$\sigma_y = \frac{K}{\sqrt{2\pi r}} \cos\frac{\theta}{2} \left[ 1 + \sin\frac{\theta}{2} \sin\frac{3\theta}{2} \right] \quad (3.4.2)$$

$$\tau_{xy} = \frac{K}{\sqrt{2\pi r}} \sin\frac{\theta}{2} \cos\frac{\theta}{2} \cos\frac{3\theta}{2} \quad (3.4.3)$$

where  $K$  is the stress intensity factor and expressed as

$$K = \sigma\sqrt{\pi a} \quad (3.4.4)$$

Along the x-axis ( $\theta = 0$ ), the stresses are:

$$\sigma_x = \sigma_y = \frac{K}{\sqrt{2\pi r}}, \quad \tau_{xy} = 0 \quad (3.4.5)$$

The practical stress intensity factor is more complex and expressed as

$$K = \alpha\sigma\sqrt{\pi a} \quad (3.4.6)$$

If the stress intensity factor,  $K$  exceeds the critical stress intensity factor,  $K_c$ , the crack extends fracture.

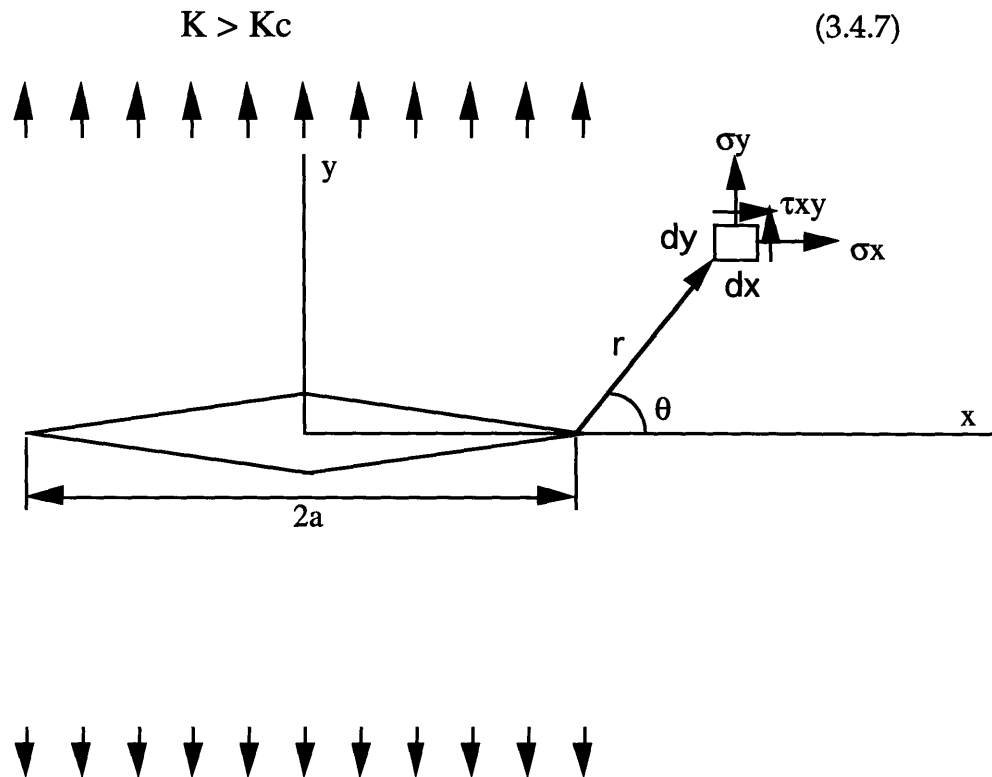


Figure 3.4.3. Crack in an infinite plate [Ref. 11]

### 3.4.2 Brittle and Ductile Fractures

The quality of metallic materials transmits from ductile to brittle as the temperature decreases, as shown in Figure 3.4.4. The fracture which occurs at the temperature in the region where the material is brittle is called a brittle fracture. Brittle fractures are usually initiated at sharp notches or cracks. On the other hand, the fracture in the region of ductile material ductile is a ductile fracture. The most familiar type of ductile fracture is by overload in tension, which produces the classic cup and cone fractures.

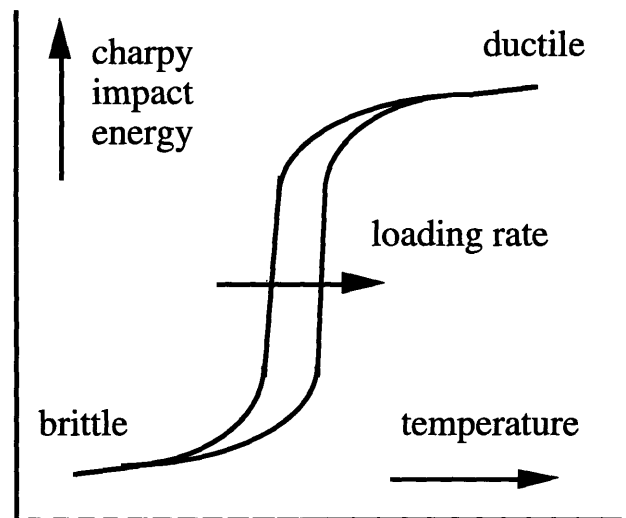


Figure 3.4.4. Brittle-Ductile transition

### 3.4.3 Fatigue Fracture

When a material is subjected to repeated loading, fracture takes place after a certain number of cycles. This is called fatigue fracture. More numbers of cycles before fracture are necessary if the applied stress is low. This is explained by a S-N diagram. Fatigue crack usually originates at the surface of materials. There are two important types of fatigue fracture, a high-cycle, low-stress fatigue and a low-cycle, high-stress fatigue. In high-cycle fatigue, the

endurance limit of a material after several million cycles or more is usually the consideration. In low-cycle fatigue, on the other hand, fracture after repeated loading of less than  $10^5$  cycles is usually considered.

### 3.4.3.1 S-N Diagram

In order to investigate failure life of a material, the S-N diagram, as shown in Figures 3.4.5 is used. It is necessary to test several similar specimens to determine the fatigue strength of a particular material under a given condition. Some materials such as steels have endurance limit . Below this stress level fatigue fracture never occurs. But most materials do not have endurance limit.

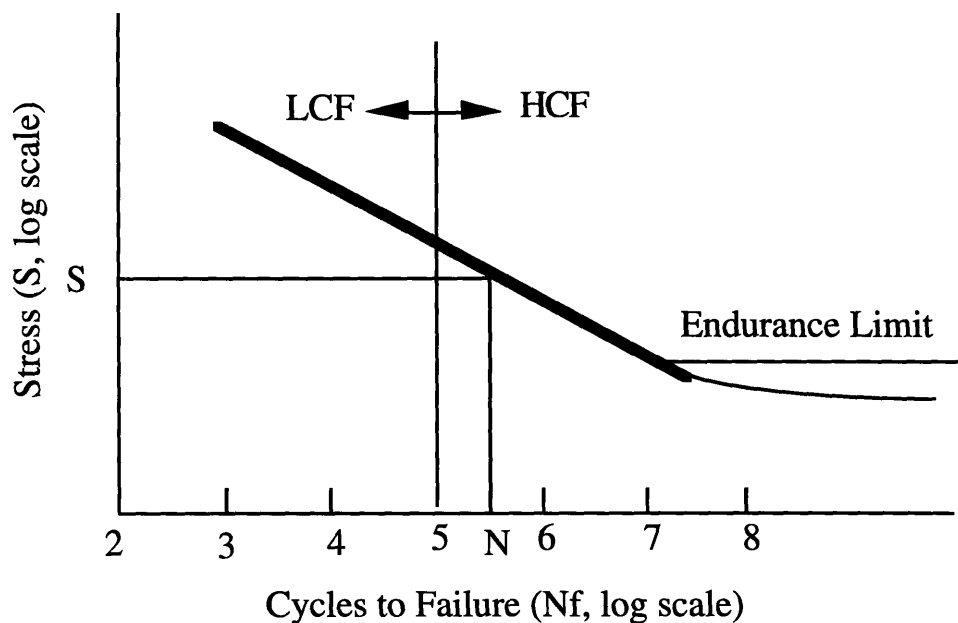


Figure 3.4.5. S-N diagram

### 3.4.3.2 Low-Cycle Fatigue and High-Cycle Fatigue

Fatigue fracture is divided into two types in terms of the stress level and the number of cycles at fracture. The failure life of low-cycle fatigue (LCF) is under approximately  $10^5$  cycles and that of high-cycle fatigue (HCF) is over it. There are many structural components in which LCF, rather than HCF, is usually the problem. For example, cracks frequently found in the hull structure of a ship are caused by LCF. For LCF the strain is a dominant factor to decrease failure life, while the stress is for HCF. LCF includes local plastic deformation. HCF is a problem in those portions of a structure subjected to fast, repeated loads, such as areas close to propellers, rotating machinery, and areas under constant vibrations. In such areas several million stress cycles can be achieved in relatively short period of time. Factors which affect the endurance limit are materials, stress concentration, and corrosion.

**Materials.** The endurance limit of a material increases as the ultimate tensile strength of the material itself increases at a ratio of 50% if the surface of the specimen is very smooth. If the surface is severely notched, the fatigue strength decreases drastically.

**Stress concentration.** The most deleterious factor affecting the fatigue life of metals is the localized stress concentration by geometric discontinuities including notches, cracks fillets, holes and various surface discontinuities especially on the surface of the specimens.

**Corrosion.** The fatigue in corrosive environments, corrosion fatigue, is one of the most serious factors which lowers endurance limit.



### 3.4.3.3 Crack Growth

A pre-existing defect or flaw may develop into a small crack under the influence of regular service loading, but such a small crack may not be fracture critical at the applied service loading. However, with the help of mechanisms of fatigue it may gradually grow and eventually reach a size at which fracture occurs at the regular service stress. The rate of fatigue crack propagation per cycle  $da/dN$  is known to depend on the stress intensity range  $\Delta K$ . It is believed to have the relation below in Region II in the figure.

$$\frac{da}{dN} = C(\Delta K)^m \quad (3.4.8)$$

where  $C$  and  $m$  are material constants. A double-logarithmic plot of  $da/dN$  versus  $\Delta K$  would then be a straight line. However, equation 3.4.8 does not represent reality. Actual experimental data fall on an S-shaped curve as shown in Figure 3.4.6. This fact infers the existence of the threshold value of  $\Delta K$  below which there is no crack growth at all. It is often difficult to verify the existence of this value,  $\Delta K_{th}$ .

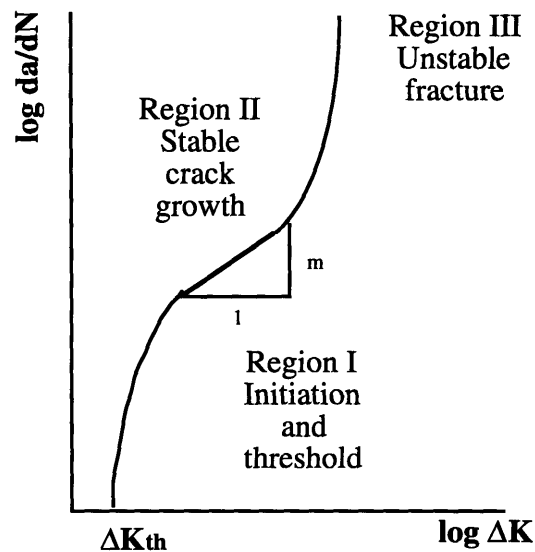


Figure 3.4.6. Relation between  $da/dN$  and  $\Delta K$  [Ref. 13]

This figure infers the possibility of existence of the threshold value  $\Delta K_{th}$  at which fatigue fracture occurs when  $\Delta K$  reaches. However, more data is necessary to study Region I.

### 3.4.3.4 Fatigue Crack Initiation

Under the action of cyclic loads cracks can be initiated as a result of cyclic plastic deformation. Even if the nominal stresses are well below the elastic limit, locally the stresses may be above yield due to stress concentrations at inclusions, mechanical notches, or various surface discontinuities and consequently plastic deformation occurs locally on a microscale.

Wood [Ref. 8] suggested one of the models, as shown in Figure 3.4.7 to explain the mechanisms of fatigue crack initiation by local plastic deformation. The cyclic slips caused by cyclic loading create the extrusions and the intrusions on the surface of materials. The picture of an example of fatigue crack initiation is shown in Figure 3.4.8.

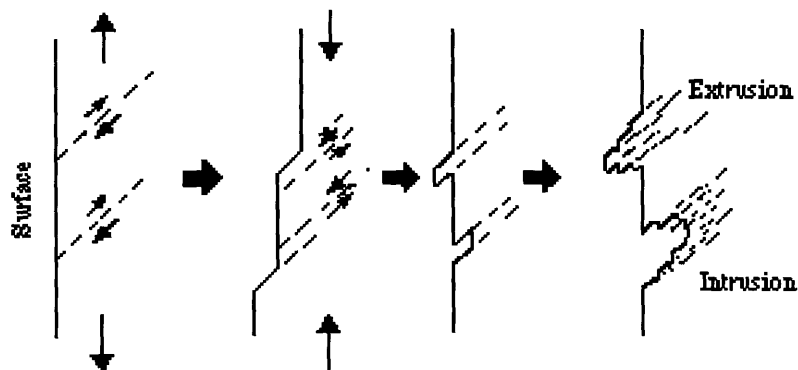


Figure 3.4.7. Wood's model for fatigue crack initiation

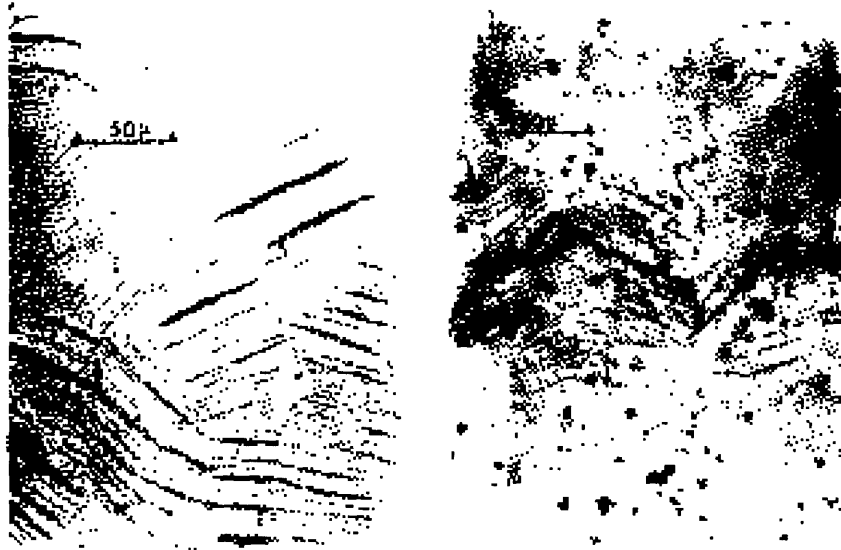


Figure 3.4.8. Example of fatigue crack initiation [Ref. 11]

Stress concentration occurs at a crack tip and plastic deformation is more likely to form. Therefore, the generation of intrusion and extrusion can occur more easily in such areas.

The cyclic opening and closing of the crack will develop a typical pattern of ripples, every new cycle adding a new ripple. These ripples show up on the fracture surface and are called fatigue striations.

## 3.5 Residual Stresses and Stress Concentration

Residual stresses and stress concentration play an important role in cracking and fracture. They are produced in the process of welding.

### 3.5.1 Residual Stresses

Residual stresses are the stresses that exist in a material without external forces or thermal gradients. Residual stresses result from welding thermal transients which induce incompatible strains and inelastic stresses. Incompatible strains are plastic strains due to solidification and solid phase transformation of the weld metal.

Residual stress fields are divided into two categories, microscopic and macroscopic residual stresses. Microscopic residual stresses are of short range and important to consider solidification phenomena, crack formation, and grain boundary effects. Macroscopic residual stresses are of long range and more important in the study of weldments.

Figure 3.5.1 shows the residual stresses due to welding. The pattern of residual stresses by welding is greatly influenced by the geometry of the joint, the number of weld passes, the type of welding processes, interpass temperatures, the materials used, and other factors.

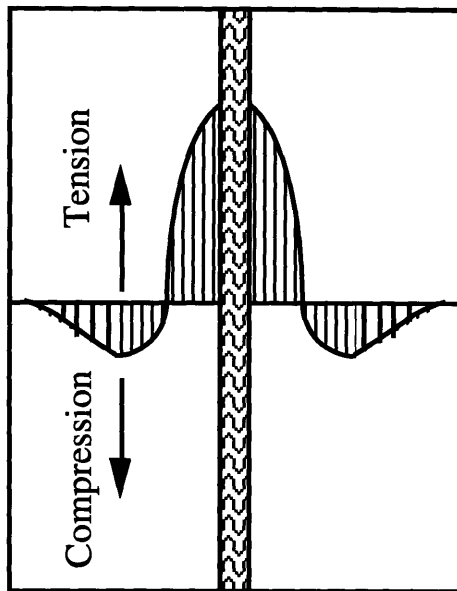


Figure 3.5.1. Residual stresses due to welding [Ref. 1]

### 3.5.2 Stress Concentrations

Geometric conditions may create the areas of stress concentration where cracks can initiate. Stress concentrations occur wherever geometric discontinuities such as sharp edges, notches, and arc strikes exist. Fatigue cracking does not require the stress concentrations, but will more likely happen at the area of the stress concentrations.

### 3.6 Non-Destructive Examination of Welds

There are various methods for non-destructive examination (NDE) of weld defects. They are as follows: [Ref. 1]

#### 1. Radiographic Examination

Radiographic examination uses short-wave length radiation such as X-rays and gamma rays which have more penetrating power than ordinary lights. There is a variation in the absorption of the rays by the weld in the defective region and those defects are shown as shadows on the picture, a radiograph. This method requires power source for an X-ray or a gamma ray and is hazardous.

#### 2. Magnetic Particle Examination

This method uses magnetic particles with colors or fluorescence to detect weld defects. There are two types, a dry method and a wet method. The dry method is more portable, but the wet method is more sensitive. To use this method, test pieces must be magnetic and are required to be demagnetized and cleaned after each test.

#### 3. Ultrasonic Examination

Ultrasonic Examination uses high-frequency sound waves to detect, locate, and help to measure discontinuities in a weldment. But it requires contact with the part of the specimen to be tested.

#### 4. Liquid-Penetrant Examination

Liquid-Penetrant Examination uses liquid of fluorescence or dye to detect and locate minute discontinuities that are open to the surface, such as cracks, pores, and leaks.

## 5. Newly Suggested CSLM and Replica Examination

John M. Cushing Jr. suggested a new non-destructive examination method which uses CSLM and a replica technique. Recent researches show that replica was found to have almost all information of the surface of the specimens. Cushing's result assures this point [Ref. 3]. Replica technique is quite handy and applicable even to very large structures such as ships and airplanes. CSLM is ideal to study replica, because it integrates all surface information into one picture. Replica does not have any information about the interior of weldments.

However, the author propose the combined use of CSLM and PVIM. PVIM is also portable and can be taken to test site. Therefore three different uses can be considered. Figure 3.6.1 illustrates the uses.

### 1. PVIM only

Only PVIM is used on the examination site. An examination is conducted directly through the lens.

### 2. Replica + PVIM

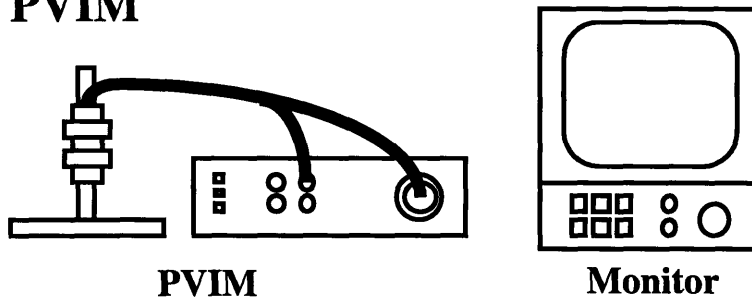
Taking replica to record the surface information of the tested piece and PVIM is used to examine the replica either at the examination site or in the laboratory.

### 3. Replica + PVIM, CSLM

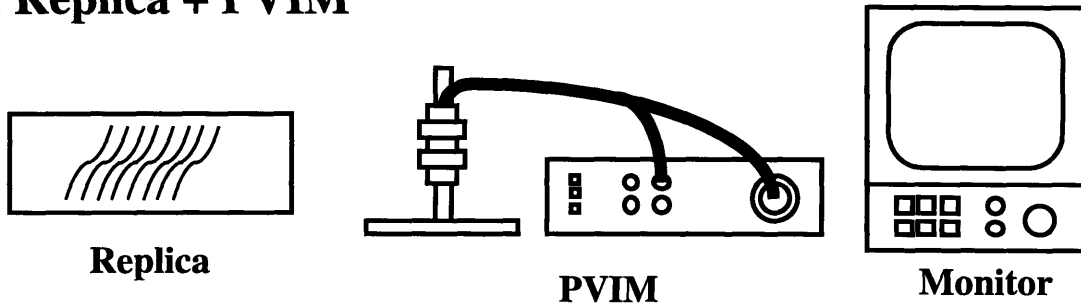
Taking replica to record the surface information of the tested piece and PVIM and CSLM are used to examine the replica either on the examination site or in the laboratory. A PVIM is for large surface irregularities and CSLM is for small ones.



### 1. PVIM



### 2. Replica + PVIM



### 3. Replica + PVIM, CSLM

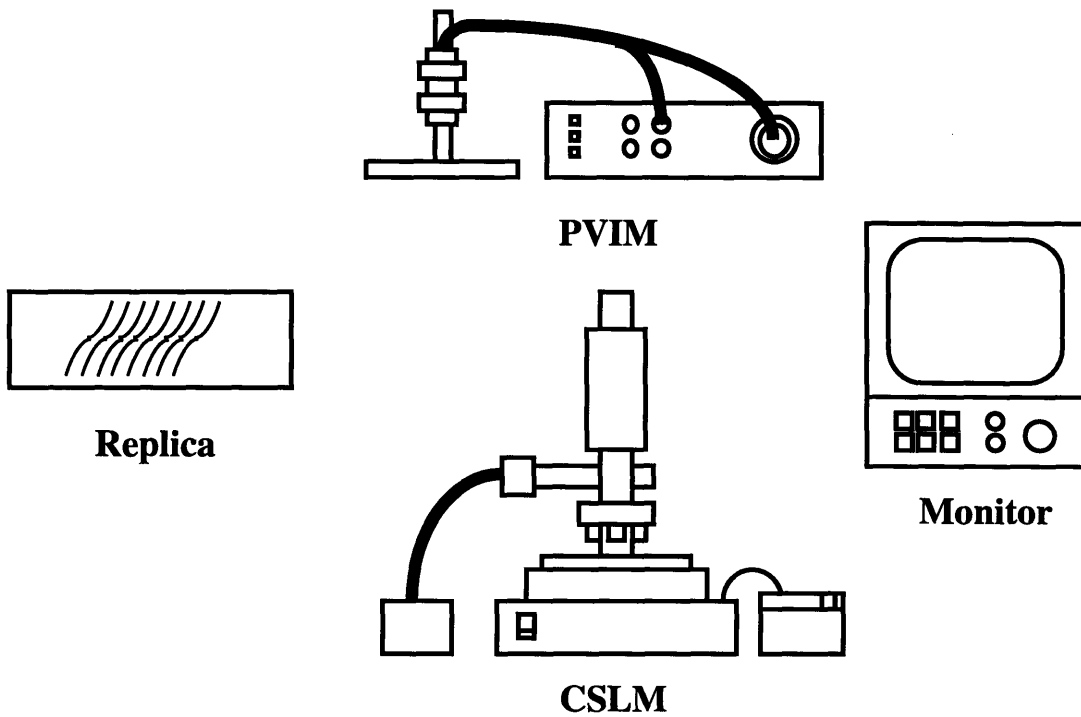


Figure 3.6.1. New Non-Destructive Examination

# Chapter 4: Observation of Welded Specimens

## 4.1 Objectives

Since fusion welding involves melting and rapid solidification, some discontinuities including porosity, cracking, and lacks of fusion are frequently formed. These discontinuities often cause fractures in welded structures, especially fatigue fracture. It has been difficult to observe the surface of a weld using ordinary optical microscopes, which focus only on a narrow area at the same height because of the three dimensional shape of welds. A scanning electron microscope has made it possible to integrate the image of whole welds. However, it is difficult to observe different locations of welds to detect defects since this microscope requires vacuum conditions. Therefore, in almost all (if not all) studies performed up to the present time, cross sections are prepared for metallurgical examination of welds. With the development of a new confocal scanning laser microscope, it is now possible to examine microscopic features of the weld surface with virtually no preparation. The information generated through the observation of the surfaces of welded materials should be useful and indispensable in studying various phenomena including fatigue fractures and a new non-destructive examination thereby helping to develop a new theory of a fatigue crack initiation.

Previous to this experimental work, two preliminary experiments were conducted. One was conducted for an Engineer's thesis by Stephanie Douglas as mentioned in 2.2 [Ref. 6]. She found the advantages and limitations of using a CSLM to observe the surface of welded structures. Based on this work, the other experiment was operated by the author [Ref. 14]. In this work the first attempt to

find the effects of specific factors such as materials, welding processes, and welding conditions was made. This work suggested the need of more numbers of observations with more consistent and carefully prepared specimens in order to know the effects of various factors to the microstructural features on the welded materials. Under these circumstances this research was planned and prepared.

There are four primary objectives:

1. Observe the surface, base metals, heat affected zones (HAZ), and weld metals of various metals welded under various conditions.
2. Classify the surface discontinuities of the specimens according to the categories stated in Chapter 3.
3. Investigate the effects of the different types of materials, welding conditions and their oxides formed through welding on the materials.
4. Verify the reliability and the advantages of using both a PVIM and a CSLM.

## 4.2 Specimen and Equipment

Figure 3.1.1 shows the system configuration. A confocal scanning laser microscope (CSLM) is used to observe microstructural features and a portable video image microscope (PVIM) is used primarily to observe oxide colors and relatively large cracks, because it utilizes ordinary light. A video recorder is used to keep track of the observation process and make a backup for a detailed investigation later. A video image printer is also used to print out the image on the monitor.

### Specimen

An example of specimens used in this research is shown in Figure 4.2.1. The weld beads on the plates are made by electron beam welding (EBW), laser beam welding (LBW) with or without after shielded, and a gas tungsten arc welding (GTAW). The materials of the specimens are low carbon steels, stainless steels, aluminum alloys, and titanium alloys, specifications of which are shown in Table 4.2.1. All the specimens used and welding conditions are summarized in Table 4.2.4.

Kawasaki Heavy Industry, Ltd. kindly prepared the welded specimens of various materials in response to our request. The welding conditions of EBW and LBW used by the company are shown in Table 4.2.2 and Table 4.2.3. A GTAW was conducted in the Welding Systems Laboratory at MIT on the specimens prepared by Kawasaki Heavy Industry, Ltd.

Material	Unit	Low-Carbon Steel	Stainless Steel	Aluminum	Titanium
----------	------	------------------	-----------------	----------	----------

Type		0.15C	SUS304	A5083	Ti-6Al-4V
Specific Heat	$\frac{J}{g \cdot ^\circ C}$	0.46	0.468	0.895	0.53
Density	$\frac{g}{cm^3}$	7.85	7.9	2.68	4.43
Thermal Conductivity	$\frac{J}{mm \cdot s \cdot K}$	0.0519	0.0655	0.21	0.0329
Thermal Expansion Rate	$\frac{cm}{^\circ C}$	11.7	17	23.9	9.6
Melting Temperature	$^\circ C$	1450-1550	1200-1450	600-750	1500-1650
Modulus of Elasticity	$\times 10^6 psi$	29	29	10.2	16
Yield Strength , Min	psi	40,000	30,000	21,000	120,000
Ultimate Strength, Min	psi	69,000	80,000	42,000	130,000

Table 4.2.1. Specifications of materials

Acceleration Voltage	150kV
Beam Current	(1) 20 mA
	(2) 30 mA
	(3) 40 mA
Welding Speed	2,000 mm/min
Welding Position	Vertical
Focus Condition	ab = 1.0
Vacuum Rate	$5 \times 10^{-4}$ torr.

Table 4.2.2. Welding conditions for EBW (CO<sub>2</sub>, 6kW)

Mode	TEM01
Power	(1) 2 kW
	(2) 3 kW
	(3) 4 kW
Welding Speed	2,000 mm/min
Mirror	Any
Focus Condition	Maximum Penetration
Assist Gas	If necessary

Table 4.2.3. Welding conditions for LBW (AF5L)

Material	No.	Sizes	Welding Processes	Welding Conditions	Qnet J/mm
<b>Mild Steel (SS400)</b>	M-1	5x50x150			
Low-Carbon Steel(GTAW)	MT-1	5x50x150	GTAW	50A*9V*82mm/min	229.427
Low-Carbon Steel(GTAW)	MT-2	5x50x150	GTAW	75A*10.5V*82mm/min	402.302
Low-Carbon Steel(GTAW)	MT-3	5x50x150	GTAW	110A*10.5V*82mm/min	590.146
Low-Carbon Steel(LBW1)	ML1-1	5x50x150	CO2 Laser w/o a.s.	2.0kw*2000mm/min	30.03
Low-Carbon Steel(LBW1)	ML1-2	5x50x150	CO2 Laser w/o a.s.	3.0kw*2000mm/min	45.045
Low-Carbon Steel(LBW1)	ML1-3	5x50x150	CO2 Laser w/o a.s.	4.0kw*2000mm/min	60.06
Low-Carbon Steel(LBW2)	ML2-1	5x50x150	CO2 Laser with a.s.	2.0kw*2000mm/min	30.03
Low-Carbon Steel(LBW2)	ML2-2	5x50x150	CO2 Laser with a.s.	3.0kw*2000mm/min	45.045
Low-Carbon Steel(LBW2)	ML2-3	5x50x150	CO2 Laser with a.s.	4.0kw*2000mm/min	60.06
Low-Carbon Steel(EBW)	ME-1	5x50x150	EB	3.0kw*2000mm/min	63.06
Low-Carbon Steel(EBW)	ME-2	5x50x150	EB	4.5kw*2000mm/min	94.6
Low-Carbon Steel(EBW)	ME-3	5x50x150	EB	6.0kw*2000mm/min	126.126
<b>Stainless (SUS304)</b>	S-1	5x50x150			
Stainless(GTAW)	ST-1	5x50x150	GTAW	50A*9.8V*96mm/min	214.375
Stainless(GTAW)	ST-2	5x50x150	GTAW	79A*10.6V*96mm/min	366.362
Stainless(GTAW)	ST-3	5x50x150	GTAW	112A*10.8V*96mm/min	529.2
Stainless(LBW1)	SL1-1	5x50x150	CO2 Laser w/o a.s.	2.0kw*2000mm/min	30.03
Stainless(LBW1)	SL1-2	5x50x150	CO2 Laser w/o a.s.	3.0kw*2000mm/min	45.045
Stainless(LBW1)	SL1-3	5x50x150	CO2 Laser w/o a.s.	4.0kw*2000mm/min	60.06
Stainless(LBW2)	SL2-1	5x50x150	CO2 Laser with a.s.	2.0kw*2000mm/min	30.03
Stainless(LBW2)	SL2-2	5x50x150	CO2 Laser with a.s.	3.0kw*2000mm/min	45.045
Stainless(LBW2)	SL2-3	5x50x150	CO2 Laser with a.s.	4.0kw*2000mm/min	60.06
Stainless(EBW)	SE-1	5x50x150	EB	3.0kw*2000mm/min	63.06
Stainless(EBW)	SE-2	5x50x150	EB	4.5kw*2000mm/min	94.6
Stainless(EBW)	SE-3	5x50x150	EB	6.0kw*2000mm/min	126.13
<b>Aluminum (A5083)</b>	A-1	5x50x150			
Aluminum(GTAW)	AT-1	5x50x150	GTAW	52A*11.5V*96mm/min	261.625
Aluminum(GTAW)	AT-2	5x50x150	GTAW	75A*12.2V*96mm/min	400.312
Aluminum(GTAW)	AT-2N	5x50x150	GTAW	75A*12.2V*96mm/min	400.312
Aluminum(GTAW)	AT-3	5x50x150	GTAW	112A*12.1V*96mm/min	529.9
Aluminum(LBW1)	AL1-1	5x50x150	CO2 Laser w/o a.s.	2.0kw*2000mm/min	30.03
Aluminum(LBW1)	AL1-2	5x50x150	CO2 Laser w/o a.s.	3.0kw*2000mm/min	45.045
Aluminum(LBW1)	AL1-3	5x50x150	CO2 Laser w/o a.s.	4.0kw*2000mm/min	60.06
Aluminum(LBW2)	AL2-1	5x50x150	CO2 Laser with a.s.	2.0kw*2000mm/min	30.03
Aluminum(LBW2)	AL2-2	5x50x150	CO2 Laser with a.s.	3.0kw*2000mm/min	45.045
Aluminum(LBW2)	AL2-3	5x50x150	CO2 Laser with a.s.	4.0kw*2000mm/min	60.06
Aluminum(EBW)	AE-1	5x50x150	EB	3.0kw*2000mm/min	63.063
Aluminum(EBW)	AE-2	5x50x150	EB	4.5kw*2000mm/min	94.6
Aluminum(EBW)	AE-3	5x50x150	EB	6.0kw*2000mm/min	126.13
<b>Titanium (Ti-6Al-4V)</b>	T-1	5x50x150			
Titanium(GTAW)	TT-1	5x50x150	GTAW	51A*9.3V*96mm/min	207.506
Titanium(GTAW)	TT-2	5x50x150	GTAW	79A*10.3V*96mm/min	355.994
Titanium(GTAW)	TT-3	5x50x150	GTAW	112A*11.0V*96mm/min	539
Titanium(LBW2)	TL2-1	5x50x150	CO2 Laser with a.s.	2.0kw*2000mm/min	30.03
Titanium(LBW2)	TL2-2	5x50x150	CO2 Laser with a.s.	3.0kw*2000mm/min	45.045
Titanium(LBW2)	TL2-3	5x50x150	CO2 Laser with a.s.	4.0kw*2000mm/min	60.06
Titanium(EBW)	TE-1	5x50x150	EB	3.0kw*2000mm/min	63.06
Titanium(EBW)	TE-2	5x50x150	EB	4.5kw*2000mm/min	94.6
Titanium(EBW)	TE-3	5x50x150	EB	6.0kw*2000mm/min	126.13

Table 4.2.4. Details of specimens

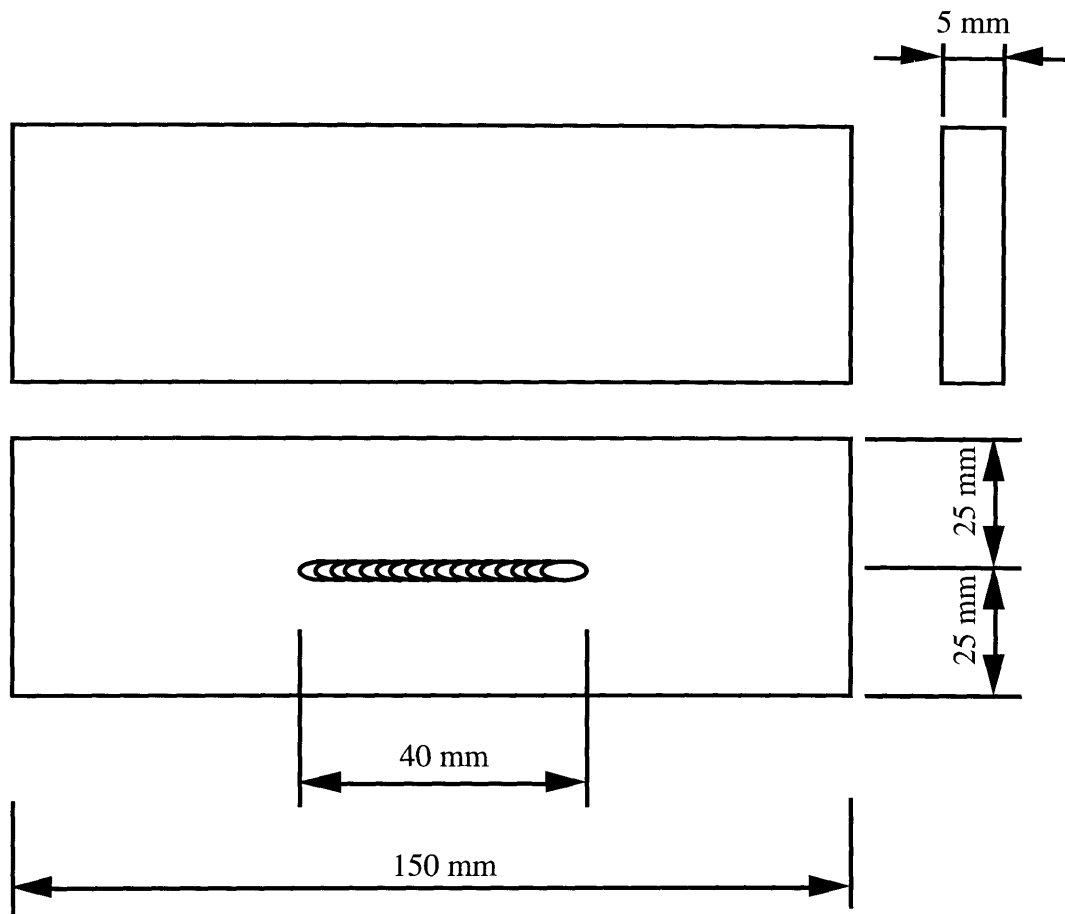


Figure 4.2.1. Specimen for observation

### 4.3 Experimental Procedure

The general procedures are described below. The examination consisted of the following three major steps and was conducted for 46 specimens.

1. First, visually inspect the specimen to see if it has any large crack and oxide.

This step helps to locate the large surface discontinuities which should not exist on the carefully prepared specimens. Oxides often have their own colors which inform one of their existence.

2. Using a PVIM with a lens 250, make observations of the surface of the specimens for base-metal, HAZ, the edge of the weldment, and the center of the weldment to find the microstructural features which affect the fatigue crack and fracture and the oxides covering the surface. The names of locations are shown in Figure 4.3.1. Then those surface discontinuities are classified into the categories mentioned in 3.2. Through the whole process, the video recorder is used to record all of the information. The detailed procedures are the following:

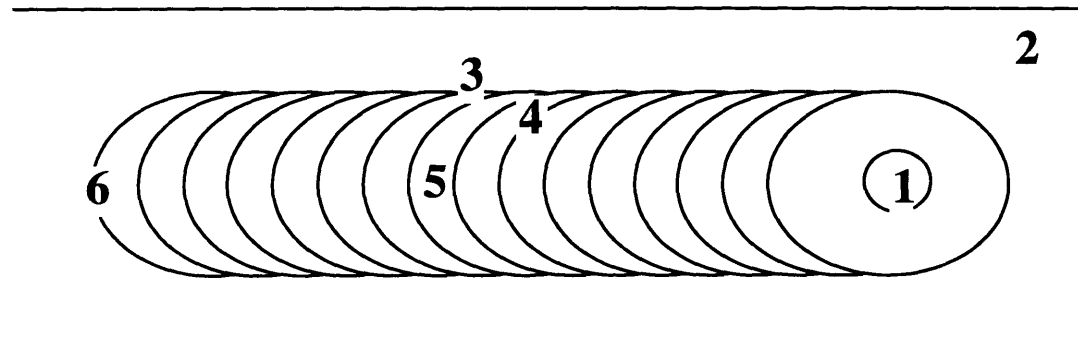
- a) Unlap the cover protecting the specimen and quickly scan it to avoid new oxide from forming and to see the color and thickness of oxides.
- b) Skim carefully all over the specimen to find special microstructural features of the specimen. If any, take a picture and describe it in the observation sheet.
- c) Describe general microstructural features of the specimen in the sheet and take pictures.

3. Using a CSLM with lenses of 10X, 20X, 40X, and 100X, make observations of the surface of the specimen for base-metal, HAZ, the edge of the weldment, and the center of the weldment to find the microstructural features which affect



the fatigue crack and fracture. Then those surface discontinuities are classified into the categories mentioned in 3.2. The detailed procedures are the following:

- a) Skim carefully all over the specimen to find special microstructural features of the specimen. If any, take a picture and describe it in the observation sheet. Use a scanning feature of the CSLM if necessary.
- b) If any surface discontinuity is found, measure its height, depth, width, length and inspect its shape. And take a picture and describe it in the sheet. Use a scanning feature of the CSLM if necessary.
- b) Describe general microstructural features of the specimen in the sheet and take pictures. Use a scanning feature of the CSLM if necessary.



**1: Weld Crater, 2: Base Metal, 3: HAZ, 4: Edge of Weld, 5: Center of Weld, 6: Start-up Toe**

Figure 4.3.1. Location of welded specimen

# Chapter 5: Experimental Results and Discussions for Observation

## 5.1 Low-Carbon Steels

Low-carbon steel specimens were welded by three different welding processes, GTAW (with and without after shield), EBW, and LBW. All observation data is shown in Appendices. Pictures of surface features observed with a PVIM and a CSLM are also shown later in this chapter.

### **Specimens Welded by GTAW (MT-1, 2, and 3)**

#### Oxide formation

A narrow band of a very thin brown oxide layer parallel to the fusion line covered the surface of HAZ. The entire weld metal of MT-1 was covered with a very thin brown oxide layer. MT-2 and MT-3 were also covered with similar oxide layers, but thicker.

#### Micro discontinuities

The appearance of the HAZ was similar to the base metal for MT-1 and MT-2. The HAZ of MT-3 was not observable due to oxide. At the edge of weld metal, a few vertical discontinuities and a few grains with random shape and 50~80  $\mu\text{m}$  diameter for MT-1, 80 ~220  $\mu\text{m}$  for MT-2, and 80 ~ 200  $\mu\text{m}$  for MT-3 were observed. Although it was difficult to find discontinuities or grains at the weld center of MT-1 due to weld ripples

covering entire weld metal, a few discontinuities, type V2 and V4, and grains were observed. At the center a few random shape grains with 40 ~ 60  $\mu\text{m}$  diameter were observed for MT-2 and MT-3.

### **Specimens Welded by LBW without After Shield (ML1-1, 2, and 3)**

#### Oxide formation

Two narrow bands of oxide layers parallel to the fusion line covered the surface of the HAZ. One was a very thin brown oxide layer and the other was a thick black layer. The weld metal of ML1-1 was entirely covered with a thin gray layer of oxidation. Only a narrow band on the weld edge had this oxidation for ML1-2 and ML1-3. The entire weld metals were covered with a very thick layer of black oxide.

#### Micro discontinuities

The only discontinuity that was able to be observed in the HAZ was grain boundaries. In many cases we found grains that were continuous to the weld metal. Although the grains were many in number, they were difficult to be observed. Their length was up to 20  $\mu\text{m}$ . The size of the subgrains in the HAZ was 2  $\mu\text{m}$ .

The discontinuities at the weld edge were grain boundaries. Their shape was round with diameter 10 ~ 15  $\mu\text{m}$ . We also observed oval shape of grains with maximum size 25 x 150  $\mu\text{m}$  on ML1-1, 20 x 30  $\mu\text{m}$  on ML1-2, and 40 x 100  $\mu\text{m}$  on ML1-3. The grain boundaries in many cases were found to have cracks. At the center the grains had the normal shape with 15 ~ 30  $\mu\text{m}$  on ML1-1, 15 ~ 40  $\mu\text{m}$  on ML1-2, and 50 ~ 80  $\mu\text{m}$  on ML1-3. The cracks

observed in the grains were mostly hot cracks on ML1-1, however, existence of transgranular cracks indicated cold cracks as well. The observation of the center of ML1-3 was difficult due to oxide. The size of the subgrains was 2 ~ 8  $\mu\text{m}$ , but for ML1-2 it was found to be 15  $\mu\text{m}$ .

### **Specimens Welded by LBW with After Shield (ML2-1, 2, and 3)**

#### Oxide formation

A 0.25 mm band of thick black oxide layer parallel to the fusion line covered the surface of the HAZ. The weld metals were covered with a very thin gray layer.

#### Discontinuities

Due to heavy oxidation, we could not see grains in the HAZ. Discontinuities observed in the area of the weld edge were grain boundaries and cracks. The use of after shielding reduced the formation of oxides significantly. Hot and cold cracks could often be observed in the grains.

In the area of the weld edge, the grains with 15 ~ 40  $\mu\text{m}$  normal shape or maximum 40 x 100  $\mu\text{m}$  oval shape for ML2-1, 15 ~ 40  $\mu\text{m}$  normal shape or maximum 40 x 200  $\mu\text{m}$  oval shape for ML2-2, and 10  $\mu\text{m}$  normal shape or maximum 60 x 300  $\mu\text{m}$  oval shape for ML2-3 were observed.

In the area of the weld center, the grains with 15 ~ 40  $\mu\text{m}$  normal shape for ML2-1, 10 ~ 40  $\mu\text{m}$  round shape for ML2-2, and maximum 25 x 3  $\mu\text{m}$  oval shape for ML2-3 were observed.

The subgrains in the weld metals were 3 ~7  $\mu\text{m}$ .

## Specimens Welded by EBW (ME-1, 2, and 3)

### Oxide formation

A band of very thin brown oxide layer parallel to the fusion line covered the surface of the HAZ. The edge of the weld metal was covered with a very thick black oxide layer. As heat input increased, the thickness of the layer and the width of the band increased.

### Micro discontinuities

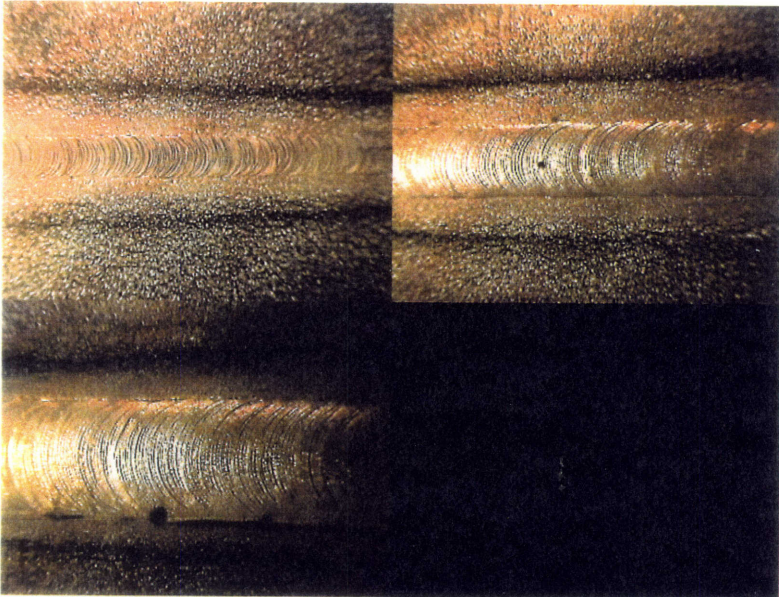
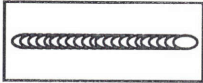
The HAZ included many horizontal discontinuities (cracks), perpendicular to the welding direction (H2). The longest, which was on ME-3, had a length of up to 35  $\mu\text{m}$ . These horizontal discontinuities were part of the grain boundaries. The shape of the grains was normal and the size was 10 ~ 30  $\mu\text{m}$ . The edge of the weld metal had almost the same appearance as the HAZ. Most of the discontinuities in the weld metals were continuous to the HAZ. The length of the horizontal discontinuities was up to 120  $\mu\text{m}$  for ME-2 and up to 150  $\mu\text{m}$  for ME-3.

The rest of the weld metals also had many horizontal discontinuities. Many of them were cold cracks. The grains in HAZ were a normal shape and the size 10 ~ 30  $\mu\text{m}$ . At the center of ME-1 the grains were round 2 ~ 5  $\mu\text{m}$  or oval 10 x 4  $\mu\text{m}$ . We also found grain-like large structures up to 50  $\mu\text{m}$  in size. For ME-2 the grains were round 2 ~ 8  $\mu\text{m}$  or oval 20 x 2  $\mu\text{m}$ , and the large structures were up to 100  $\mu\text{m}$ . For ME-3 the grains were round 2 ~ 7  $\mu\text{m}$  or oval 25 x 5  $\mu\text{m}$ , and the large structures were up to 90  $\mu\text{m}$ .

# Surface Appearance of Welded Low-Carbon Steels

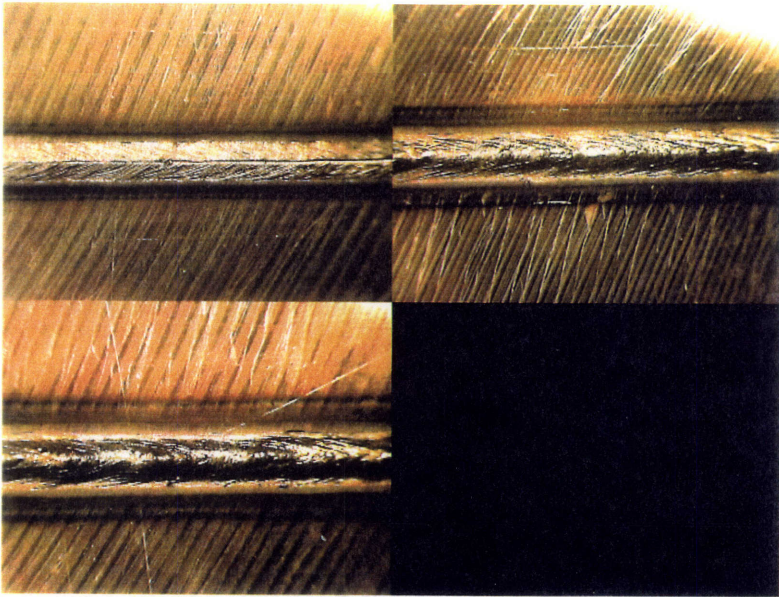
PVIM

MT-1 42X	MT-2 42X
MT-3 42X	



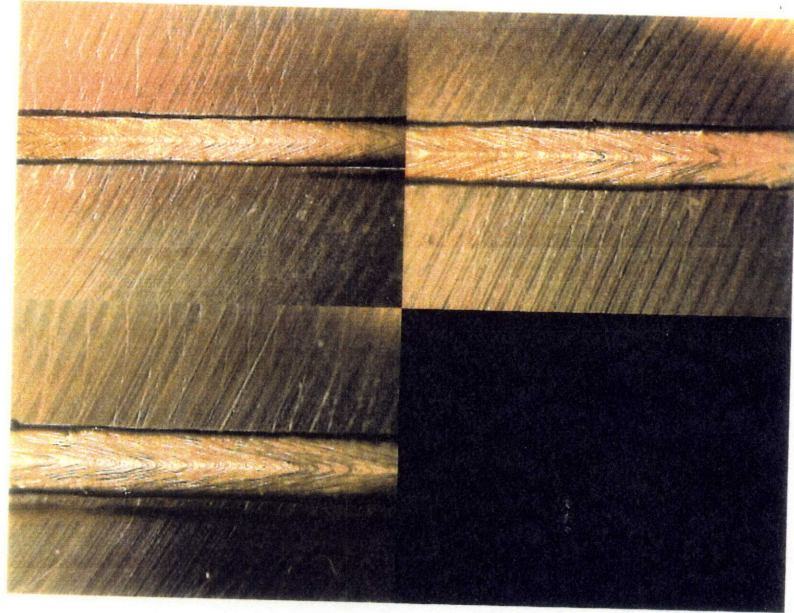
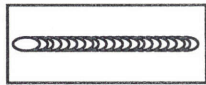
PVIM

ML1-1 42X	ML1-2 42X
ML1-3 42X	



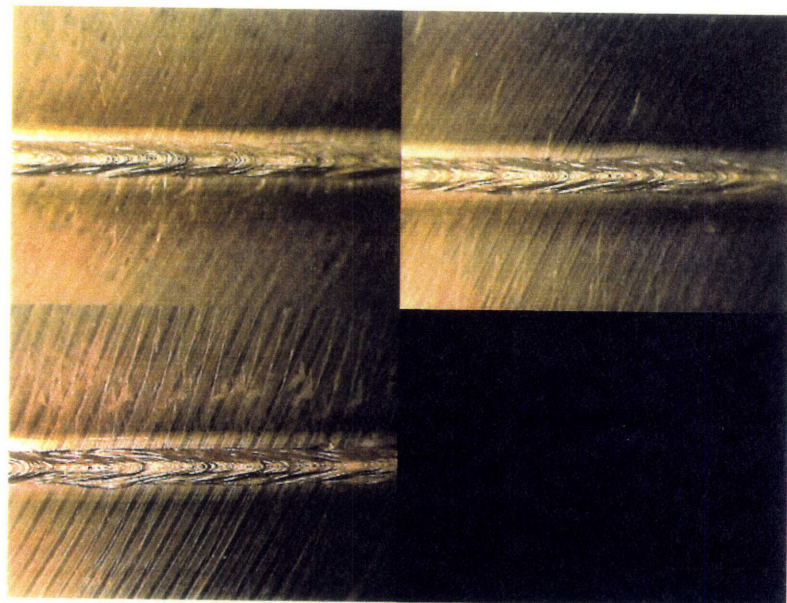
PVIM

ML2-1 42X	ML2-2 42X
ML2-3 42X	



PVIM

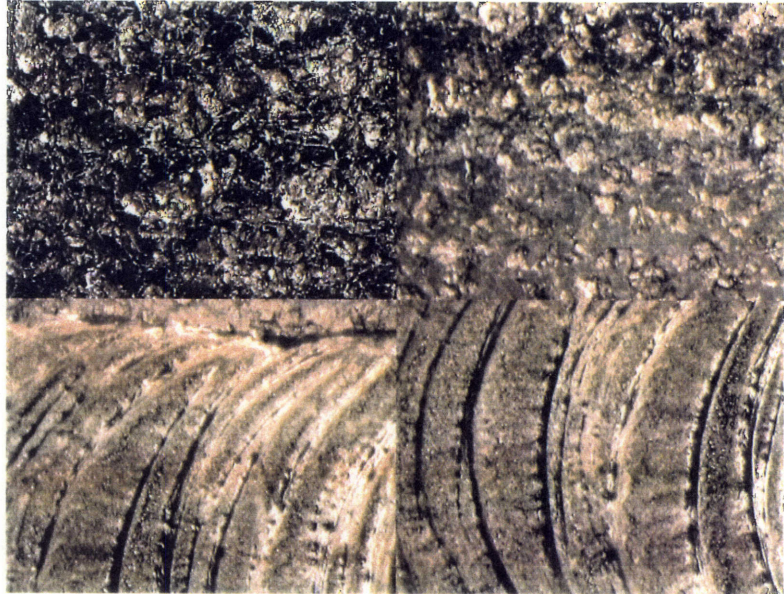
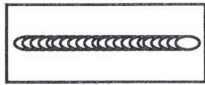
ME-1 42X	ME-2 42X
ME-3 42X	



**MT-1** (SS400-GTAW-50A x 9V x 82mm/min)

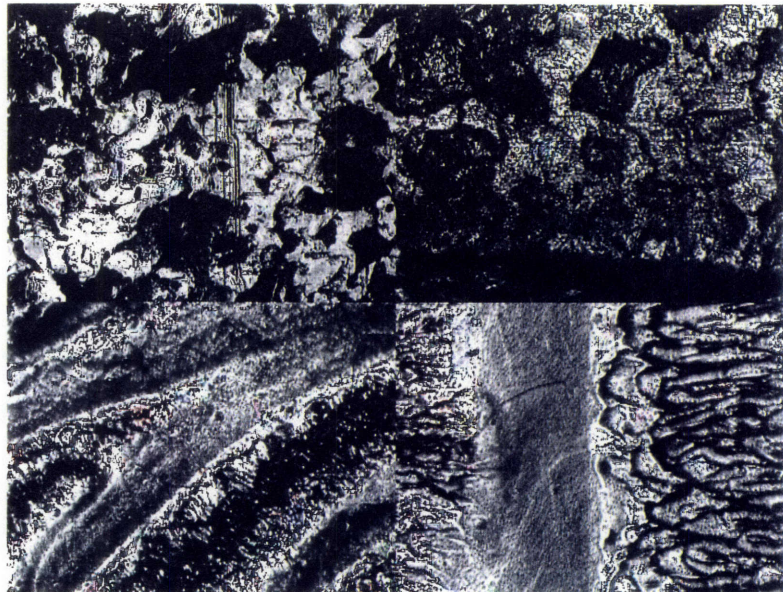
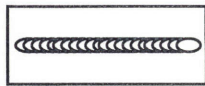
**PVIM**

B.M. 42X	HAZ 42X
Edge 42X	Center 42X



**CSLM**

B.M. 113X	HAZ 113X
Edge 225X	Center 450X

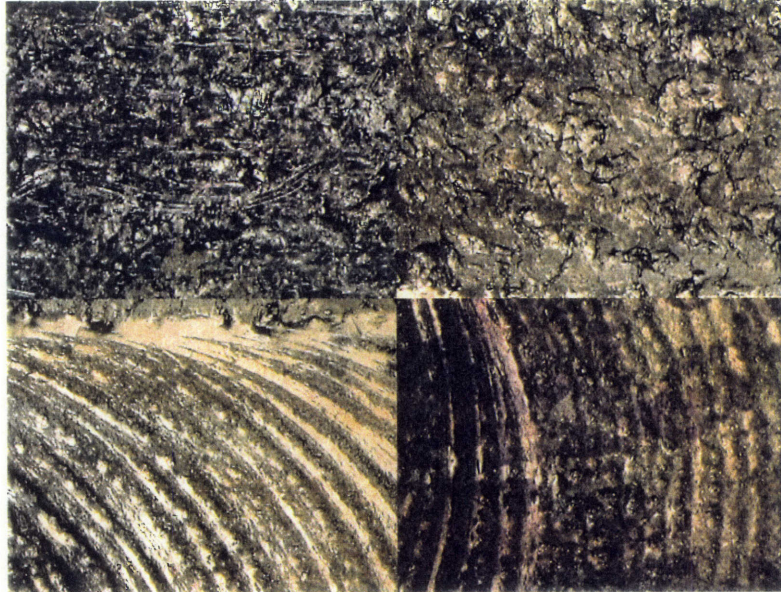
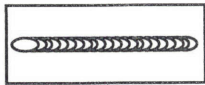




**MT-2** (SS400-GTAW-75A x 10.5V x 82mm/min)

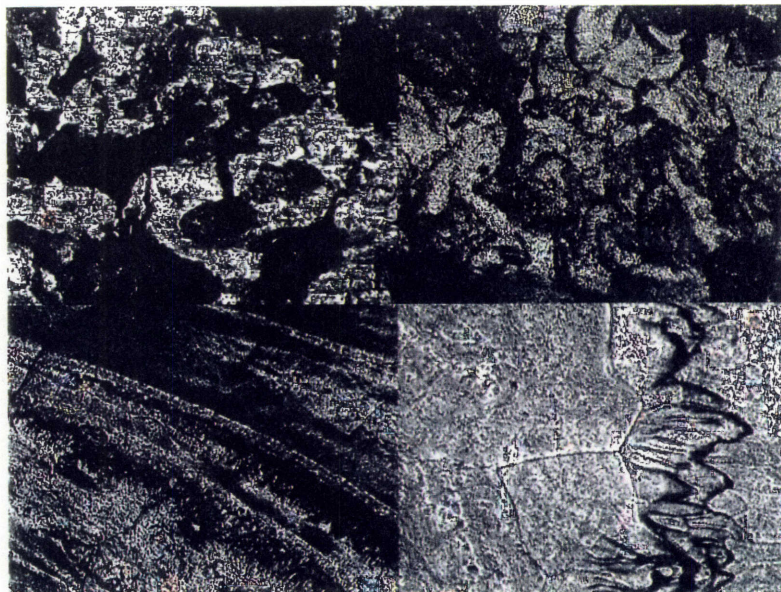
**PVIM**

B.M.	HAZ
42X	42X
Edge	Center
42X	42X



**CSLM**

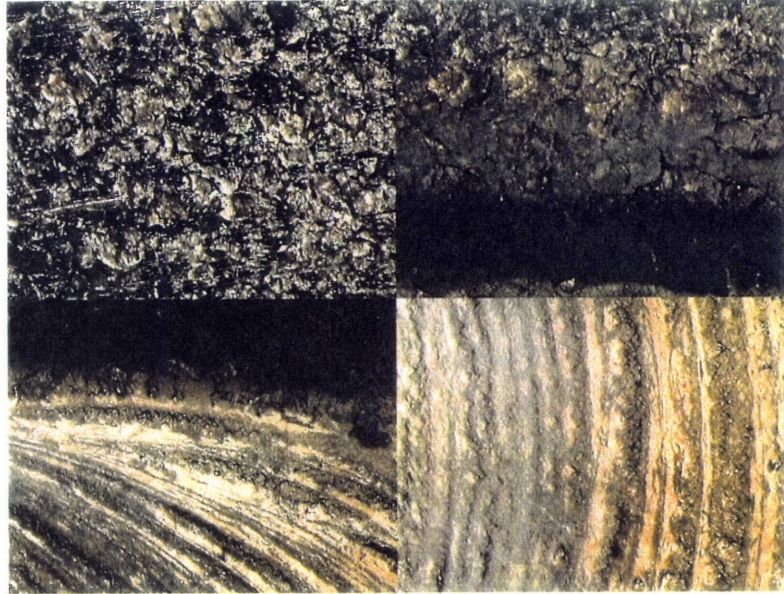
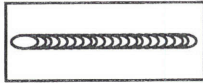
B.M.	HAZ
113X	113X
Edge	Center
113X	450X



**MT-3** (SS400-GTAW-110A x 10.5V x 82mm/min)

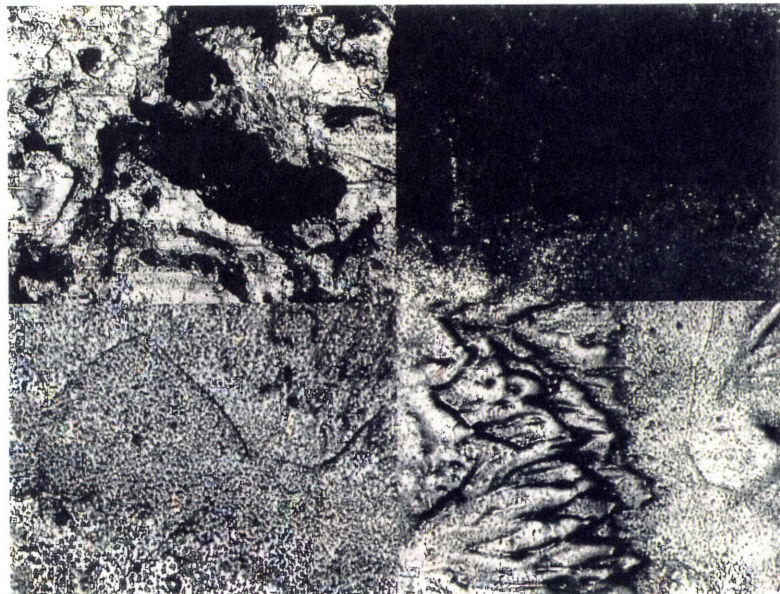
**PVIM**

B.M. 42X	HAZ 42X
Edge 42X	Center 42X



**CSLM**

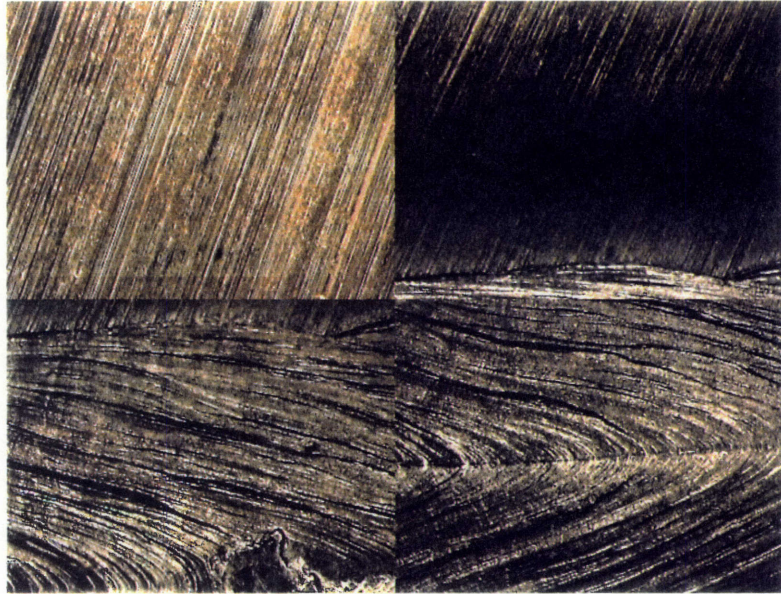
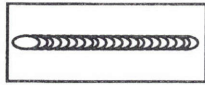
B.M. 113X	HAZ 113X
Edge 450X	Center 450X



**ML1-1** (SS400-LBW1-2.0kW x 2000mm/min)

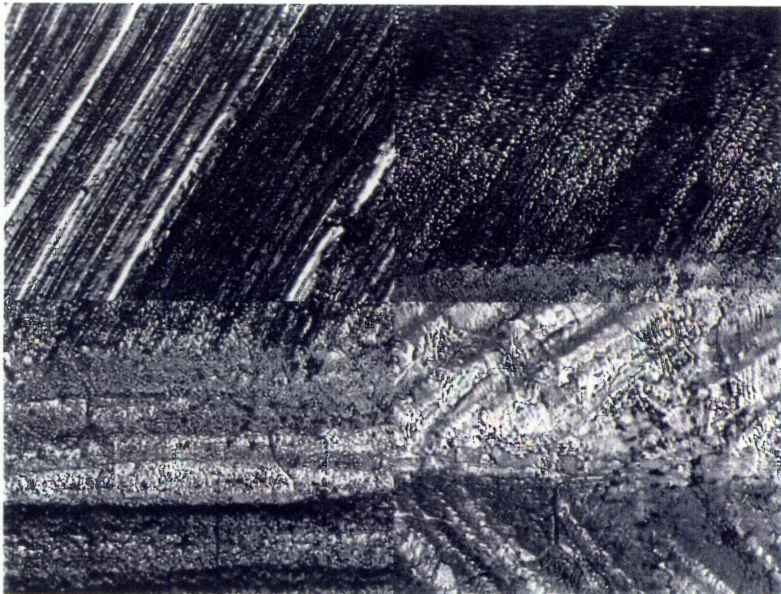
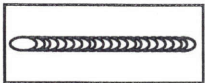
**PVIM**

B.M.	HAZ
42X	42X
Edge	Center
42X	42X



**CSLM**

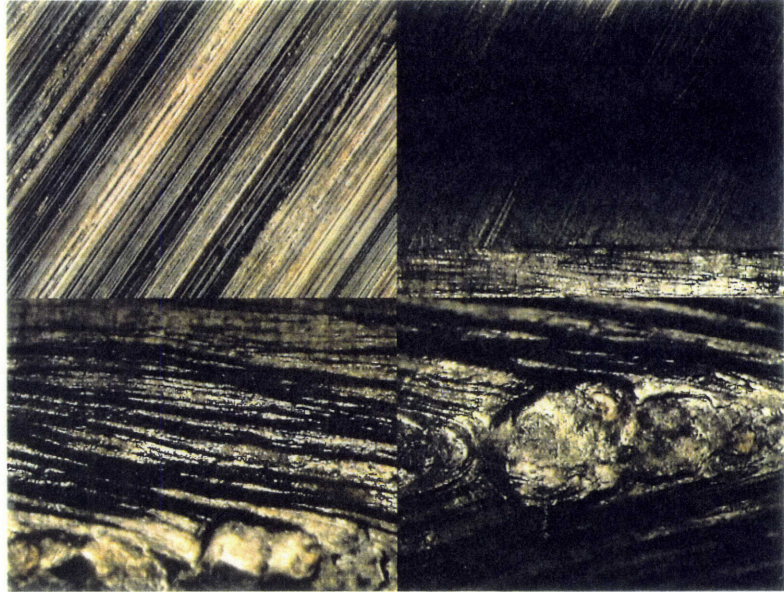
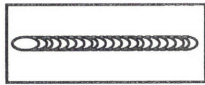
B.M.	HAZ
450X	450X
Edge	Center
450X	450X



**ML1-2** (SS400-LBW1-3.0kW x 2000mm/min)

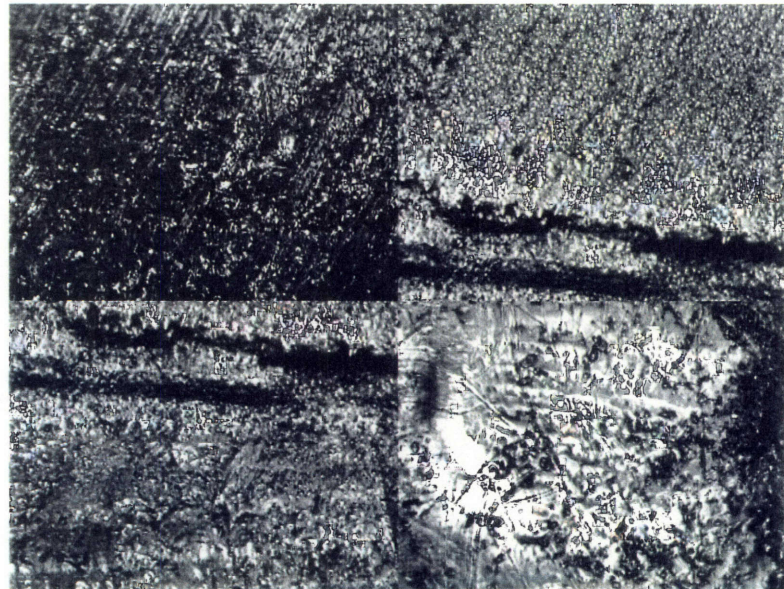
**PVIM**

B.M. 42X	HAZ 42X
Edge 42X	Center 42X



**CSLM**

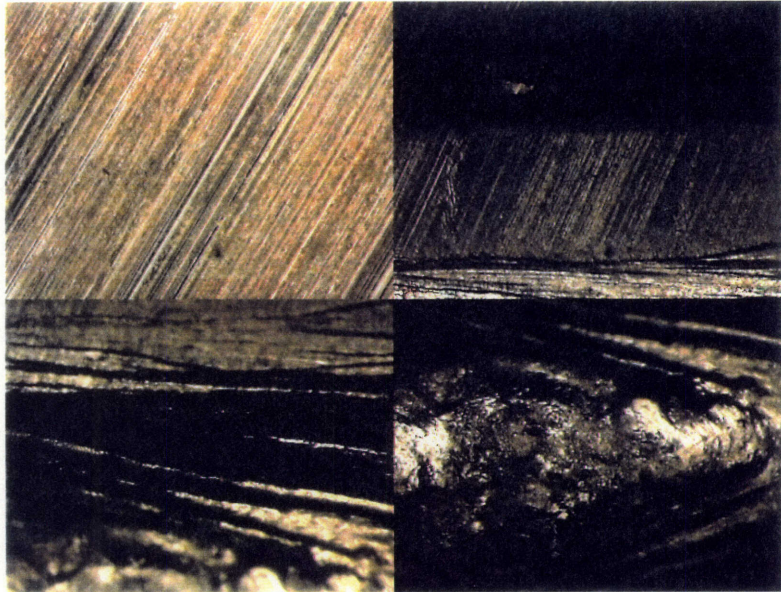
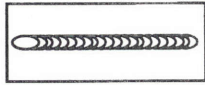
B.M. 450X	HAZ 450X
Edge 450X	Center 450X



**ML1-3** (SS400-LBW1-4.0kW x 2000mm/min)

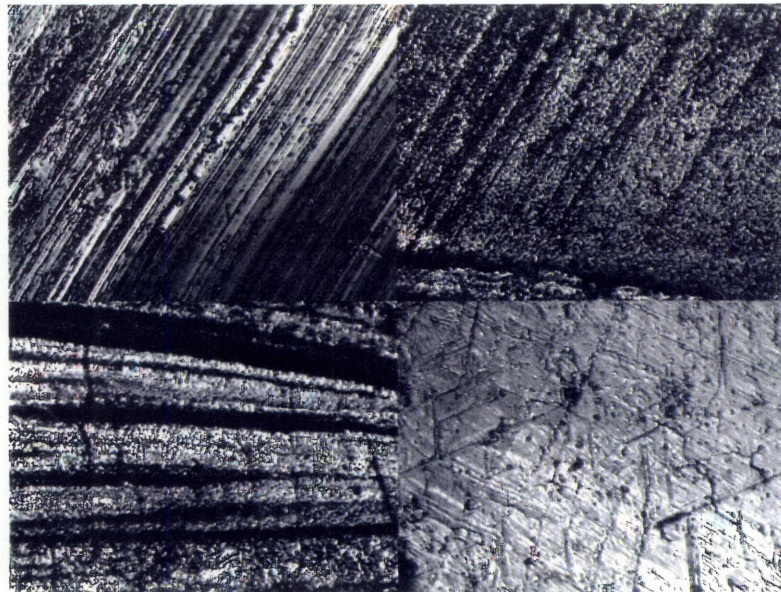
**PVIM**

B.M. 42X	HAZ 42X
Edge 42X	Center 42X



**CSLM**

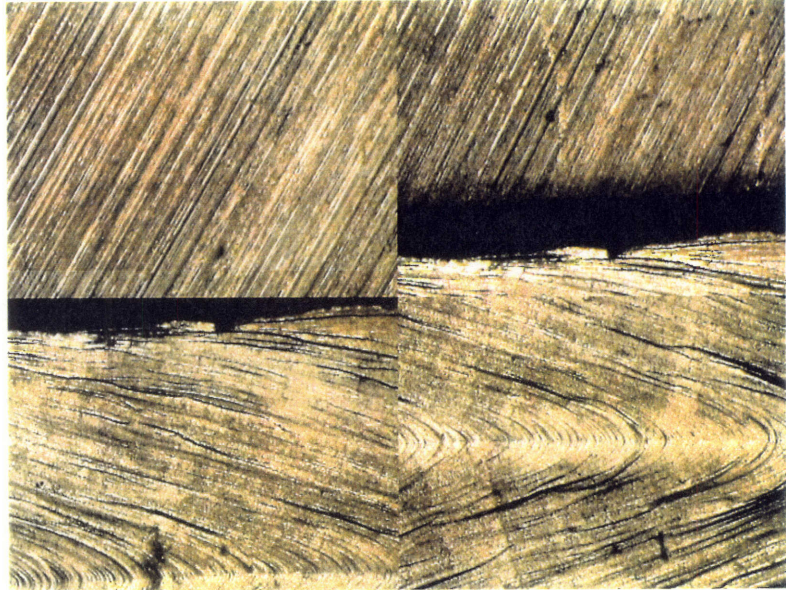
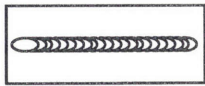
B.M. 450X	HAZ 450X
Edge 450X	Center 450X



**ML2-1** (SS400-LBW2-2.0kW x 2000mm/min)

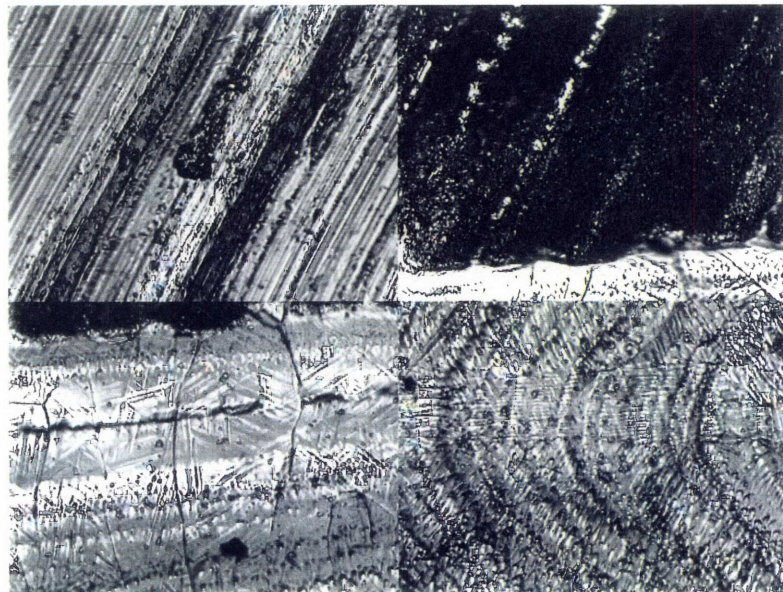
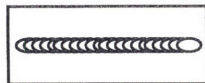
**PVIM**

B.M. 42X	HAZ 42X
Edge 42X	Center 42X



**CSLM**

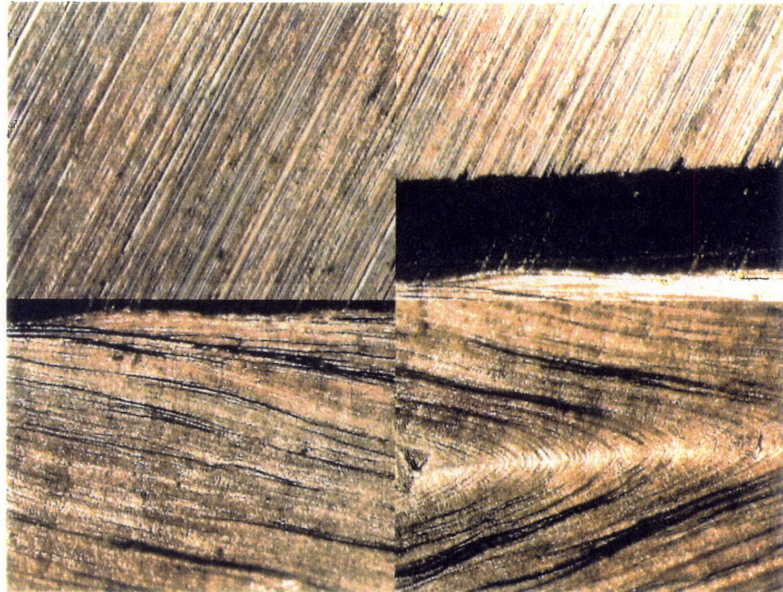
B.M. 450X	HAZ 450X
Edge 450X	Center 450X



**ML2-2** (SS400-LBW2-3.0kW x 2000mm/min)

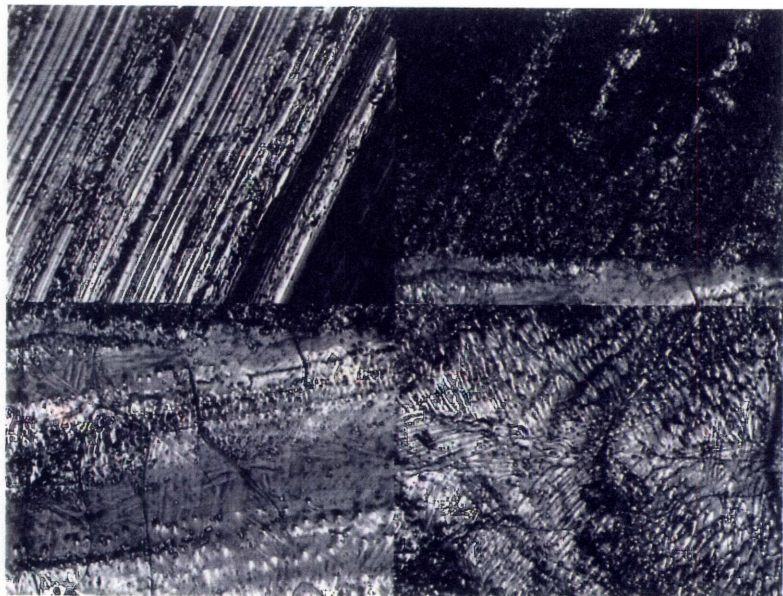
**PVIM**

B.M. 42X	HAZ 42X
Edge 42X	Center 42X



**CSLM**

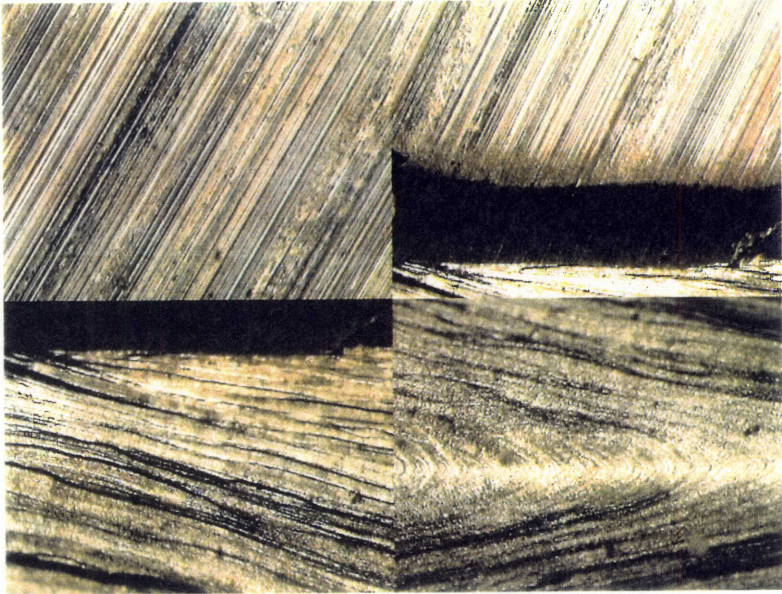
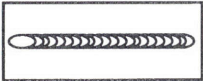
B.M. 450X	HAZ 450X
Edge 450X	Center 450X



**ML2-3** (SS400-LBW2-4.0kW x 2000mm/min)

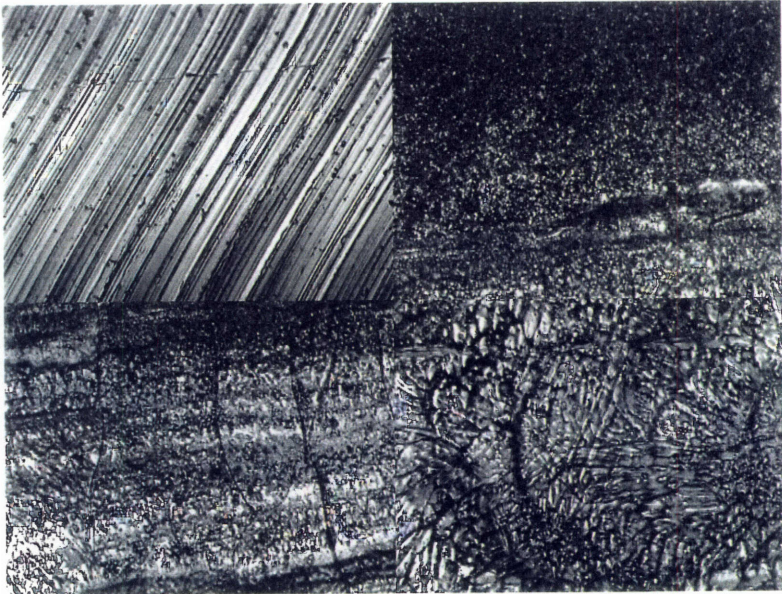
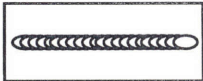
**PVIM**

B.M.	HAZ
42X	42X
Edge	Center
42X	42X



**CSLM**

B.M.	HAZ
450X	450X
Edge	Center
450X	450X

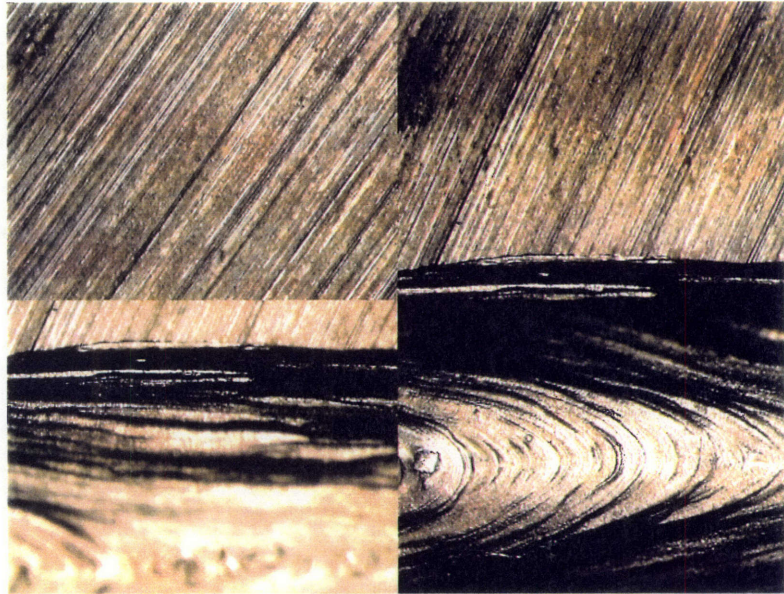
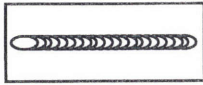




**ME-1** (SS400-EBW2-3.0kW x 2000mm/min)

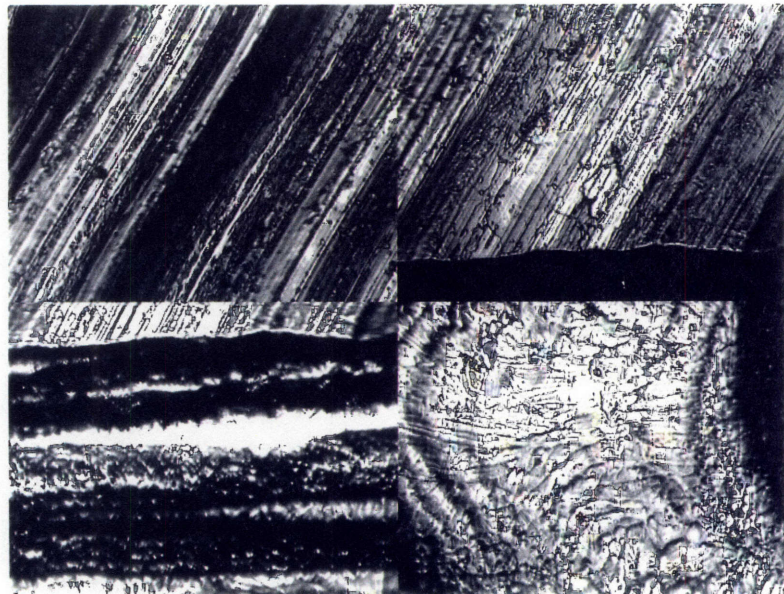
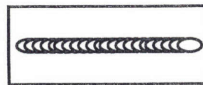
PVIM

B.M. 42X	HAZ 42X
Edge 42X	Center 42X



CSLM

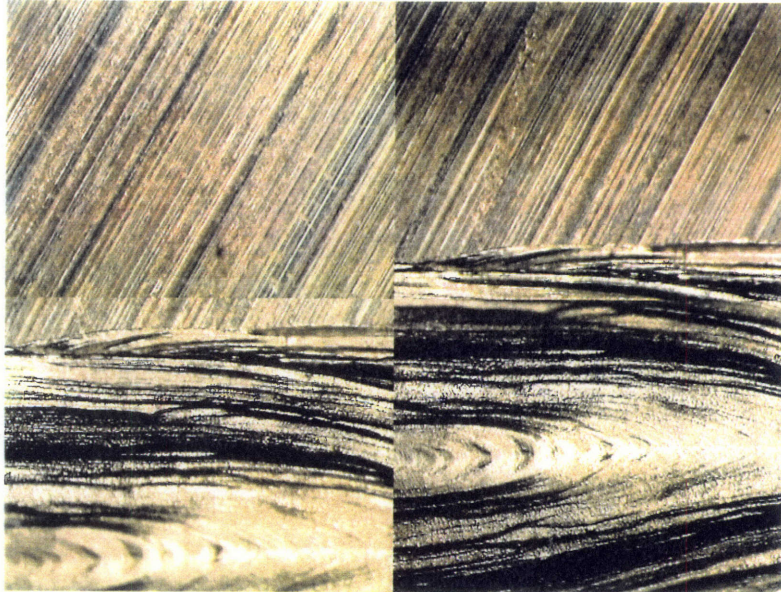
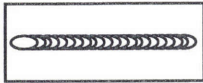
B.M. 450X	HAZ 450X
Edge 450X	Center 450X



**ME-2** (SS400-EBW2-4.5kW x 2000mm/min)

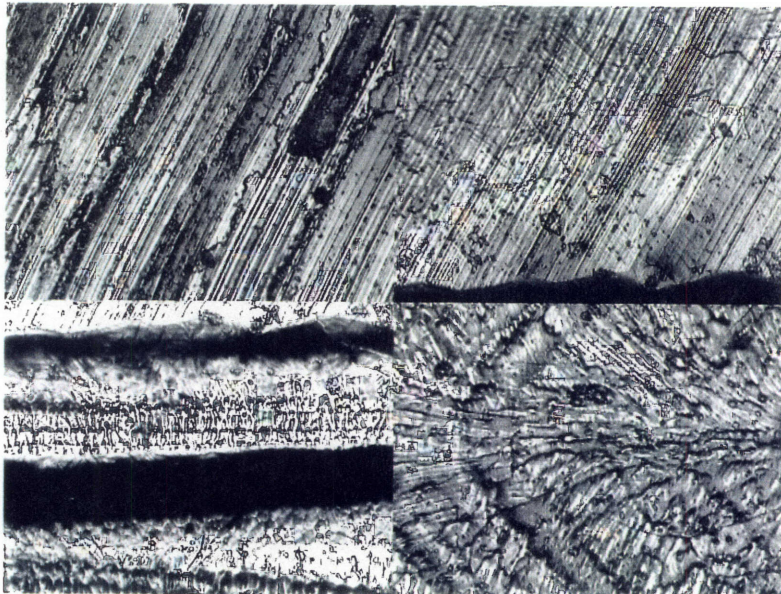
**PVIM**

B.M.	HAZ
42X	42X
Edge	Center
42X	42X



**CSLM**

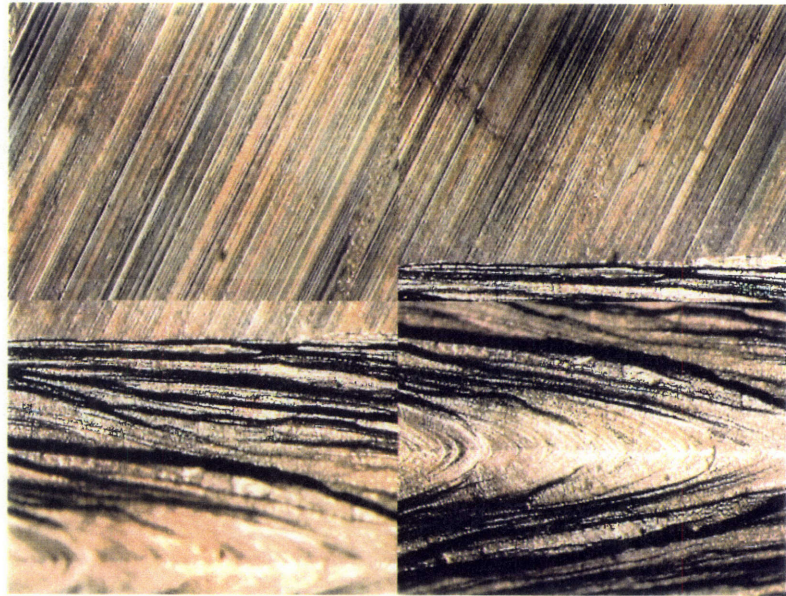
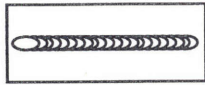
B.M.	HAZ
450X	450X
Edge	Center
450X	450X



**ME-3** (SS400-EBW2-6.0kW x 2000mm/min)

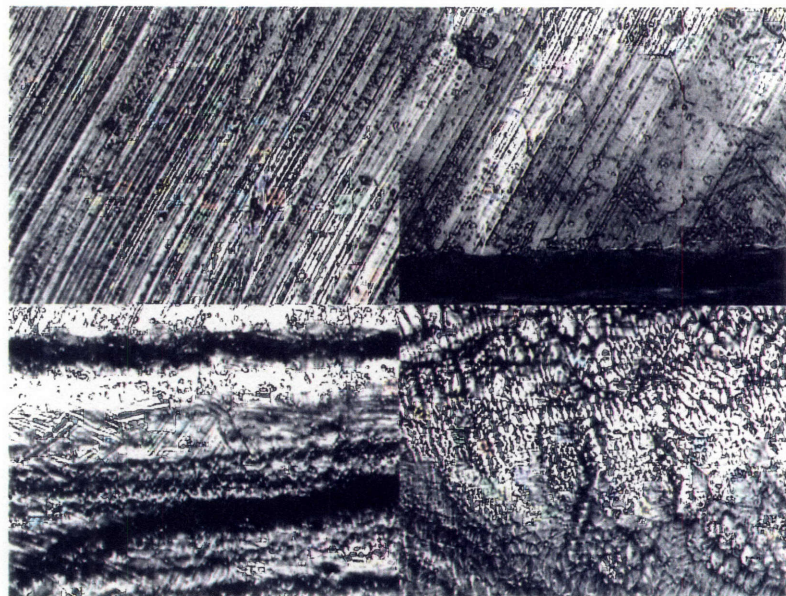
PVIM

B.M. 42X	HAZ 42X
Edge 42X	Center 42X



CSLM

B.M. 450X	HAZ 450X
Edge 450X	Center 450X



## 5.2 Stainless Steels

Stainless steel specimens were welded by three different welding processes, GTAW (with and without after shield), EBW, and LBW. All observation data is shown in Appendices. Pictures of surface features observed with a PVIM and a CSLM are also shown later in this chapter.

### **Specimens Welded by GTAW (ST-1, 2, and 3)**

#### Oxide formation

The HAZ of all the specimens was covered with several narrow bands of thick oxide layers. From the outside of the weld metals there were four bands: a 0.3 mm dark violet band, a 0.4 mm dark green and blue band, a 0.1 mm light gray band, and a 0.3 mm white green band on ST-1. On ST-2 there were six bands: a 1.0 mm brown band, a 0.5 mm dark violet band, a 0.8 mm blue band, a 0.3 mm green band: a 0.3 mm violet band, and a 0.3 mm black band. On ST-3 there were four bands: a 2.8 mm green & violet band, a 2.1 mm blue band, a 0.8 mm green band, and a 1.1 mm black band.

#### Micro discontinuities

For ST-1 many vertical discontinuities (V3.1), to 300  $\mu\text{m}$  in size, were observed in the HAZ. For ST-2 horizontal discontinuities (cracks) with the length of 20 ~ 70  $\mu\text{m}$  were observed as well as V3.1. The weld metals of all specimens were covered with ripples. No grains were found.

## **Specimens Welded by LBW without After Shield (SL1-1, 2, and 3)**

### Oxide formation

The surfaces of all the specimens were covered with very thick oxides. The thickness of the layers was increased as the heat input increased.

### Micro discontinuities

The thick oxides prevented us from observing the surface features such as discontinuities or grains.

## **Specimens Welded by LBW with After Shield (SL2-1, 2, and 3)**

### Oxide formation

The surfaces of all the weld metals were entirely covered with a brown layer of oxides. The thickness of the layer increased as the heat input increased. There was a black layer of oxide observed along the ripples. This black layer made observation of the edge and SL2-2 and SL2-3 difficult. The HAZ also was covered with a thick black layer which made observation impossible.

### Micro discontinuities

The HAZ was impossible to be observed due to thick oxides. The appearance of the outside of the HAZ was almost the same as the base metal.

Vertical discontinuities going in all directions were found at the edge of the weld metals. Grains with 3  $\mu\text{m}$  for SL2-1 and 10  $\mu\text{m}$  for SL2-2 in diameter were observed. No grains were found on SL2-3.

Many of the vertical discontinuities having the transverse direction were also found to be horizontal discontinuities (H2) with the length up to 300  $\mu\text{m}$ . Most of them started from the fusion line. Many horizontal discontinuities were observed for SL2-2 in the transverse direction with the length up to 800  $\mu\text{m}$ .

Subgrains were observed at the center of the weld metal. They were round or elongated in the transverse direction with the size of 3  $\mu\text{m}$  for the round shape and 3 x 6 ~ 15  $\mu\text{m}$  for the elongated.

### **Specimens Welded by EBW (SE-1, 2, and 3)**

#### Oxide formation

The surfaces of all the weld metals were entirely covered with a thin brown layer of oxides. The thickness of the layer increased as the heat input increased. There was a thick dark brown layer of oxide observed along the ripples. This black layer made observation of the edge and SL2-2 and SL2-3 difficult. The HAZ was also covered with a similar brown layer of oxides.

#### Micro discontinuities

The HAZ had almost the same kind of discontinuities as the unaffected base metal. However, some discontinuities continuous from the weld metal. Grain boundaries with 10  $\mu\text{m}$  diameter were observed on SE-3. The area of the weld edge had many vertical discontinuities (V3.2), most of

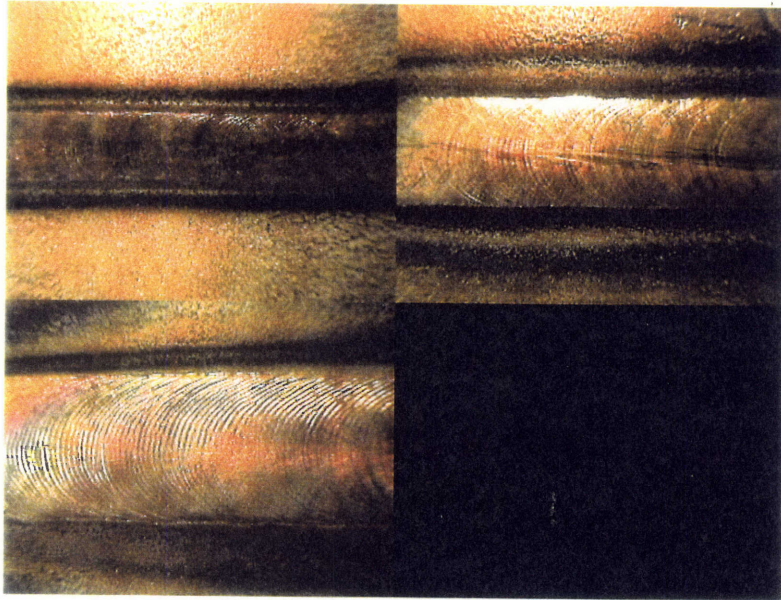
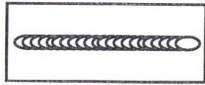
which were perpendicular to the welding direction. None of them had cracks.

In the weld metals we found other types of structures which had grain-like shapes, but it was not clear if they were grains or subgrains. At the edge those shapes were round, while at the center they were round or elongated.

# Surface Appearance of Welded Stainless Steels

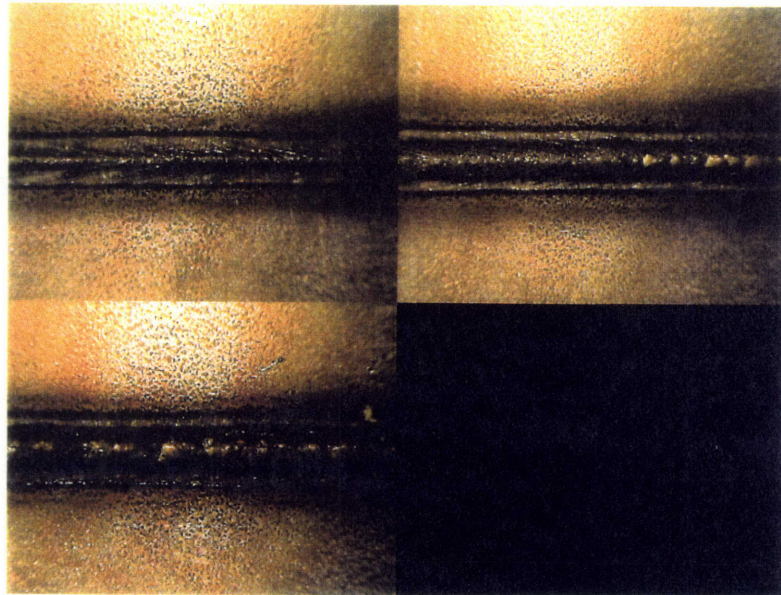
PVIM

ST-1 42X	ST-2 42X
ST-3 42X	



PVIM

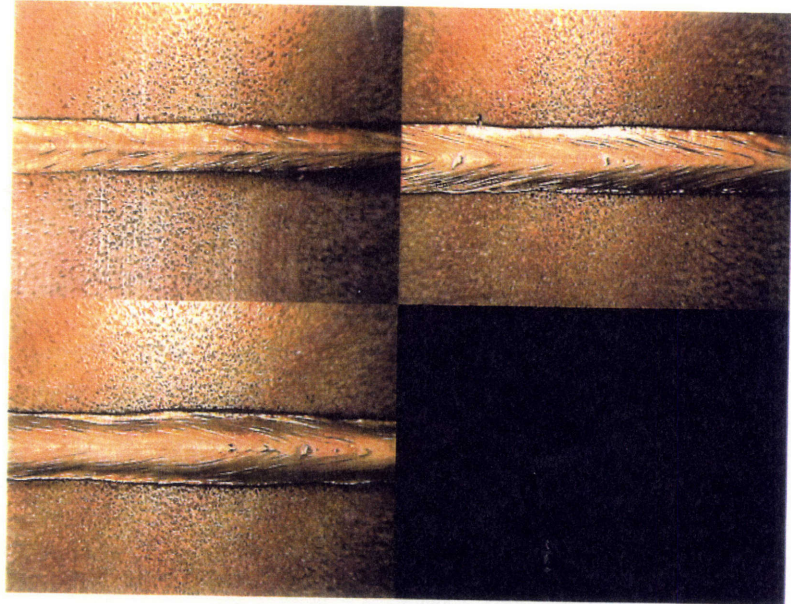
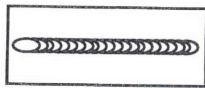
SL1-1 42X	SL1-2 42X
SL1-3 42X	





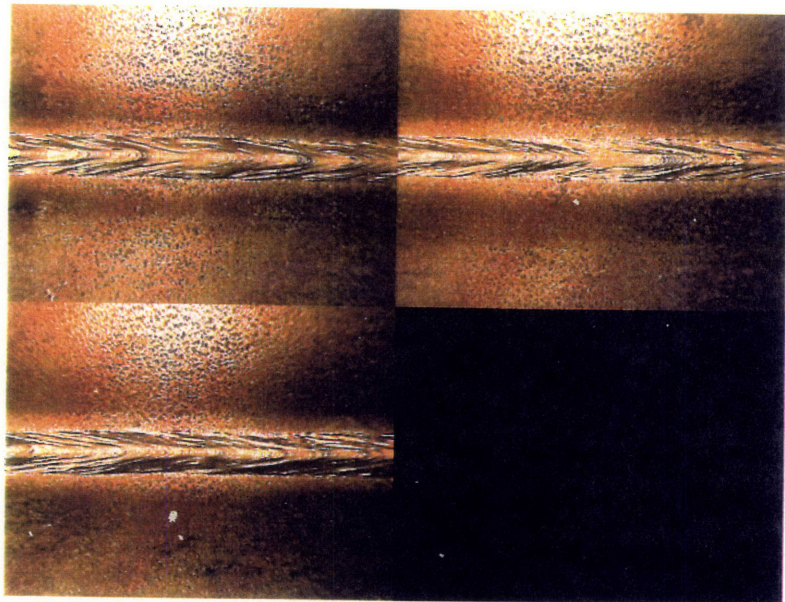
PVIM

SL2-1 42X	SL2-2 42X
SL2-3 42X	



PVIM

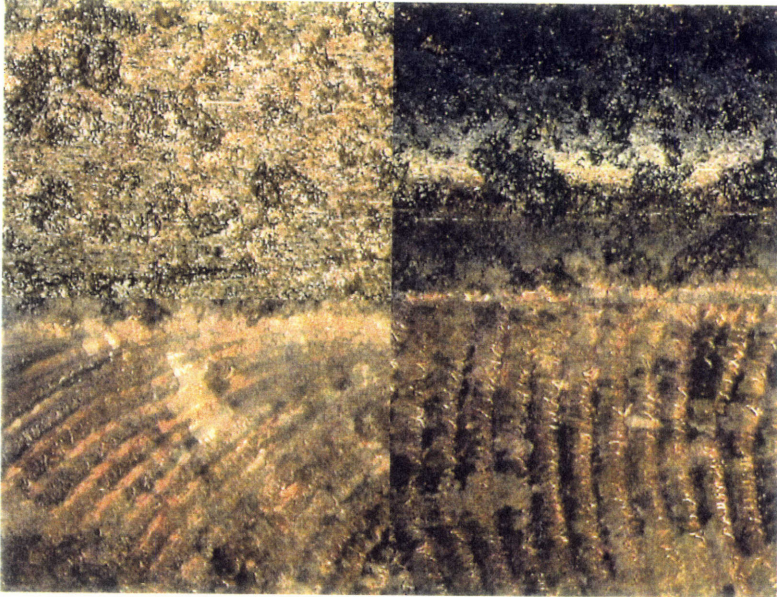
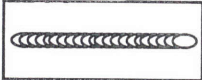
SE-1 42X	SE-2 42X
SE-3 42X	



**ST-1** (SUS304-GTAW-50A x 9.8V x 96mm/min)

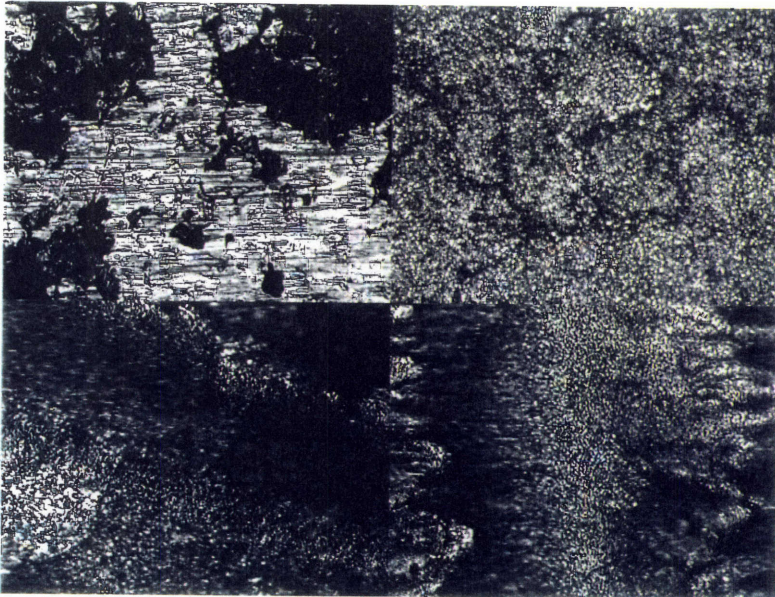
**PVIM**

B.M. 42X	HAZ 42X
Edge 42X	Center 42X



**CSLM**

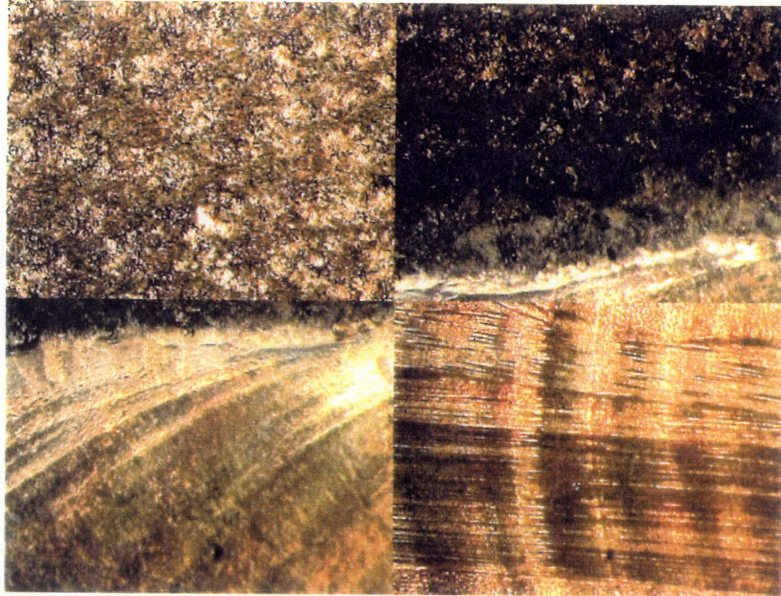
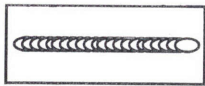
B.M. 225X	HAZ 450X
Edge 450X	Center 450X



**ST-2** (SUS304-GTAW-79A x 10.6V x 96mm/min)

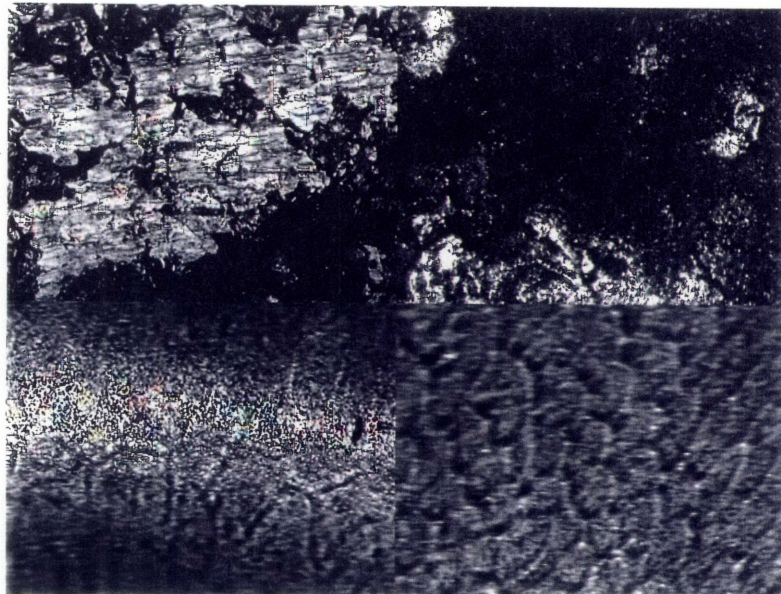
**PVIM**

B.M. 42X	HAZ 42X
Edge 42X	Center 42X



**CSLM**

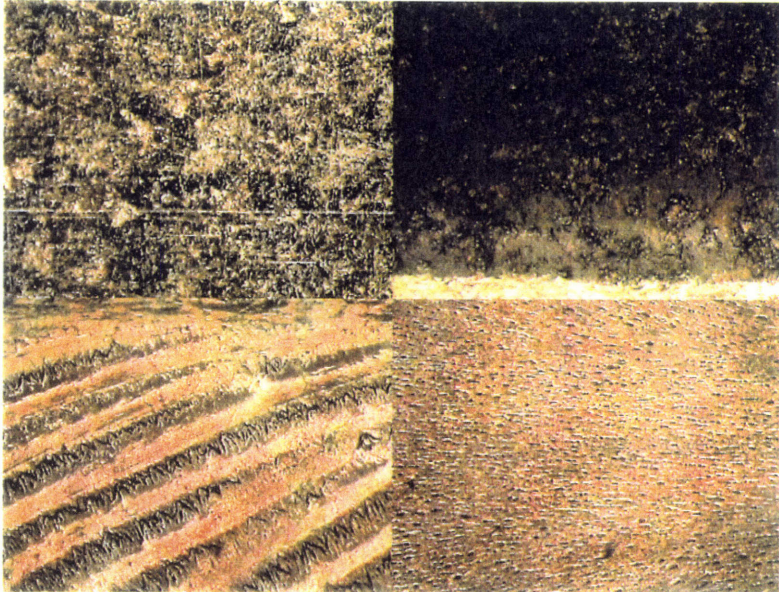
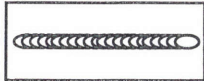
B.M. 225X	HAZ 450X
Edge 450X	Center 450X



**ST-3** (SUS304-GTAW-112A x 10.8V x 96mm/min)

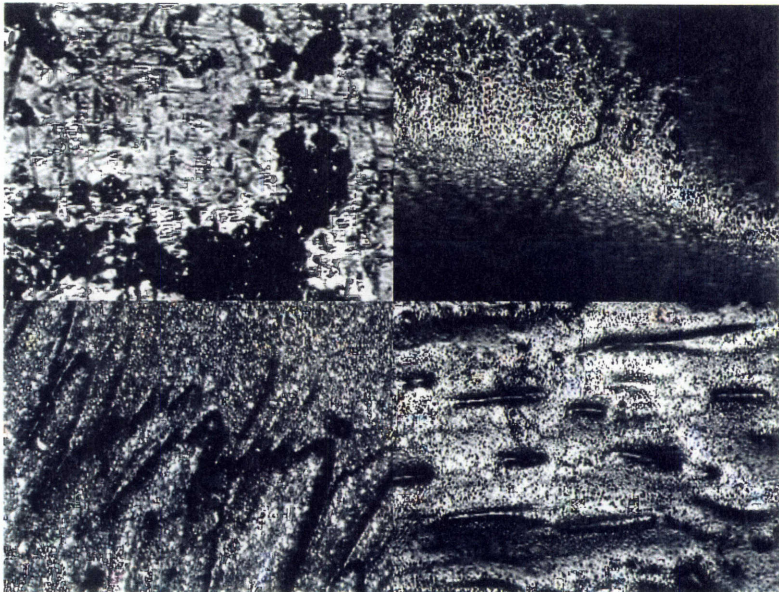
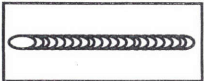
**PVIM**

B.M. 42X	HAZ 42X
Edge 42X	Center 42X



**CSLM**

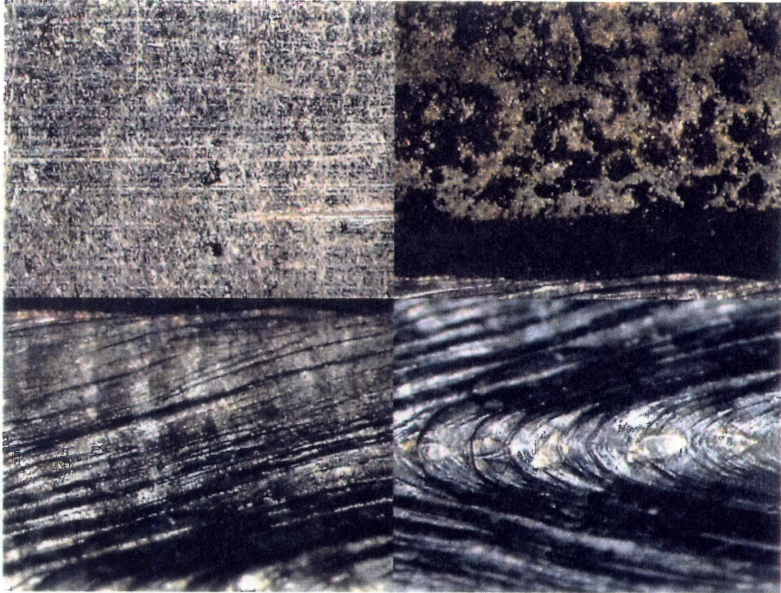
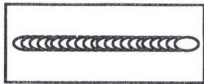
B.M. 225X	HAZ 450X
Edge 450X	Center 450X



**SL1-1** (SUS304-LBW1-2.0kW x 2000mm/min)

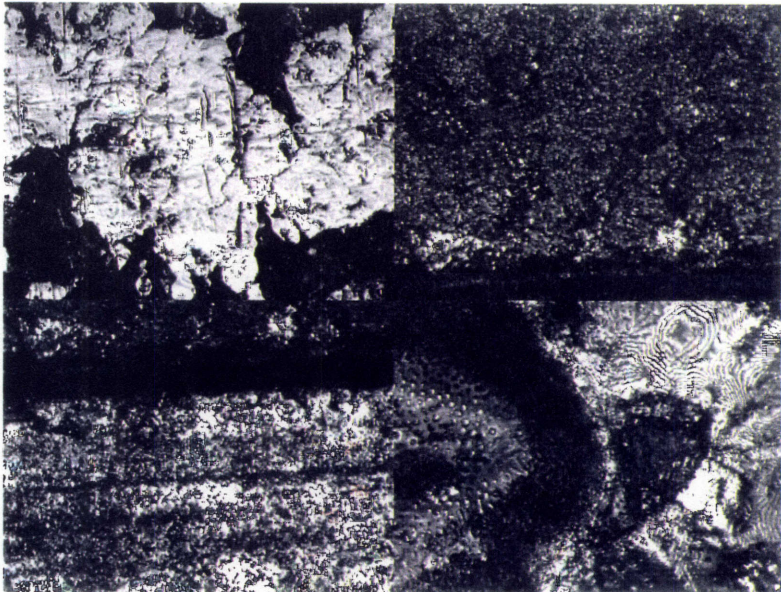
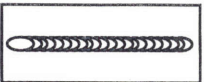
**PVIM**

B.M. 42X	HAZ 42X
Edge 42X	Center 42X



**CSLM**

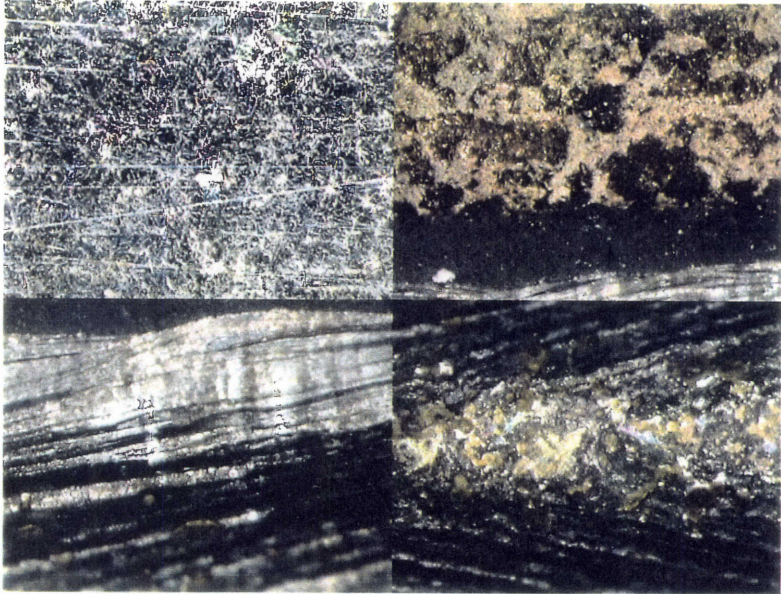
B.M. 450X	HAZ 450X
Edge 450X	Center 450X



**SL1-2** (SUS304-LBW1-3.0kW x 2000mm/min)

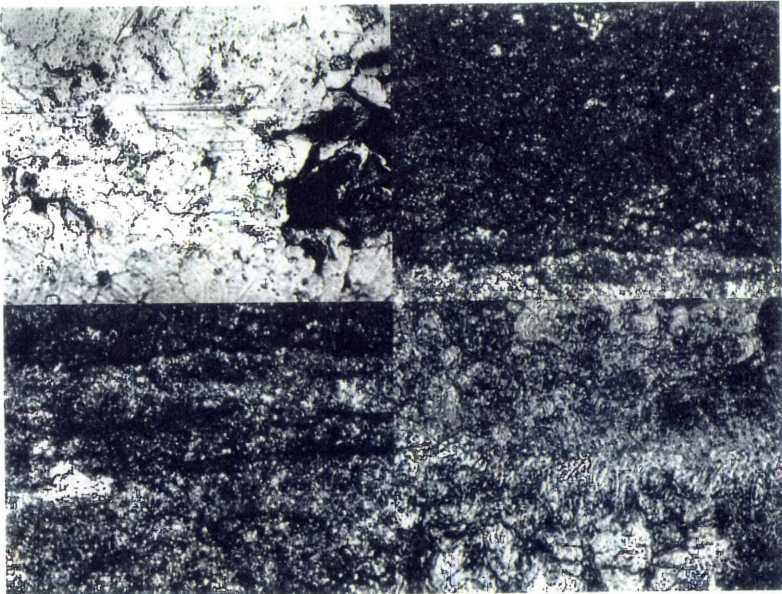
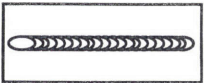
**PVIM**

B.M.	HAZ
42X	42X
Edge	Center
42X	42X



**CSLM**

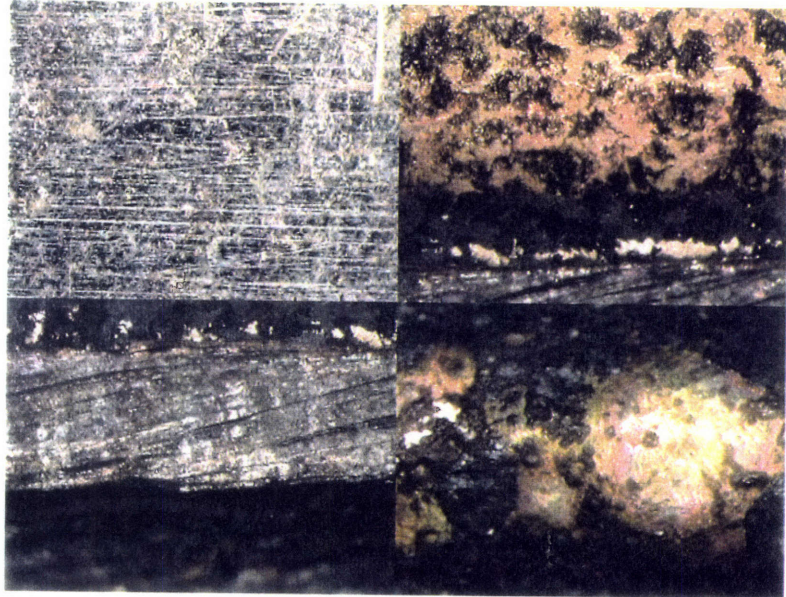
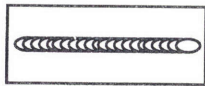
B.M.	HAZ
450X	450X
Edge	Center
450X	450X



**SL1-3** (SUS304-LBW1-4.0kW x 2000mm/min)

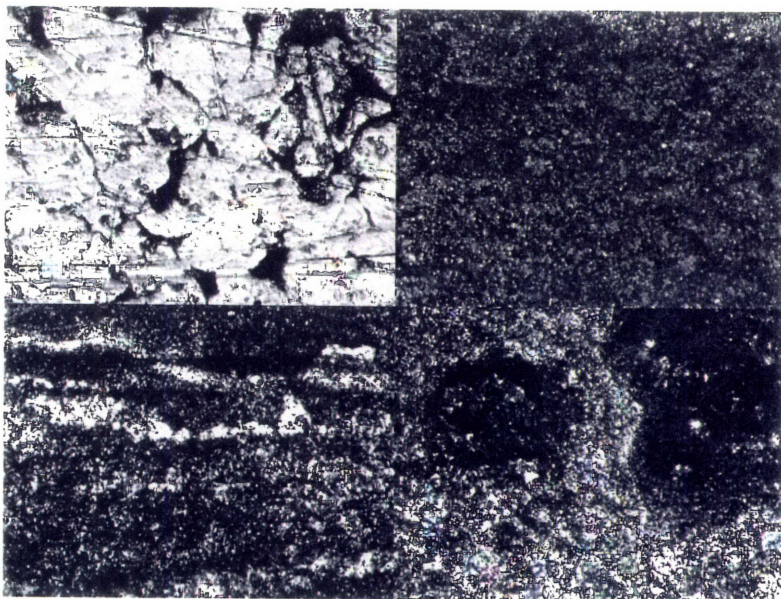
**PVIM**

B.M. 42X	HAZ 42X
Edge 42X	Center 42X



**CSLM**

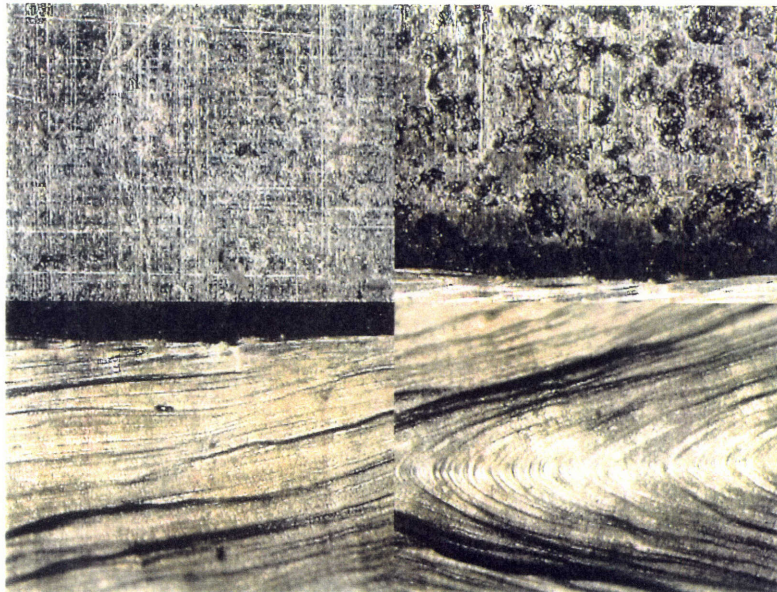
B.M. 450X	HAZ 450X
Edge 450X	Center 450X



**SL2-1** (SUS304-LBW2-2.0kW x 2000mm/min)

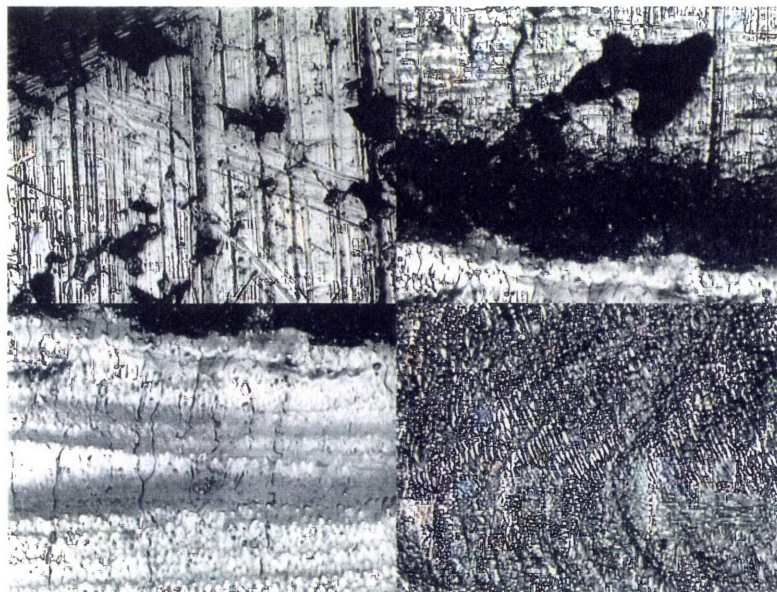
**PVIM**

B.M. 42X	HAZ 42X
Edge 42X	Center 42X



**CSLM**

B.M. 450X	HAZ 450X
Edge 450X	Center 450X

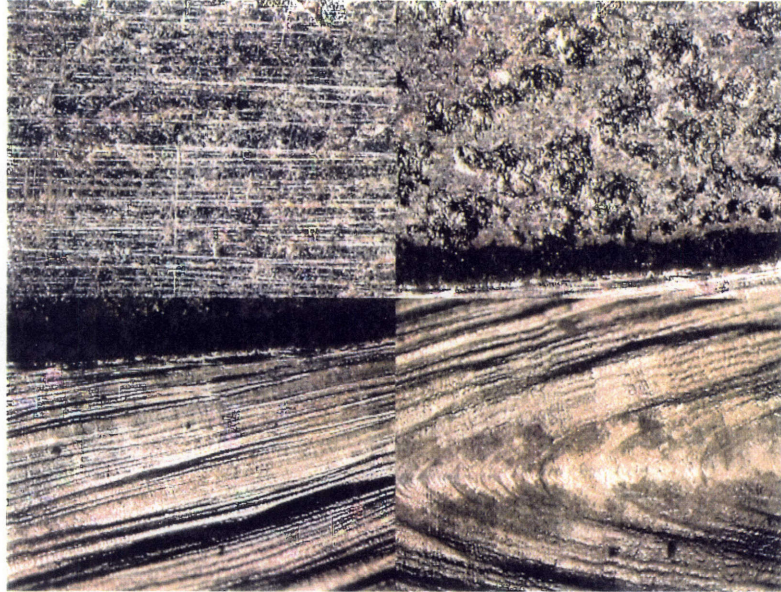
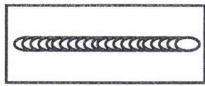




**SL2-2** (SUS304-LBW2-3.0kW x 2000mm/min)

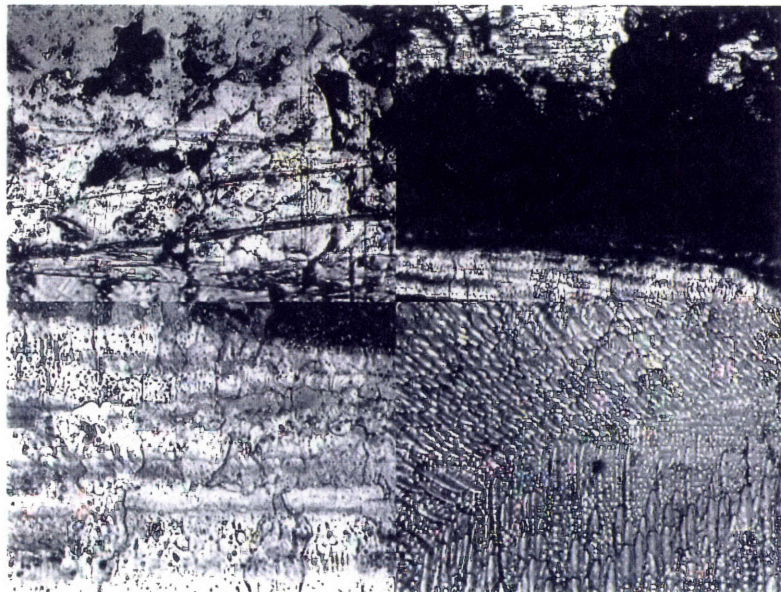
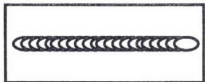
**PVIM**

B.M. 42X	HAZ 42X
Edge 42X	Center 42X



**CSLM**

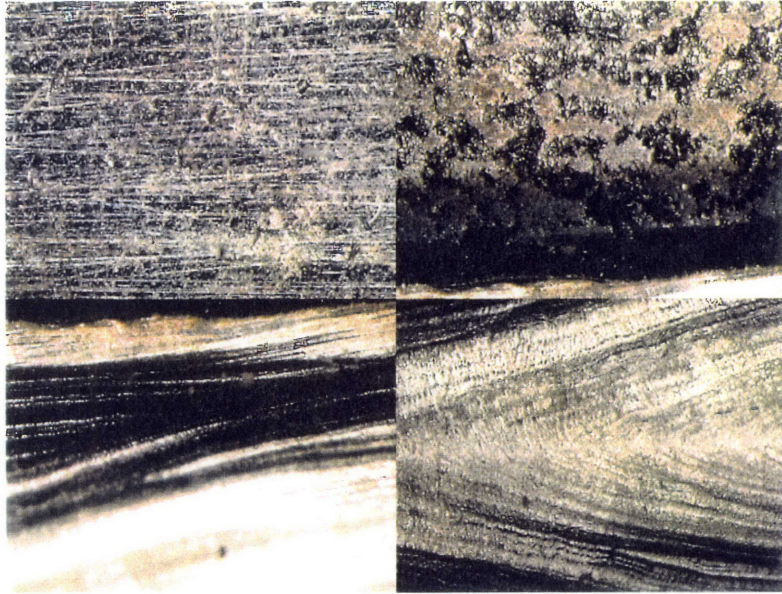
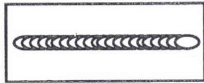
B.M. 450X	HAZ 225X
Edge 450X	Center 450X



**SL2-3** (SUS304-LBW2-4.0kW x 2000mm/min)

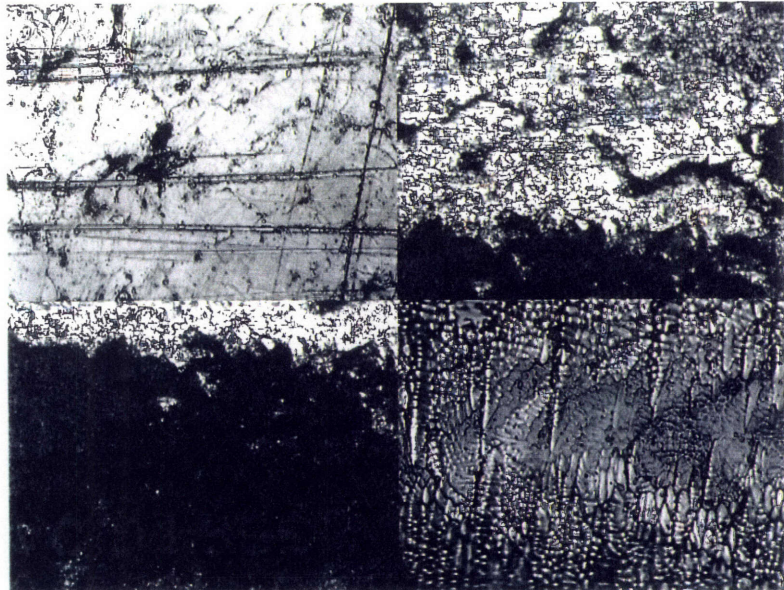
**PVIM**

B.M.	HAZ
42X	42X
Edge	Center
42X	42X



**CSLM**

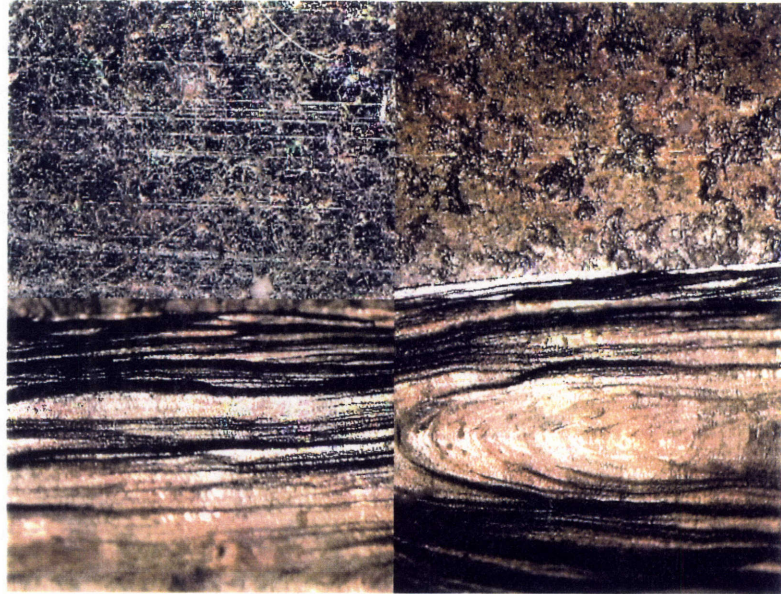
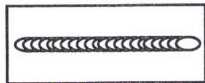
B.M.	HAZ
450X	225X
Edge	Center
450X	450X



**SE-1** (SUS304-EBW2-3.0kW x 2000mm/min)

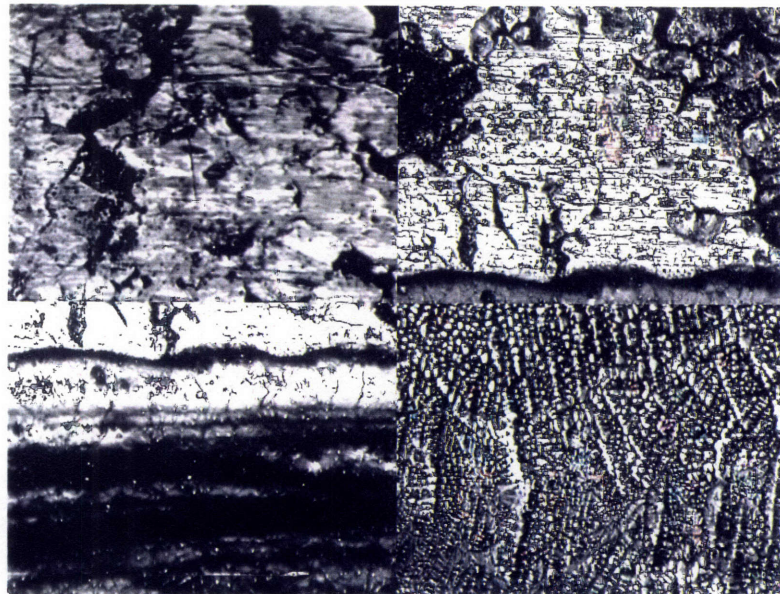
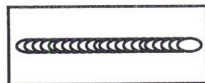
**PVIM**

B.M. 42X	HAZ 42X
Edge 42X	Center 42X



**CSLM**

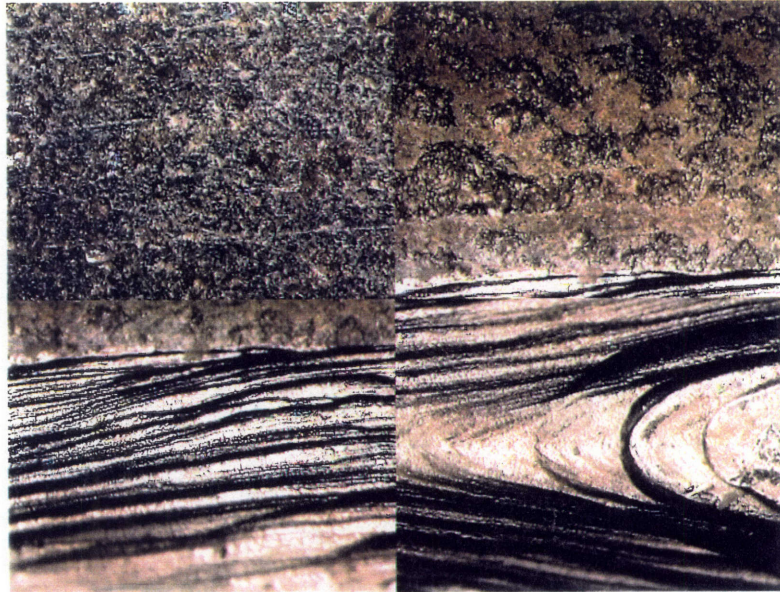
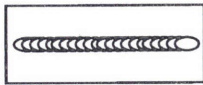
B.M. 450X	HAZ 450X
Edge 450X	Center 450X



**SE-2** (SUS304-EBW2-4.5kW x 2000mm/min)

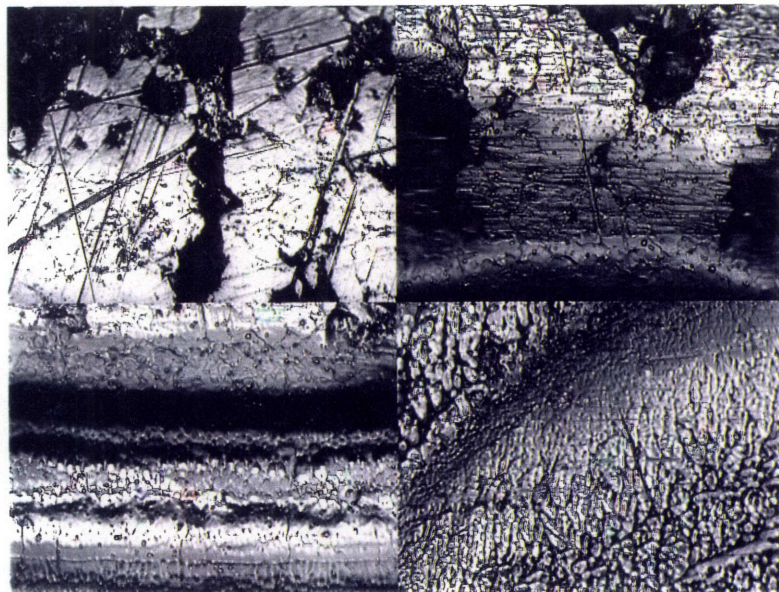
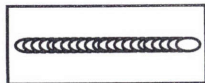
**PVIM**

B.M.	HAZ
42X	42X
Edge	Center
42X	42X



**CSLM**

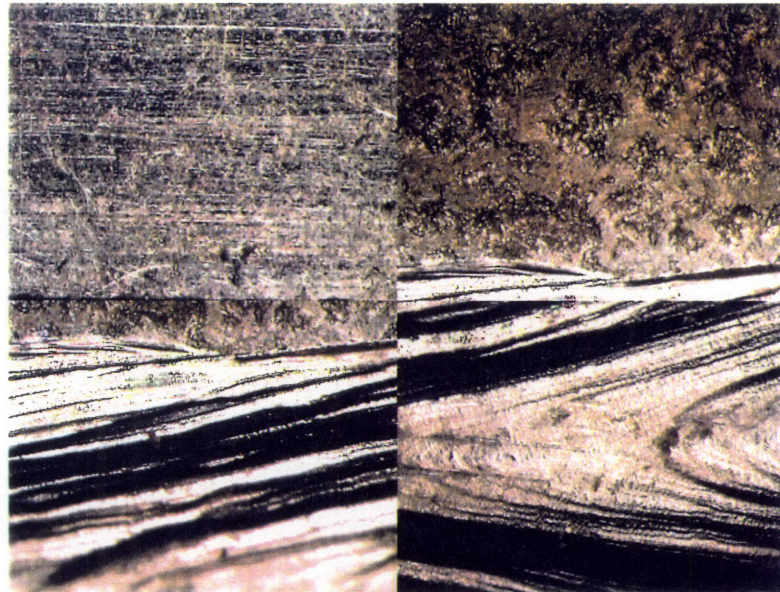
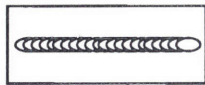
B.M.	HAZ
450X	450X
Edge	Center
450X	450X



**SE-3** (SUS304-EBW2-6.0kW x 2000mm/min)

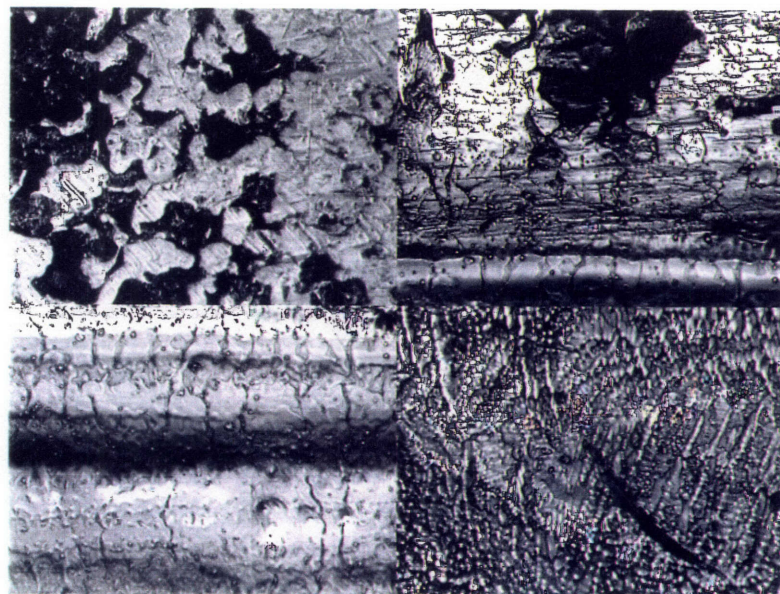
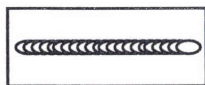
**PVIM**

B.M. 42X	HAZ 42X
Edge 42X	Center 42X



**CSLM**

B.M. 450X	HAZ 450X
Edge 450X	Center 450X



## 5.3 Aluminum Alloys

Aluminum alloy specimens were welded by three different welding processes, GTAW (with and without after shield), EBW, and LBW. AT-1N and AT-2N were polished prior to welding. All observation data is shown in the Appendices. Pictures of surface features observed with a PVIM and a CSLM are also shown later in this part. Consequently, the surface of aluminum alloys are the most difficult to observe with these microscopes.

### **Specimens Welded by GTAW (AT-1N, 2N, 2, and 3)**

#### Oxide formation

The surfaces of all the specimens were covered with very thick oxides. Most oxides had more mountain-like shapes. The thickness of the layers was increased as the heat input increased. The oxides were thin light brown or thick black with many metallic spots. Although the entire weld metals were covered with thick oxides, some parts of the oxides were peeled off, thus making it observable through those breaks.

#### Micro discontinuities

The appearance of the HAZ was similar to the base metals. However, the weld metals were not observable due to thick oxides.

### **Specimens Welded by LBW without After Shield (AL1-1, 2, and 3)**

### Oxide formation

All the specimens had the surface of the weld metals covered with black thick layers. The thickness of the layers was increased as the heat input increased. Although entire weld metals were covered with thick oxides, some parts of oxides were peeled off, thus observable through those breaks.

### Micro discontinuities

Due to thick oxides, we were not able to observe the HAZ. Only through the peeled off areas, could we observe some structures which looked like grains with the sizes 2  $\mu\text{m}$  for AL1-1 and AL1-2, and 2 ~ 4  $\mu\text{m}$  for AL1-3.

## **Specimens Welded by LBW with After Shield (AL2-1, 2, and 3)**

### Oxide formation

The HAZ of all the specimens was the same as the unaffected base metals except AL2-2 which has a very thin oxide layer on it.

At the edge of all the specimens and along the fusion lines, there were thick black bands (0.2 mm wide) of oxide layers. For AL2-1 and AL2-2 the thick black layer covered the weld ripples, while for AL2-3 the entire surface of weld metal was covered with very thick black layers of oxides.

All specimens had many spots with different colors. For AL2-1 and AL2-2 they were blue or orange and for AL2-3 they were very thick layers of green or orange.

### Micro discontinuities

Due to thick oxides, we were not able to observe any surface discontinuity in the rough surface of the weld metals.

### **Specimens Welded by EBW (AE-1, 2, and 3)**

#### Oxide formation

The HAZ of all the specimens was covered with black thick oxide layers. All the surface of the weld metals was also covered with thick oxide layers with the color brown or gray.

#### Micro discontinuities

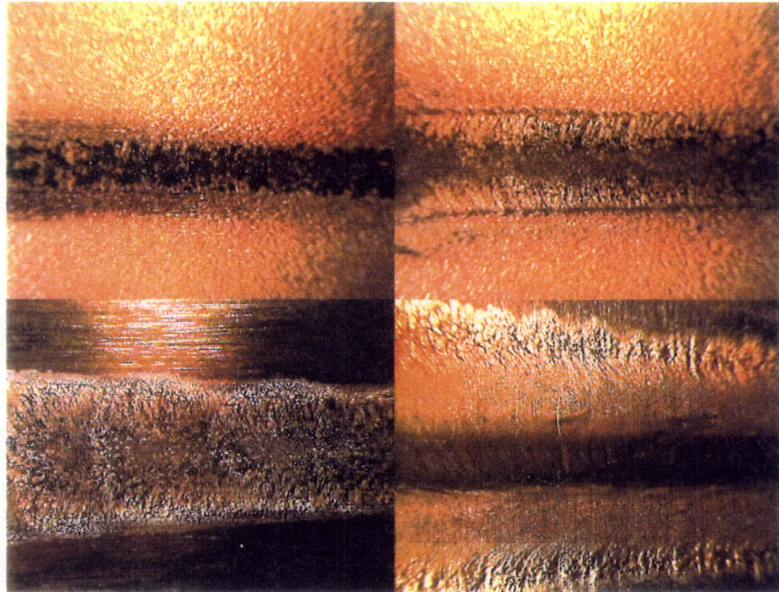
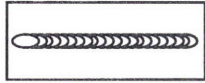
Due to heavy oxidation, we were not able to observe any surface discontinuity in the rough surface of the weld metals. However, grain-like structures were observed to cover all the surface. Their size was 2 ~ 3  $\mu\text{m}$ . We could not determine whether they were grains of the alloys or oxides.



# Surface Appearance of Welded Aluminum Alloys

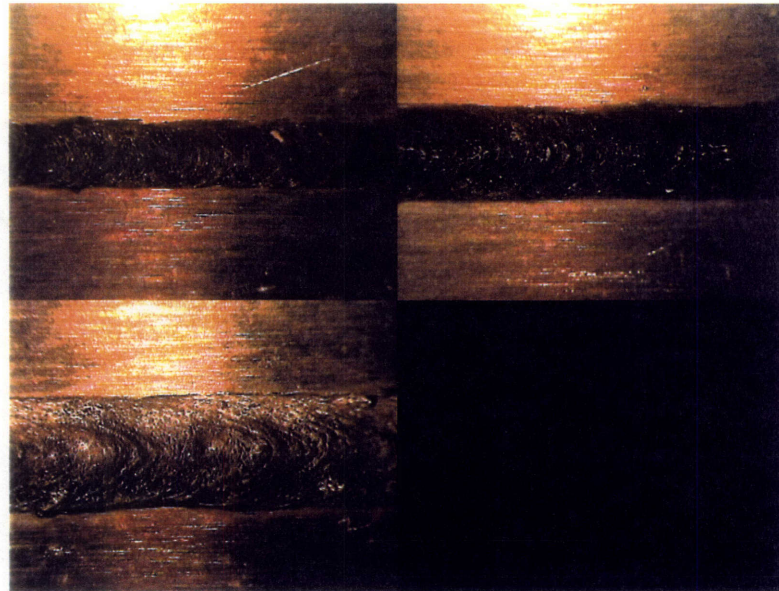
## PVIM

AT-1N 42X	AT-2N 42X
AT-2 42X	AT-3 42X



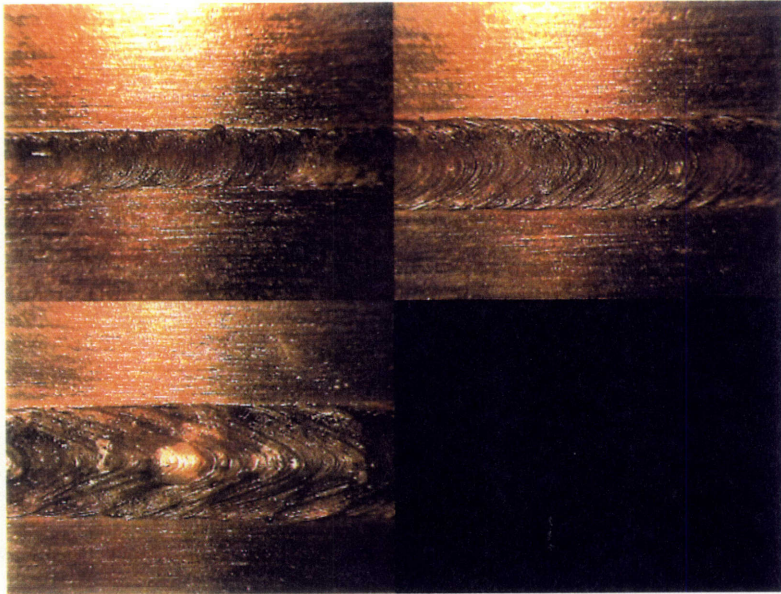
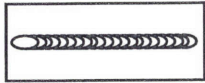
## PVIM

AL1-1 42X	AL1-2 42X
AL1-3 42X	



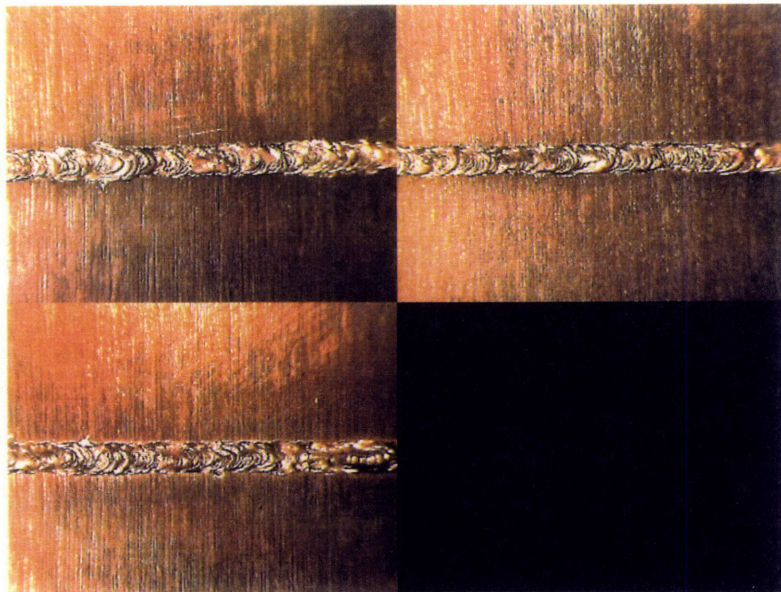
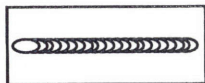
### PVIM

AL2-1 42X	AL2-2 42X
AL2-3 42X	



### PVIM

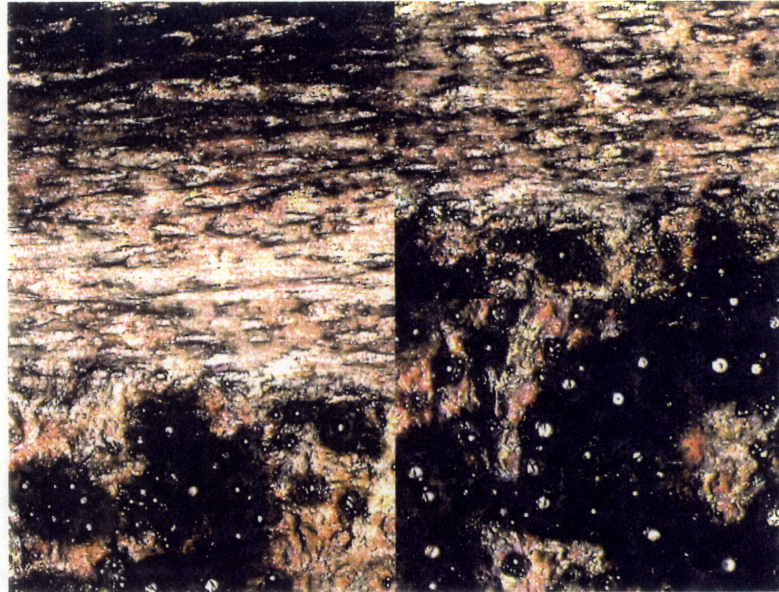
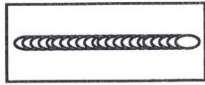
AE-1 42X	AE-2 42X
AE-3 42X	



**AT-1N** (A5083-GTAW-52A x 11.5V x 96mm/min)

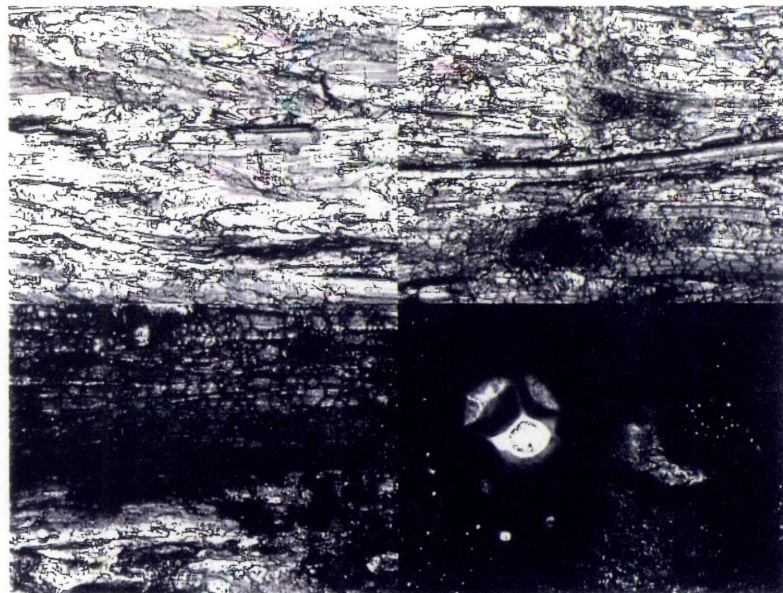
**PVIM**

B.M. 42X	HAZ 42X
Edge 42X	Center 42X



**CSLM**

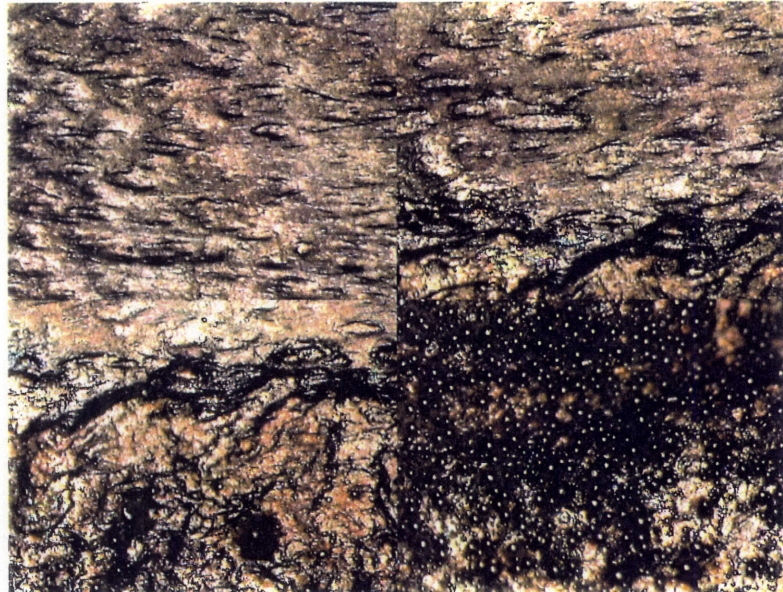
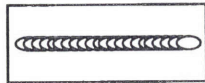
B.M. 450X	HAZ 450X
Edge 450X	Center 450X



**AT-2N** (A5083-GTAW-75A x 12.2V x 96mm/min)

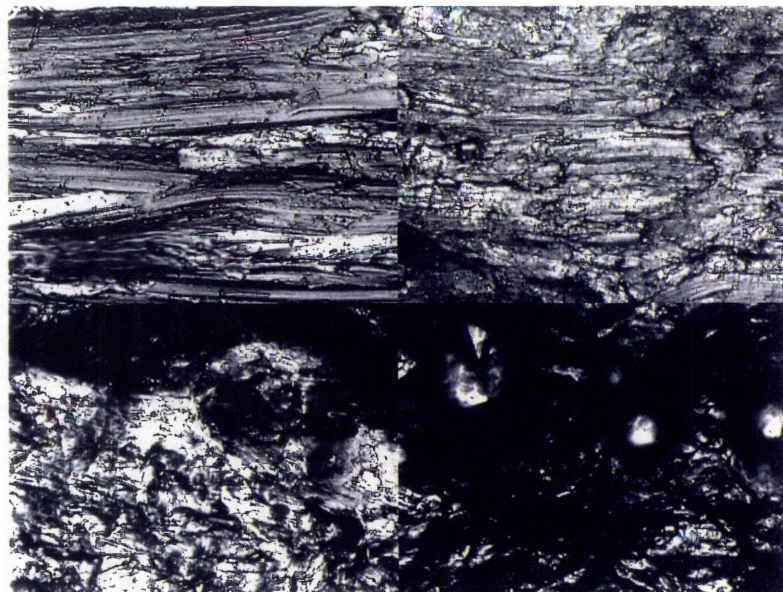
**PVIM**

B.M.	HAZ
42X	42X
Edge	Center
42X	42X



**CSLM**

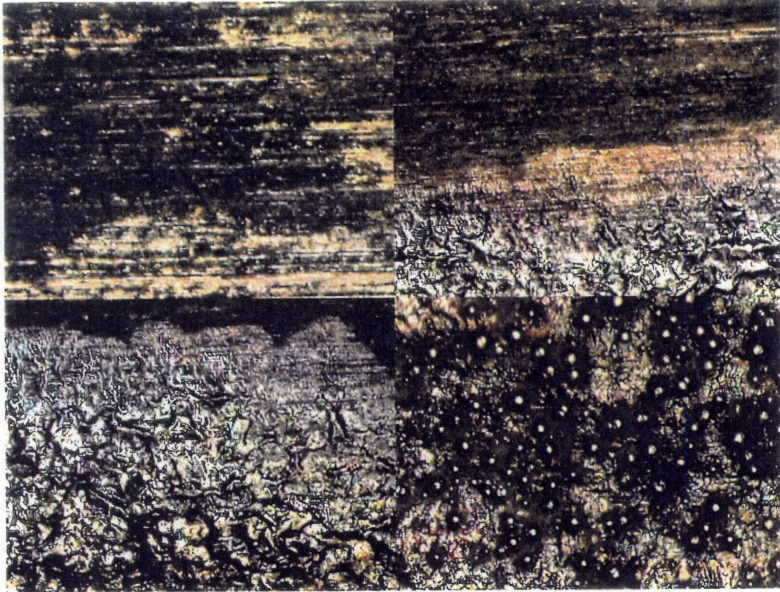
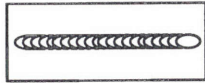
B.M.	HAZ
450X	450X
Edge	Center
450X	450X



**AT-2** (A5083-GTAW-75A x 12.2V x 96mm/min)

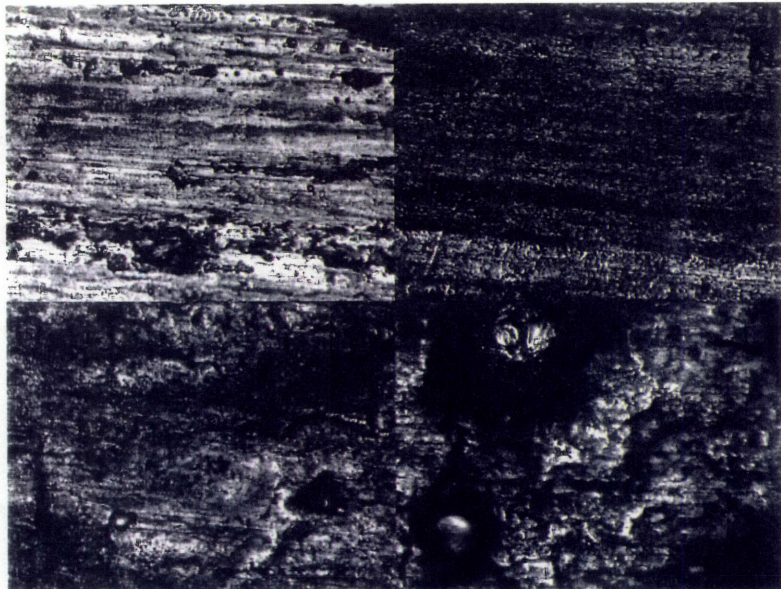
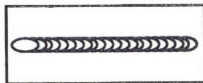
**PVIM**

B.M. 42X	HAZ 42X
Edge 42X	Center 42X



**CSLM**

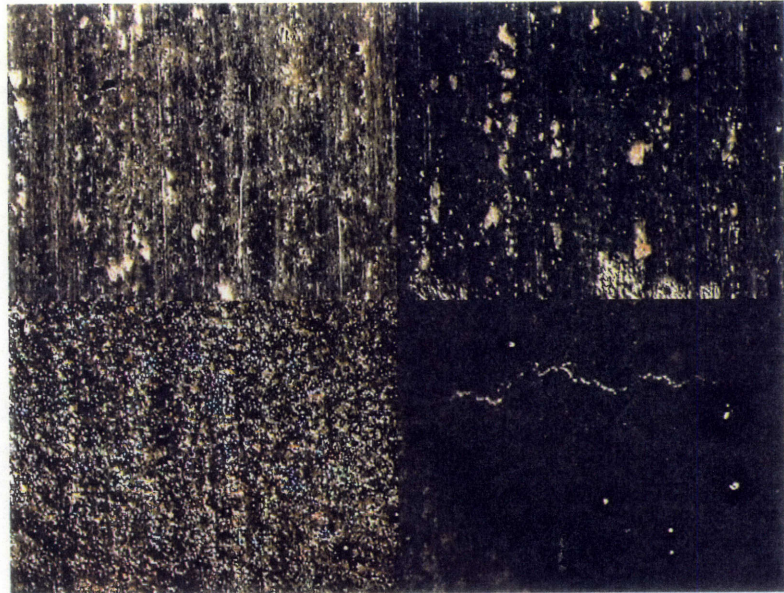
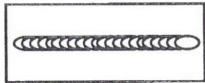
B.M. 450X	HAZ 450X
Edge 450X	Center 450X



**AT-3** (A5083-GTAW-112A x 12.1V x 96mm/min)

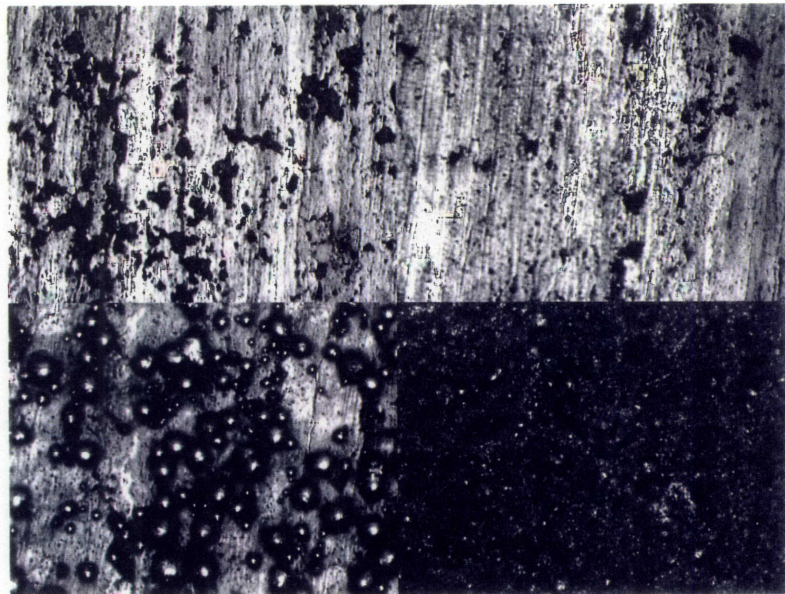
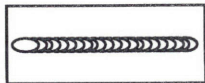
**PVIM**

B.M. 42X	HAZ 42X
Edge 42X	Center 42X



**CSLM**

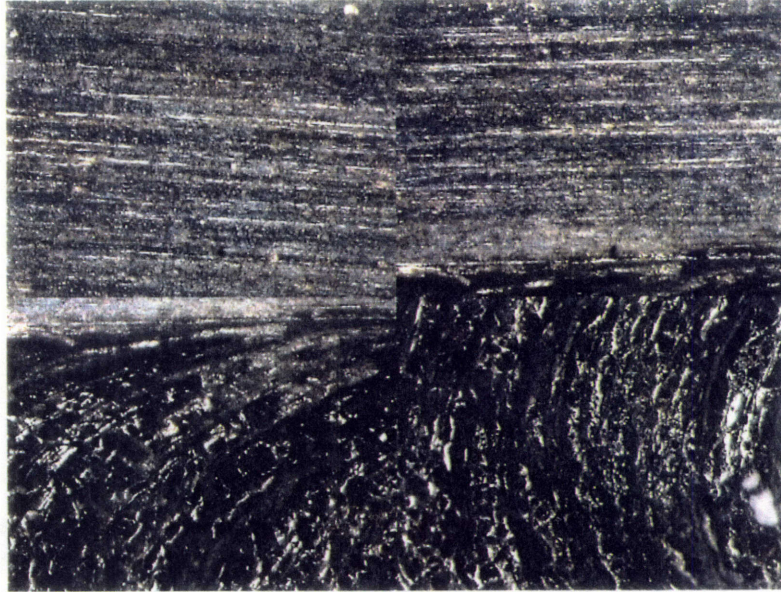
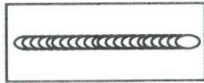
B.M. 450X	HAZ 450X
Edge 450X	Center 450X



**AL1-1** (A5083-LBW1-2.0kW x 2000mm/min)

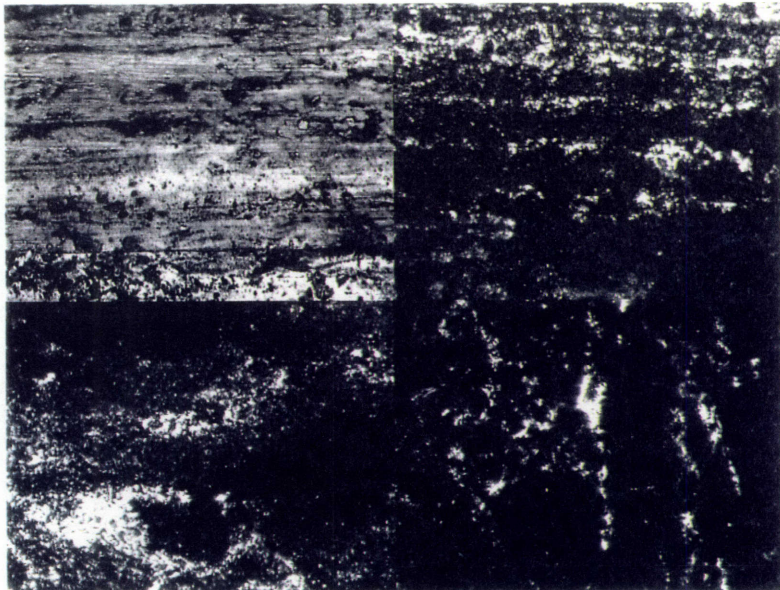
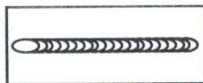
**PVIM**

B.M. 42X	HAZ 42X
Edge 42X	Center 42X



**CSLM**

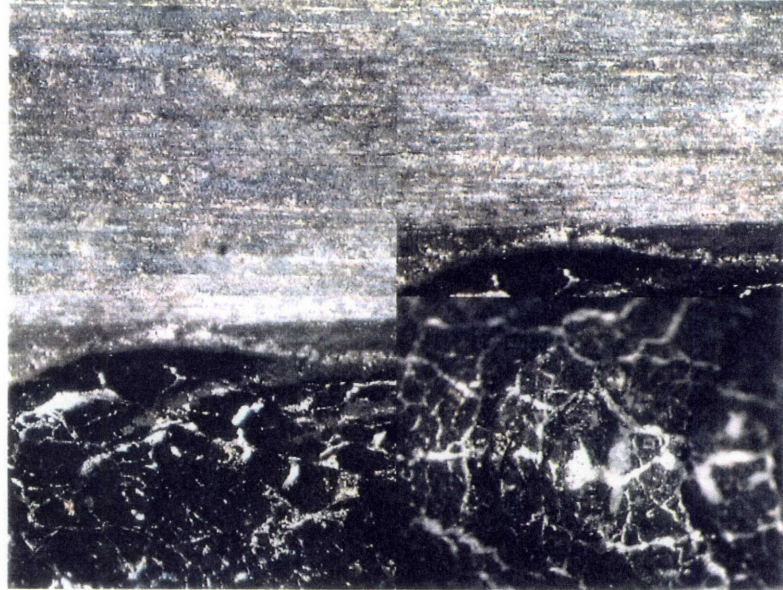
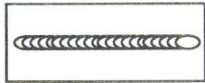
B.M. 450X	HAZ 450X
Edge 450X	Center 450X



**ALI-2** (A5083-LBW1-3.0kW x 2000mm/min)

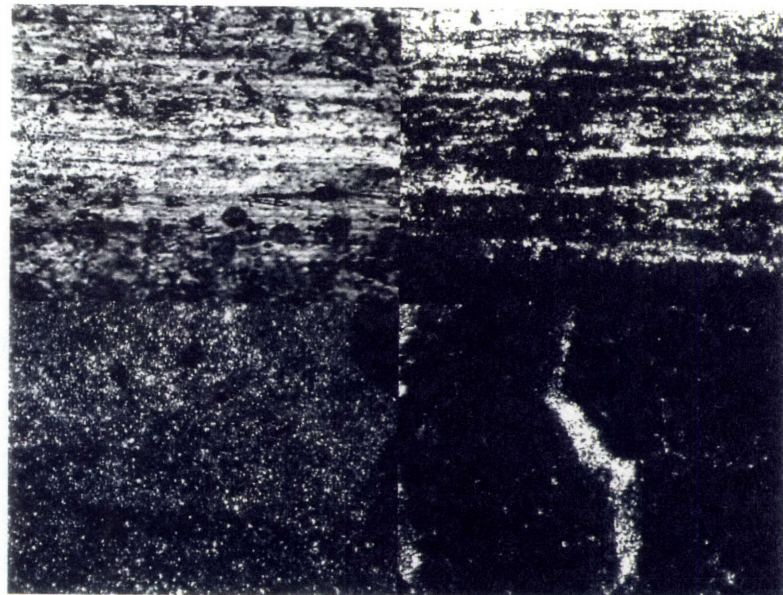
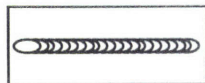
**PVIM**

B.M.	HAZ
42X	42X
Edge	Center
42X	42X



**CSLM**

B.M.	HAZ
450X	450X
Edge	Center
450X	450X

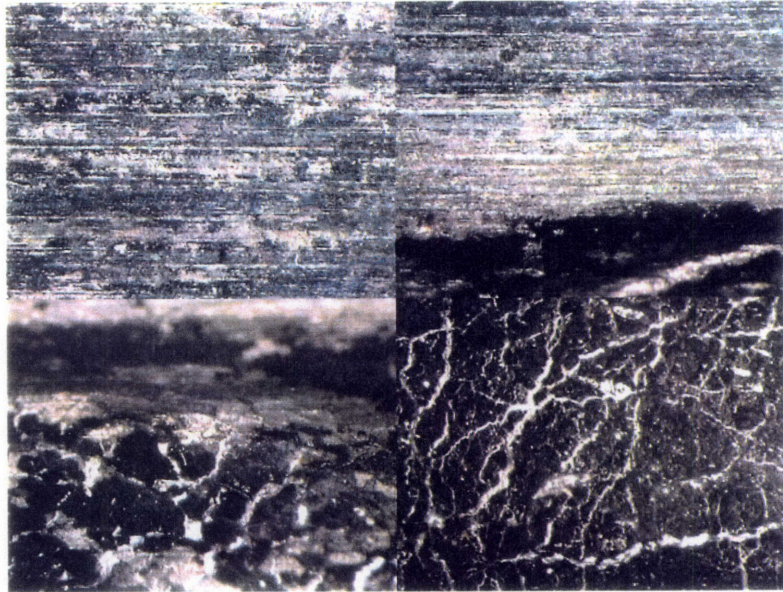
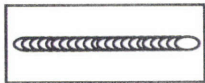




**AL1-3** (A5083-LBW1-4.0kW x 2000mm/min)

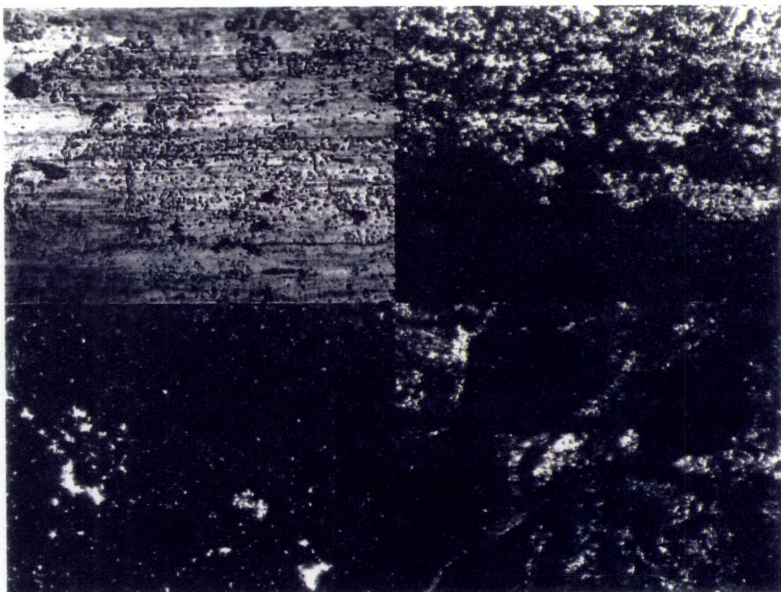
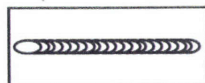
**PVIM**

B.M. 42X	HAZ 42X
Edge 42X	Center 42X



**CSLM**

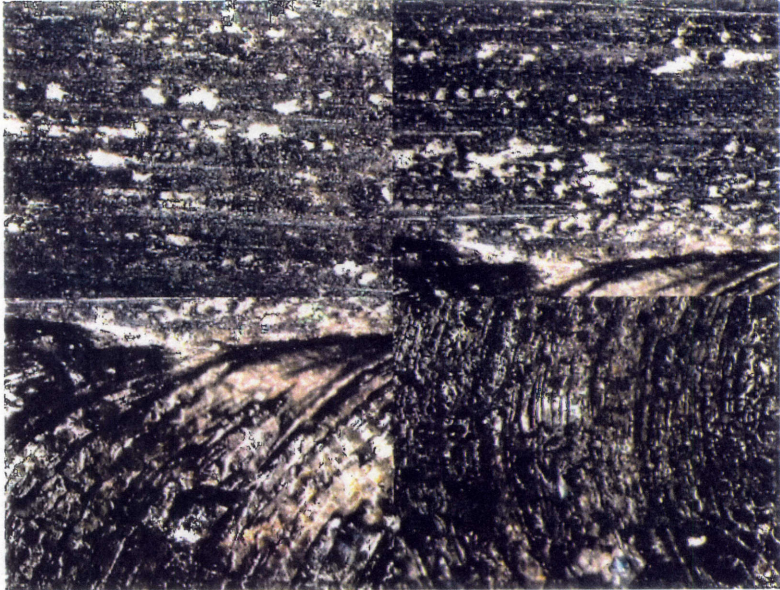
B.M. 450X	HAZ 450X
Edge 450X	Center 450X



**AL2-1** (A5083-LBW2-2.0kW x 2000mm/min)

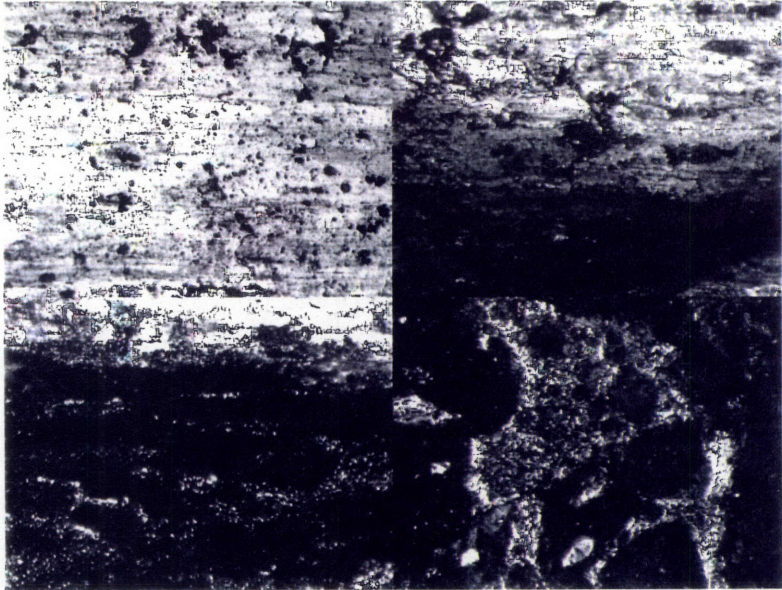
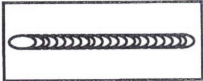
**PVIM**

B.M. 42X	HAZ 42X
Edge 42X	Center 42X



**CSLM**

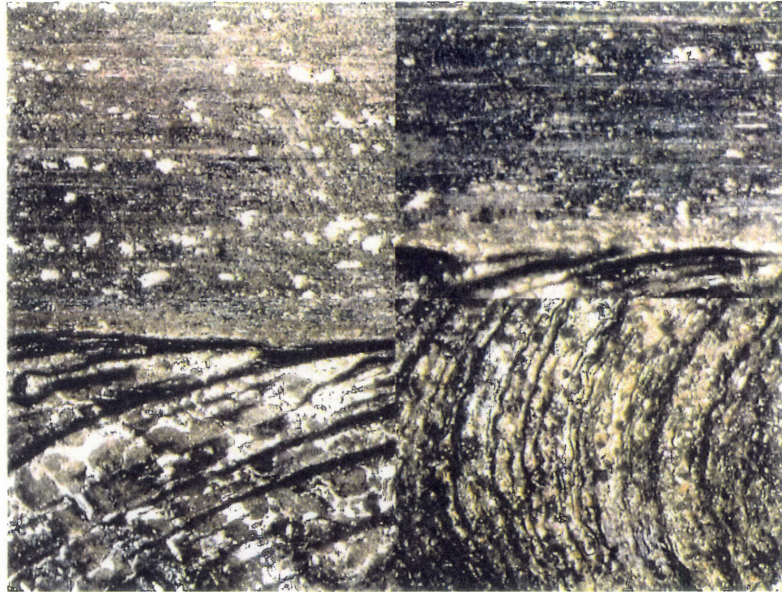
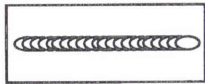
B.M. 450X	HAZ 450X
Edge 450X	Center 450X



**AL2-2** (A5083-LBW2-3.0kW x 2000mm/min)

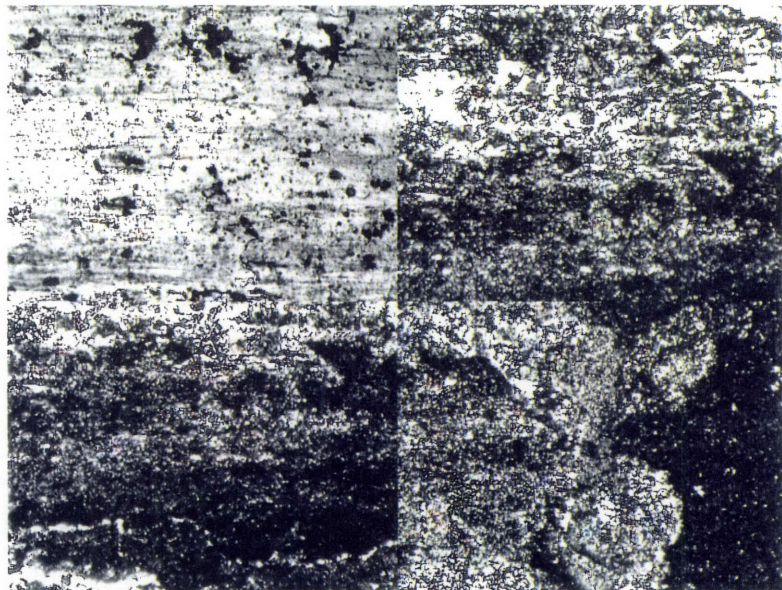
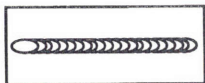
**PVIM**

B.M. 42X	HAZ 42X
Edge 42X	Center 42X



**CSLM**

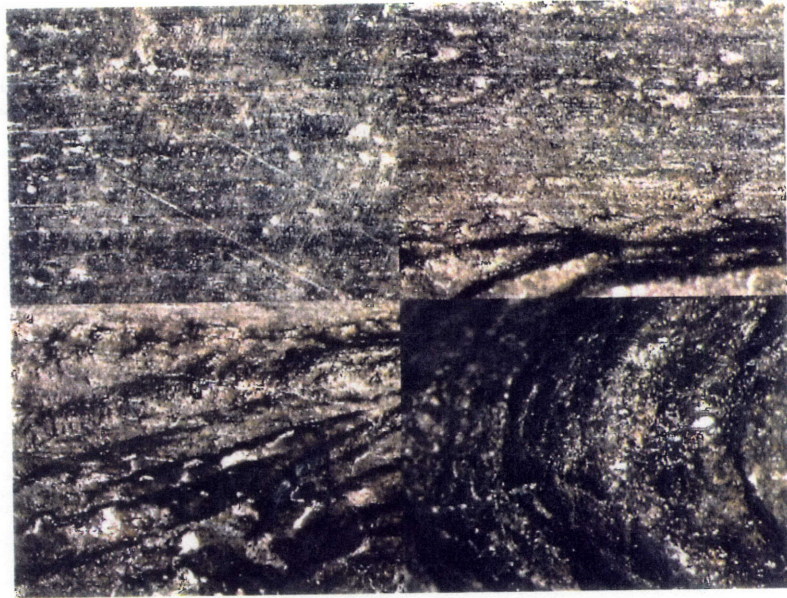
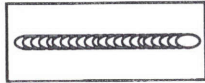
B.M. 450X	HAZ 450X
Edge 450X	Center 450X



**AL2-3** (A5083-LBW2-4.0kW x 2000mm/min)

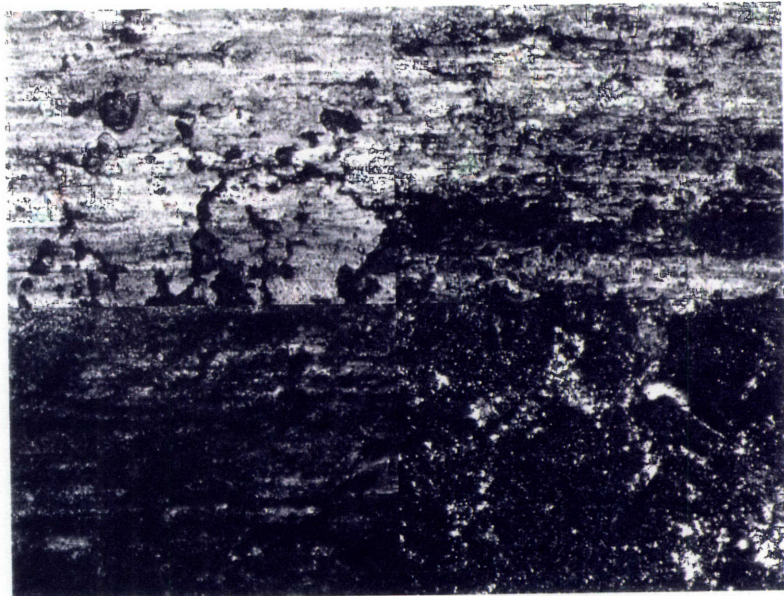
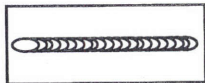
**PVIM**

B.M. 42X	HAZ 42X
Edge 42X	Center 42X



**CSLM**

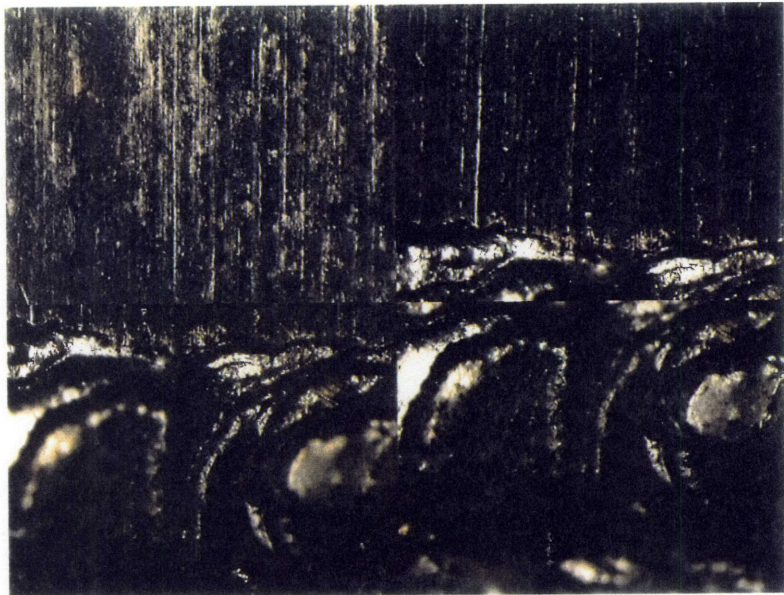
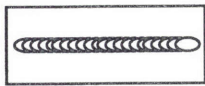
B.M. 450X	HAZ 450X
Edge 450X	Center 450X



**AE-1** (A5083-EBW2-3.0kW x 2000mm/min)

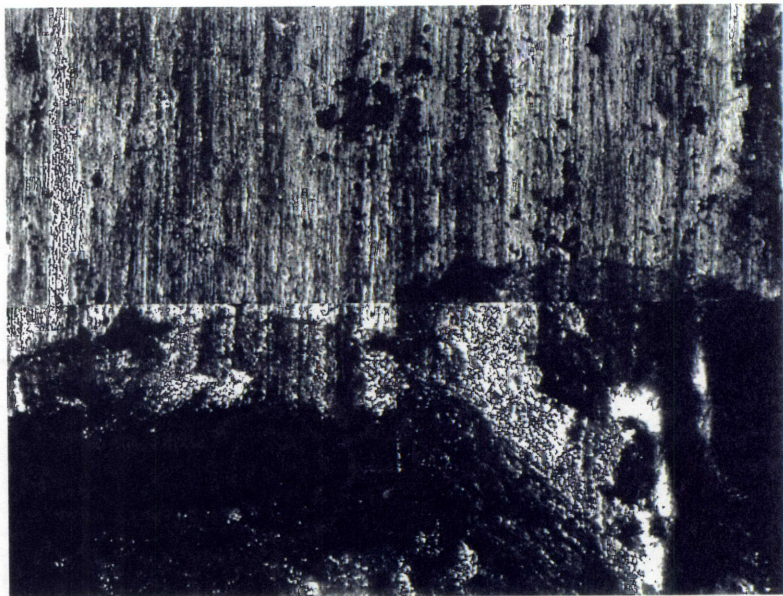
**PVIM**

B.M. 42X	HAZ 42X
Edge 42X	Center 42X



**CSLM**

B.M. 450X	HAZ 450X
Edge 450X	Center 450X



**AE-2** (A5083-EBW2-4.5kW x 2000mm/min)

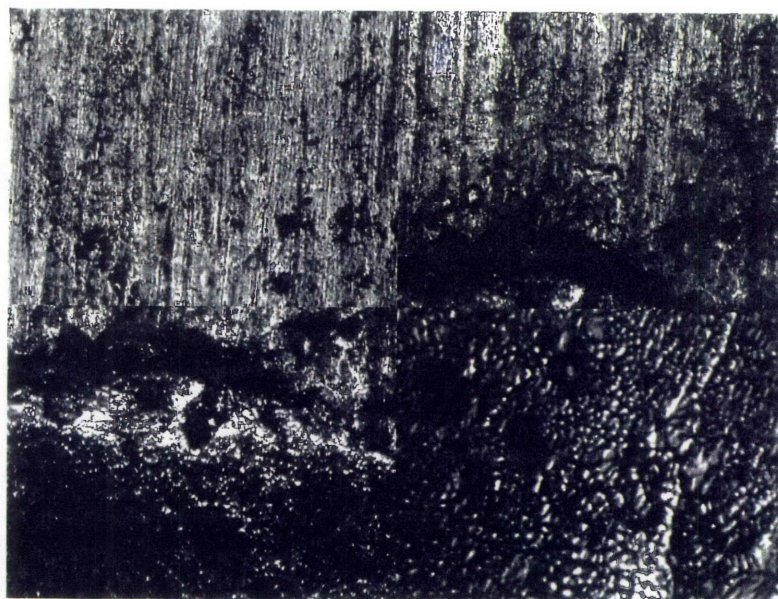
**PVIM**

B.M.	HAZ
42X	42X
Edge	Center
42X	42X



**CSLM**

B.M.	HAZ
450X	450X
Edge	Center
450X	1130X



**AE-3** (A5083-EBW2-6.0kW x 2000mm/min)

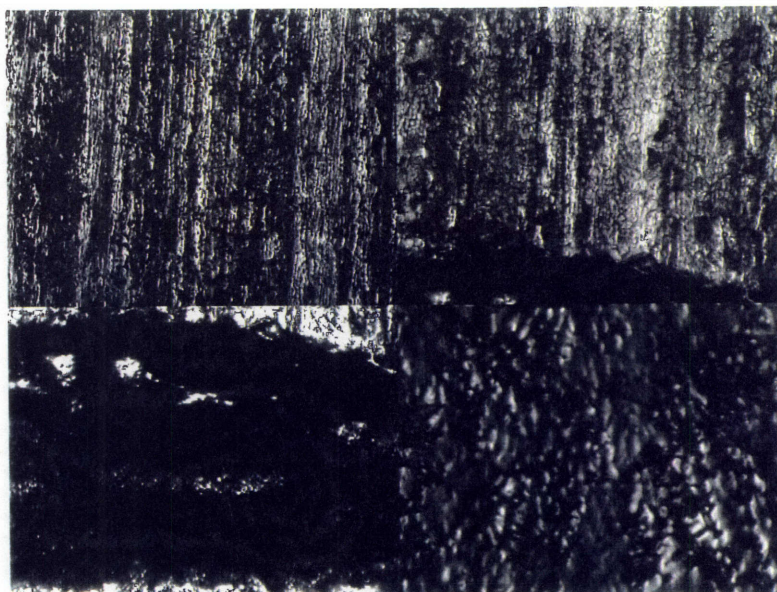
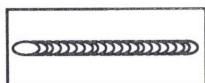
**PVIM**

B.M. 42X	HAZ 42X
Edge 42X	Center 42X



**CSLM**

B.M. 450X	HAZ 450X
Edge 450X	Center 1130X



## 5.4 Titanium Alloys

Titanium alloy specimens were welded by three different welding processes, GTAW (with after shield), EBW, and LBW. All observation data is shown in Appendices. Pictures of surface features observed with a PVIM and a CSLM are also shown later in this chapter.

### **Specimens Welded by GTAW (TT-1, 2, and 3)**

#### Oxide formation

The surface of the weld metals of the TE-1 and TE-2 was all covered with a thin yellow oxide layer. The surface of the weld metals of the TE-3 was all covered with a thin violet and blue oxide layer.

#### Micro discontinuities

The only type of discontinuity observed was the grain boundaries. Large grain structure were apparent in all specimens. These large grains were continuous into the HAZ. The grains in the HAZ were 10 ~ 400  $\mu\text{m}$  for TT-1, 400 ~ 1200  $\mu\text{m}$  for TT-2, and ~ 800  $\mu\text{m}$  for TT-3 in diameter.

The grains in the weld metals were 200 ~ 500  $\mu\text{m}$  for TT-1, 200 ~ 650  $\mu\text{m}$  for TT-2, and ~ 800  $\mu\text{m}$  for TT-3 in diameter.

The grains were normal in shape.



## **Specimens Welded by LBW with After Shield (TL2-1, 2, and 3)**

### Oxide formation

The surface of all the specimens were covered with a thin oxide layer. The thickness of the layer increased as the heat input increased. However, the layer of even TL2-3 with the most heat input was still thin. At the center of the specimens a narrow black band of a thin oxide layer was observed. However, a thick black layer was present on TL2-3 in the area of the weld edge along the fusion line and near the weld center.

### Micro discontinuities

Due to thick oxides, we were not able to observe grains in the HAZ of TL2-3. The grains in the HAZ of TL2-1 and TL2-2 had a normal shape and the diameter was 15 ~ 25  $\mu\text{m}$ .

In the weld metals the observed grains had normal shapes and the diameter of the grains at the edge along the fusion line was 20 ~ 30  $\mu\text{m}$  for TL2-1, 30 ~ 50  $\mu\text{m}$  for TL2-2, and about 70  $\mu\text{m}$  for TL2-3. At the center we were able to observe grains with the size up to 500  $\mu\text{m}$  for TL2-1 and TL2-2, and 1,600  $\mu\text{m}$  for TL2-3.

Near the center there were elongated grains perpendicular to the welding direction and their size was 100 x 400  $\mu\text{m}$  for TL2-2 and 200 x 500  $\mu\text{m}$  for TL2-3. Although no crack was actually found in weld metals, large vertical discontinuities with the height 0.4  $\mu\text{m}$  were often observed at the grain boundaries.

## Specimens Welded by EBW (TE-1, 2, and 3)

### Oxide formation

The surface of the weld metals and the HAZ of the TE-2 and TE-3 was all covered with a thin brown oxide layer. The thickness of the layer increased as the heat input increased. In the HAZ a band which was not covered with oxides was observed. The width of the band was about 1 mm for TE-2 and TE-3.

Along the ripple, there was also a thick dark brown oxide, which was thicker on the specimens with larger heat input. The center of the weld was not covered with this black layer.

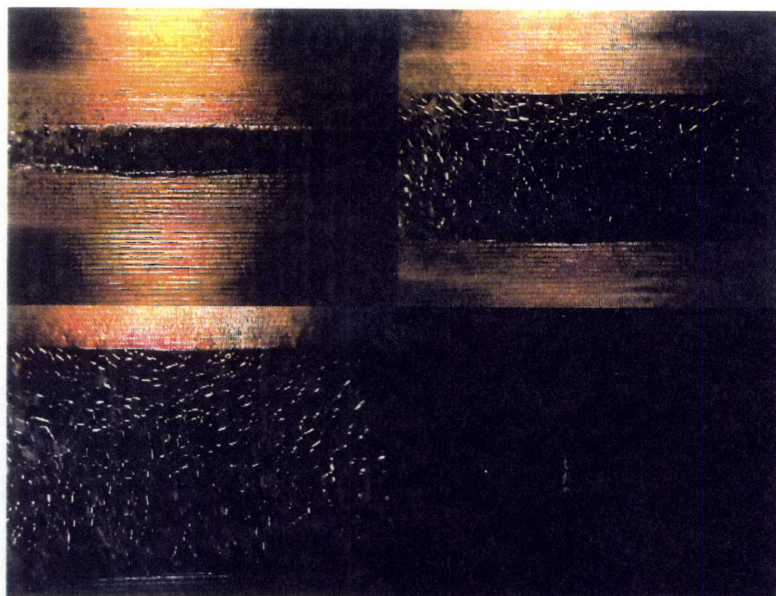
### Micro discontinuities

The only type of discontinuity observed was the grain boundaries. Large grain structure was apparent in all specimens. These large grains were continuous into the HAZ. The grains in the HAZ were 12 ~ 40  $\mu\text{m}$  for TE-1, 10 ~ 30  $\mu\text{m}$  for TE-2, and 20 ~ 50  $\mu\text{m}$  for TE-3 in diameter. The grains in the weld metals were often elongated in the direction perpendicular to the welding direction and their maximum sizes were 60 x 160  $\mu\text{m}$  for TE-1, 60 x 160  $\mu\text{m}$  for TE-2, and 60 x 100  $\mu\text{m}$  for TE-3. Generally, the grains had normal shape and their sizes were 30 ~ 160  $\mu\text{m}$ .

# Surface Appearance of Welded Titanium Alloys

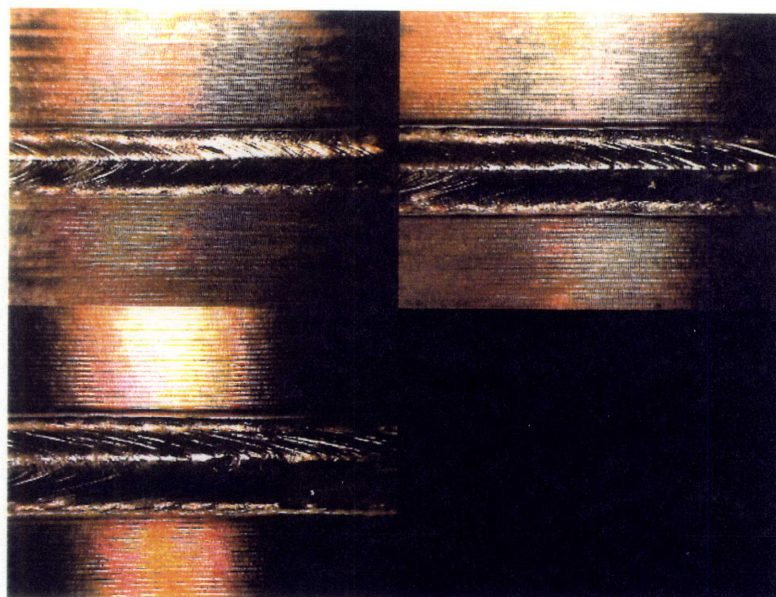
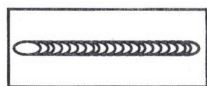
## PVIM

TT-1 42X	TT-2 42X
TT-3 42X	



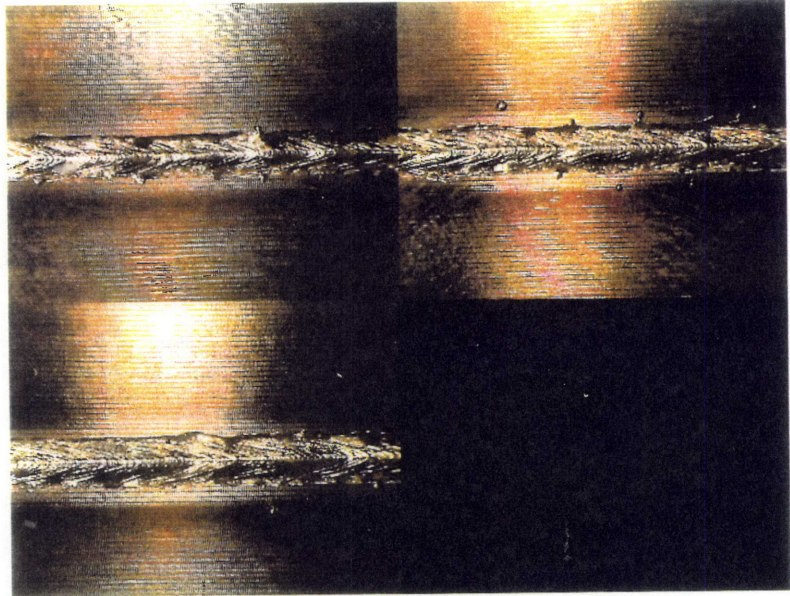
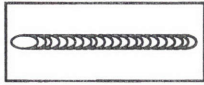
## PVIM

TL2-1 42X	TL2-2 42X
TL2-3 42X	



PVIM

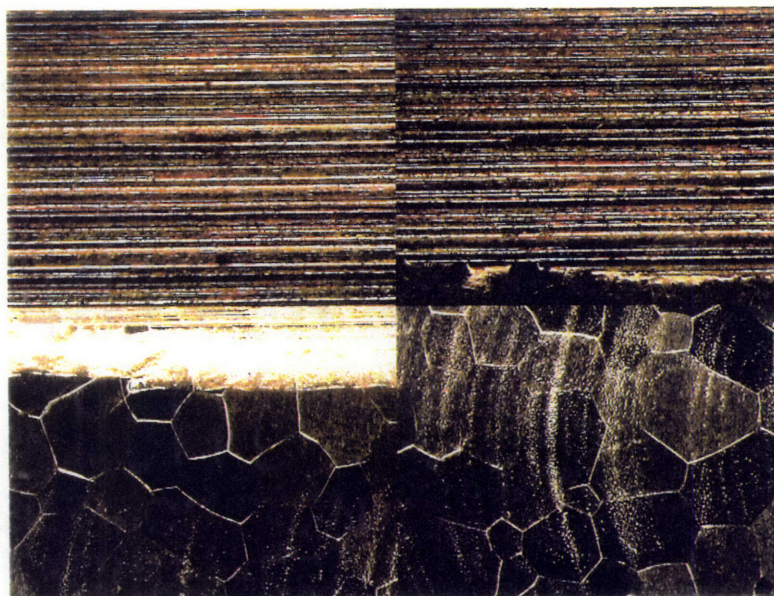
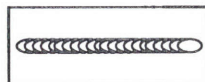
TE-1 42X	TE-2 42X
TE-3 42X	



**TT-1** (Ti-6Al-4V-GTAW-51A x 9.3V x 96mm/min)

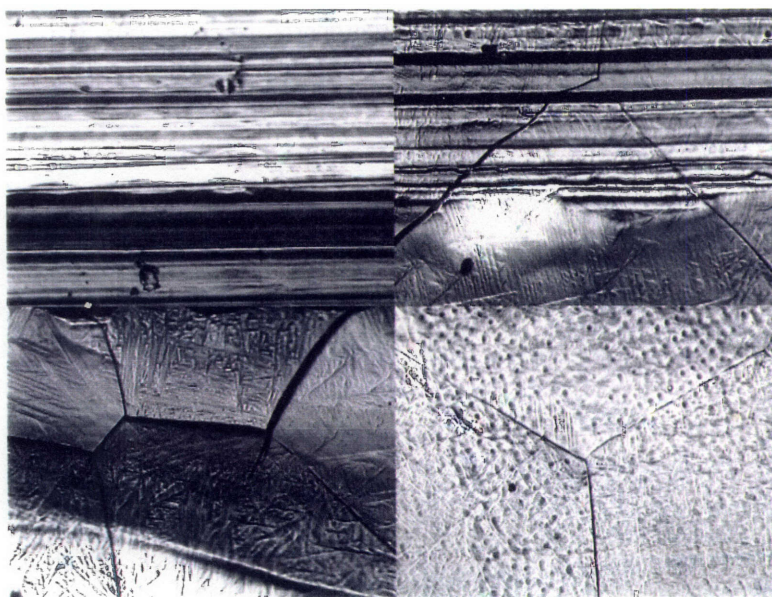
**PVIM**

B.M.	HAZ
42X	42X
Edge	Center
42X	42X



**CSLM**

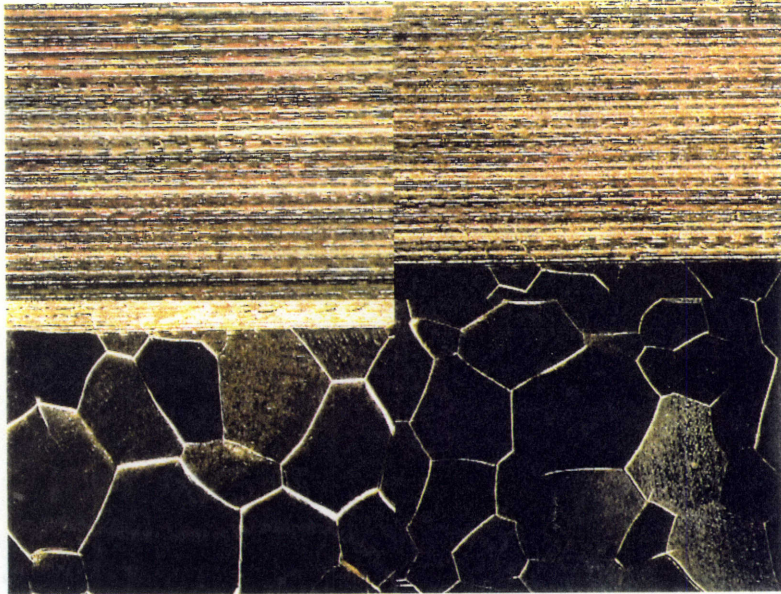
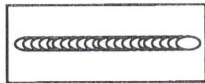
B.M.	HAZ
225X	225X
Edge	Center
225X	225X



**TT-2** (Ti-6Al-4V-GTAW-79A x 10.3V x 96mm/min)

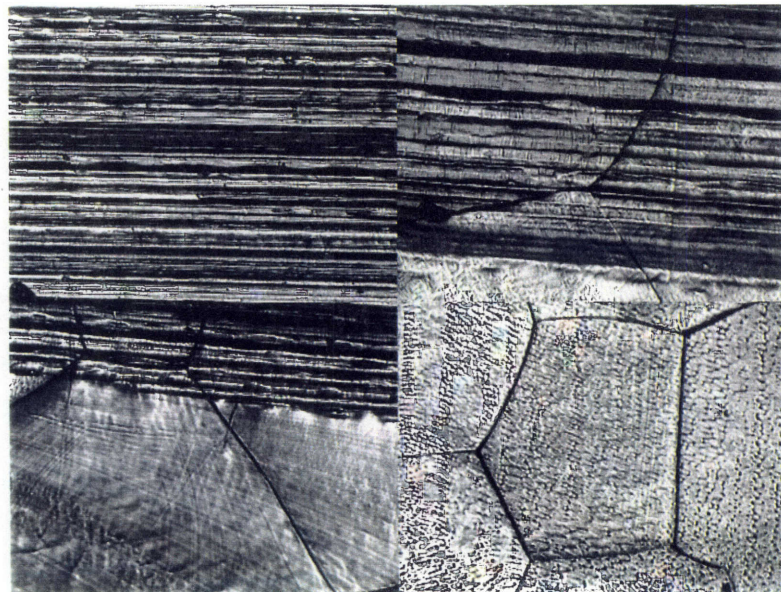
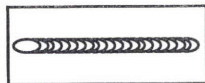
**PVIM**

B.M.	HAZ
42X	42X
Edge	Center
42X	42X



**CSLM**

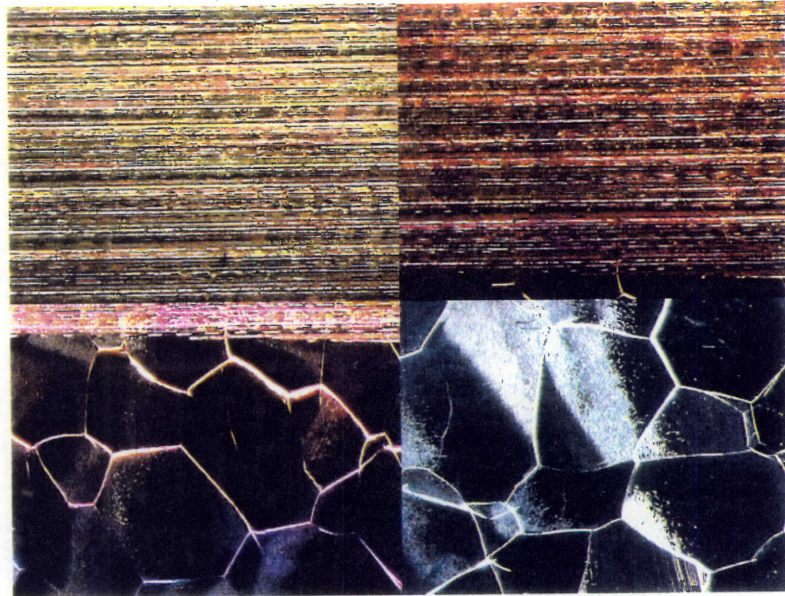
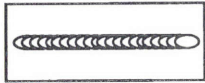
B.M.	HAZ
113X	113X
Edge	Center
113X	113X



**TT-3** (Ti-6Al-4V-GTAW-112A x 11.0V x 96mm/min)

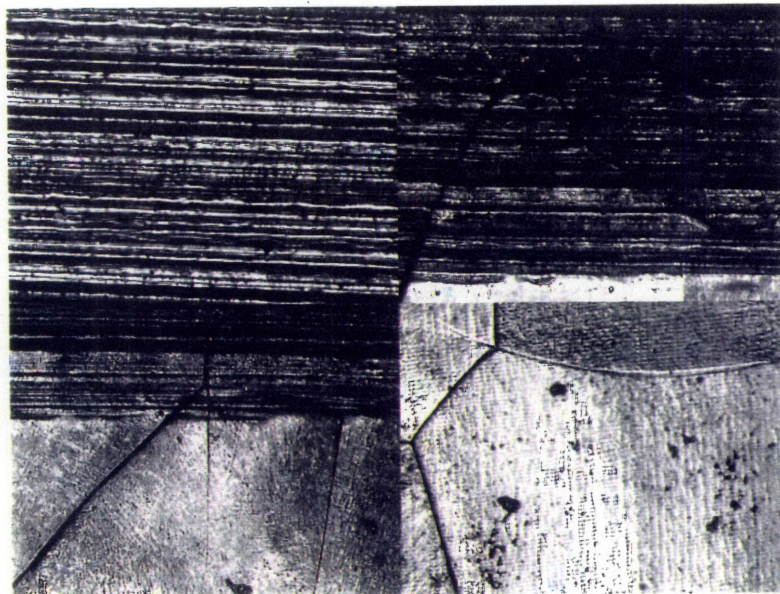
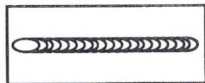
**PVIM**

B.M.	HAZ
42X	42X
Edge	Center
42X	42X



**CSLM**

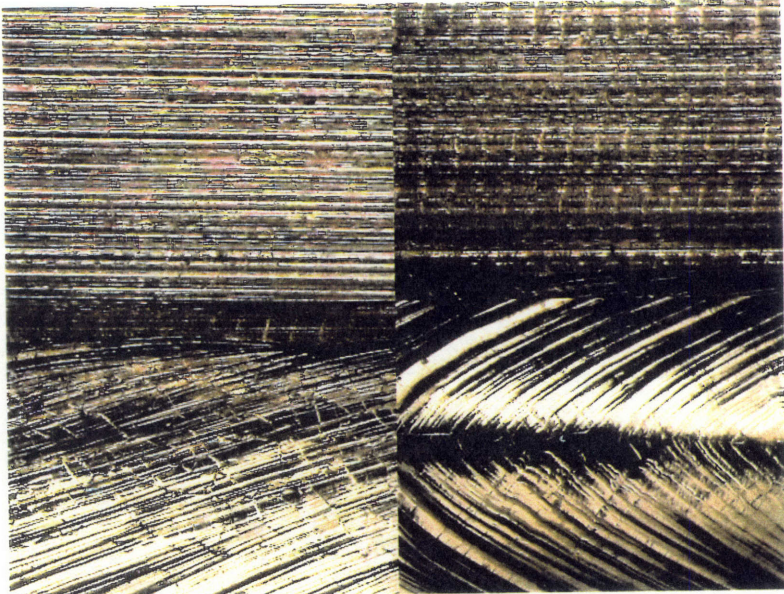
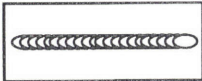
B.M.	HAZ
113X	113X
Edge	Center
113X	113X



**TL2-1** (Ti-6Al-4V-LBW2-2.0kW x 2000mm/min)

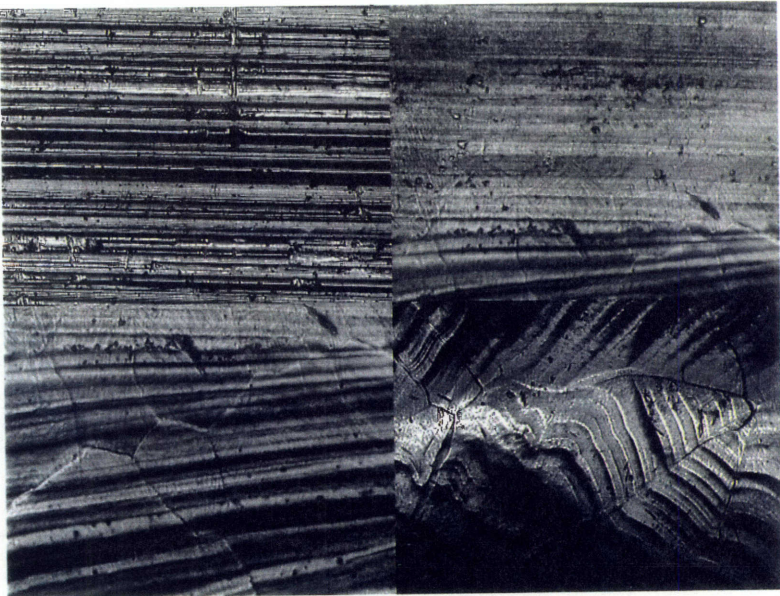
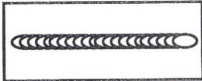
**PVIM**

B.M.	HAZ
42X	42X
Edge	Center
42X	42X



**CSLM**

B.M.	HAZ
113X	450X
Edge	Center
450X	113X

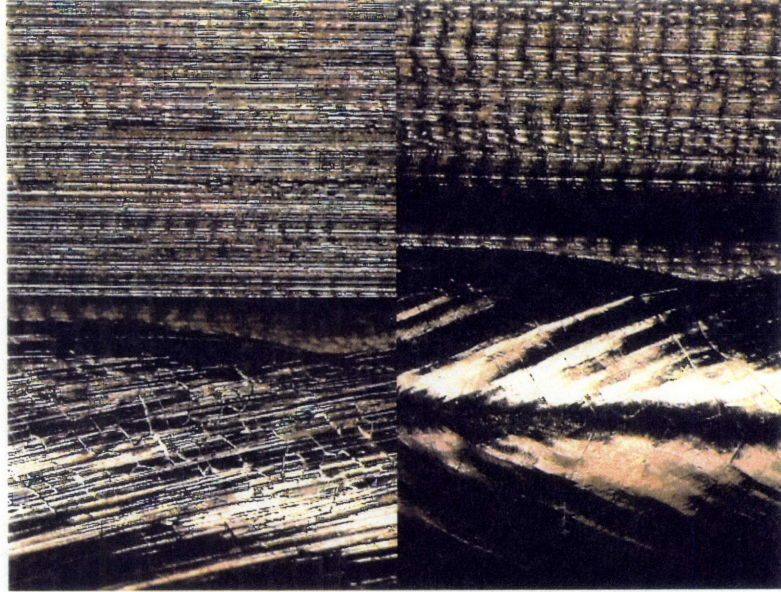
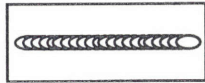




**TL2-2** (Ti-6Al-4V-LBW2-3.0kW x 2000mm/min)

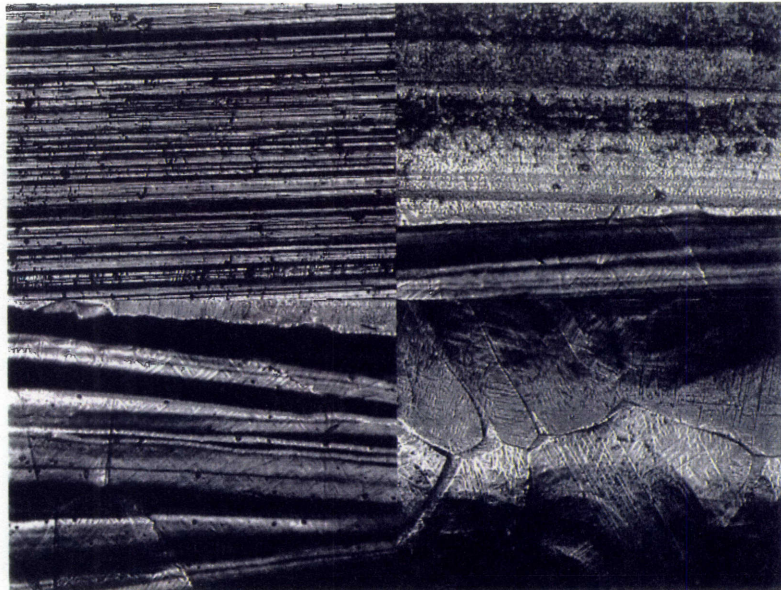
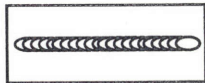
**PVIM**

B.M. 42X	HAZ 42X
Edge 42X	Center 42X



**CSLM**

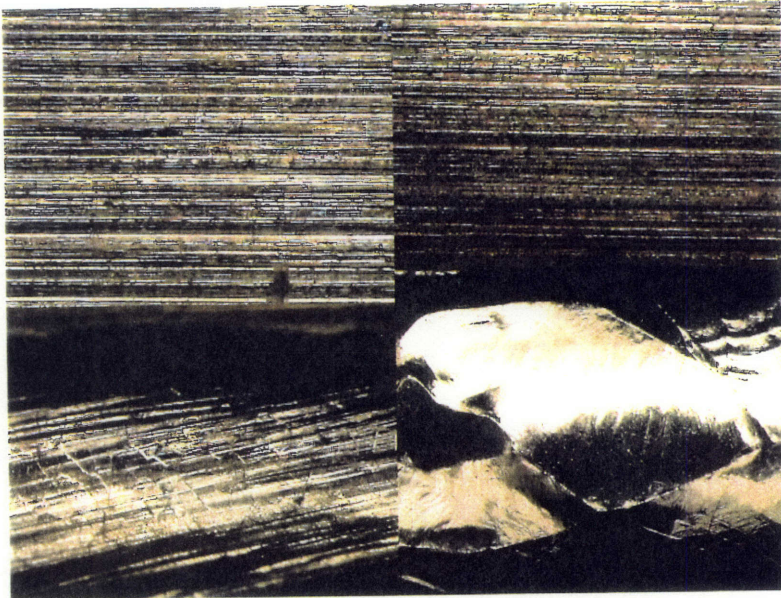
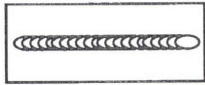
B.M. 113X	HAZ 225X
Edge 450X	Center 113X



**TL2-3** (Ti-6Al-4V-LBW2-4.0kW x 2000mm/min)

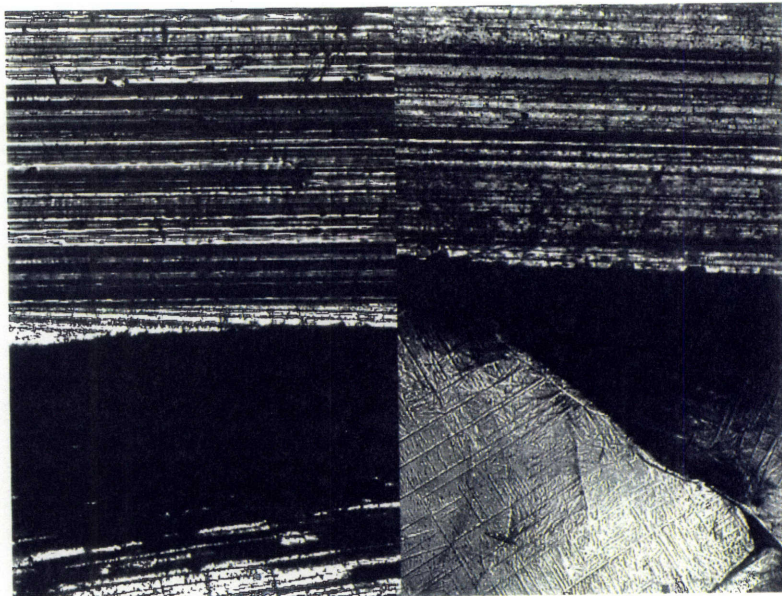
**PVIM**

B.M.	HAZ
42X	42X
Edge	Center
42X	42X



**CSLM**

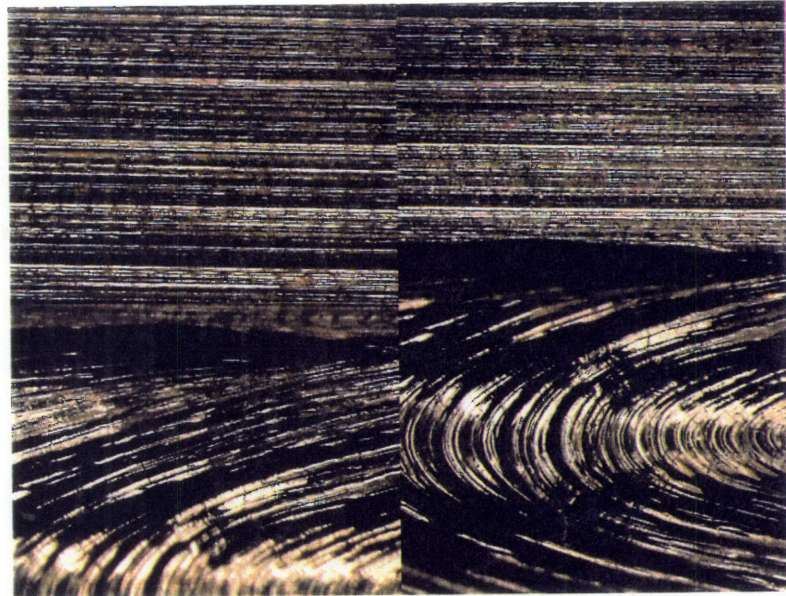
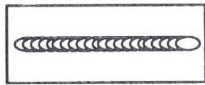
B.M.	HAZ
113X	113X
Edge	Center
113X	113X



**TE-1** (Ti-6Al-4V-EBW2-3.0kW x 2000mm/min)

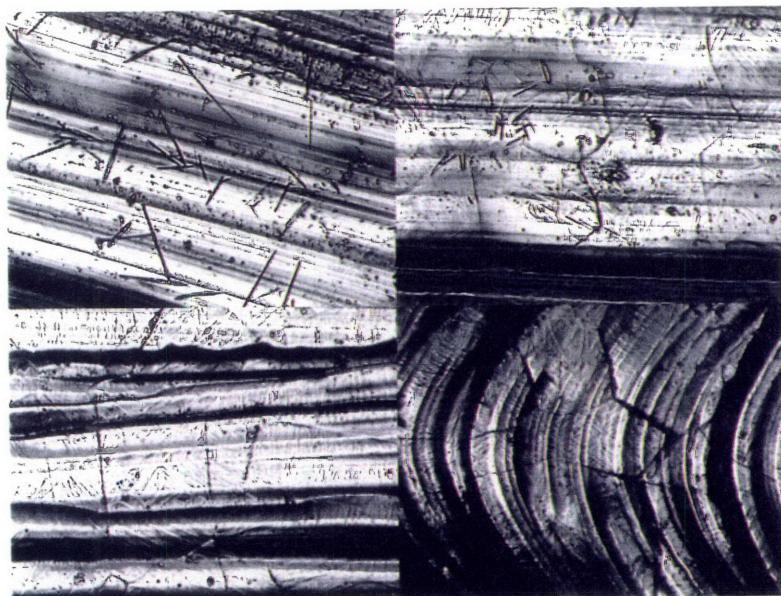
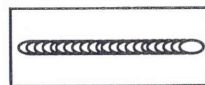
**PVIM**

B.M.	HAZ
42X	42X
Edge	Center
42X	42X



**CSLM**

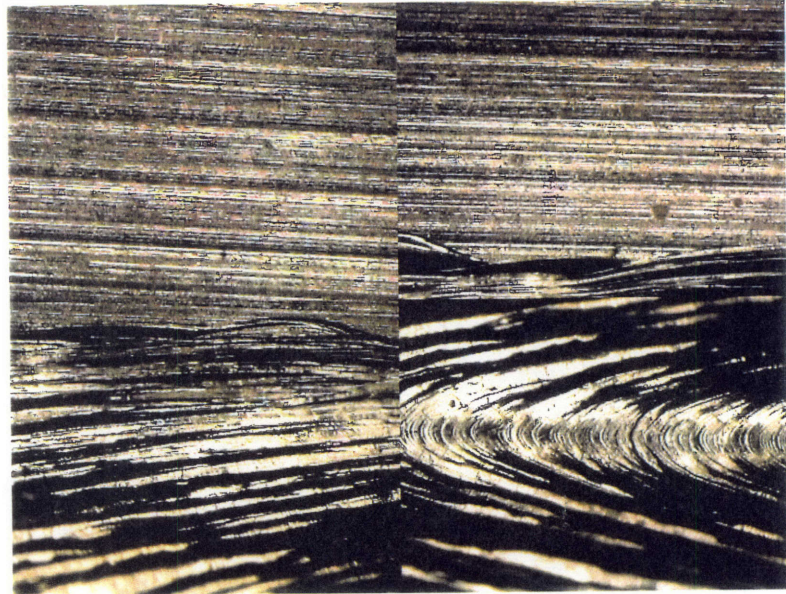
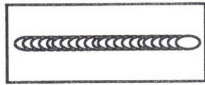
B.M.	HAZ
450X	450X
Edge	Center
450X	225X



**TE-2** (Ti-6Al-4V-EBW2-4.5kW x 2000mm/min)

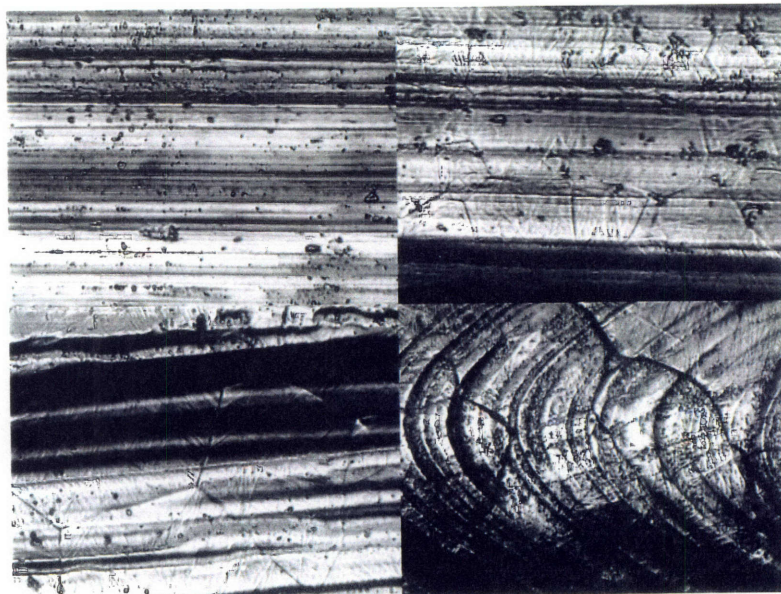
**PVIM**

B.M.	HAZ
42X	42X
Edge	Center
42X	42X



**CSLM**

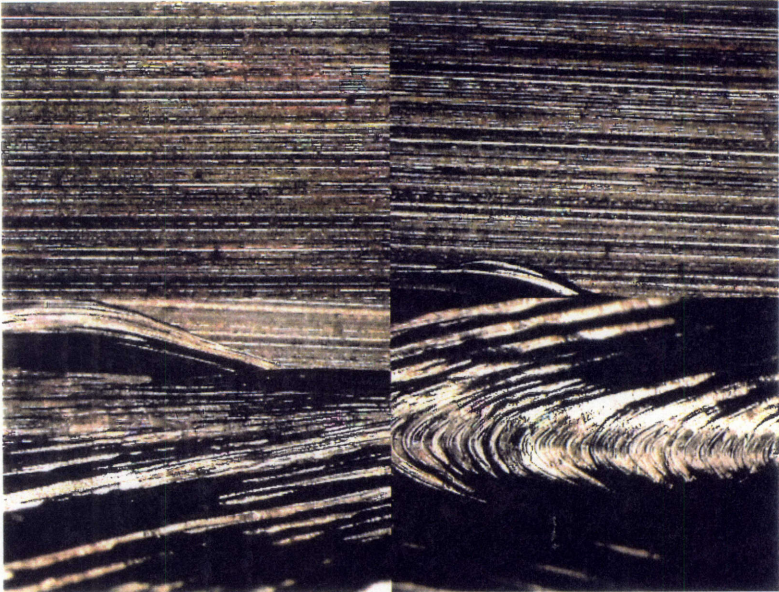
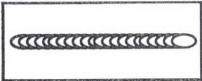
B.M.	HAZ
450X	450X
Edge	Center
450X	225X



**TE-3** (Ti-6Al-4V-EBW2-6.0kW x 2000mm/min)

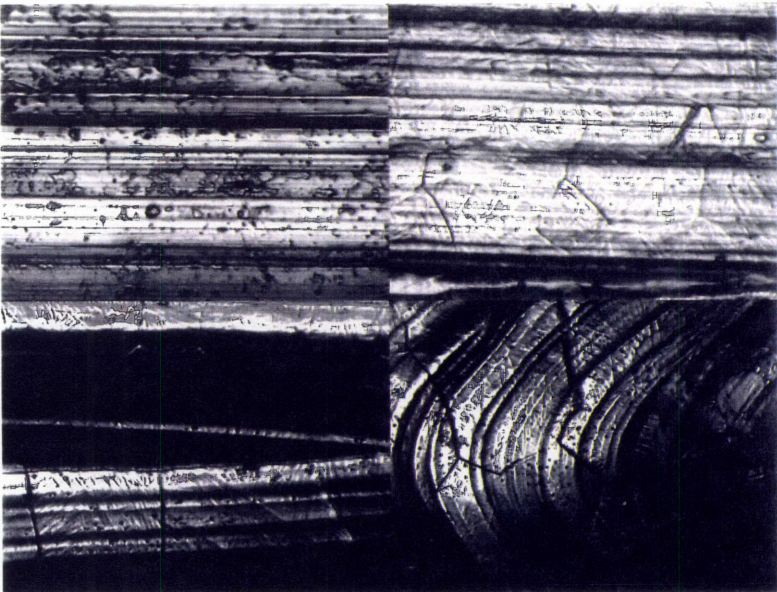
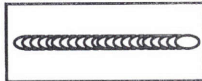
**PVIM**

B.M. 42X	HAZ 42X
Edge 42X	Center 42X



**CSLM**

B.M. 450X	HAZ 450X
Edge 450X	Center 225X



# Chapter 6 : Experiments on Fatigue Crack Initiation

## 6.1 Objectives

A fatigue crack generally initiates at the surface of materials, especially near the area where stress concentrations exist. There are several types of surface discontinuities which result from cracks, grain boundaries, undercuts, inclusions, arc strikes, porosity, and craters. When there are surface discontinuities around an area of stress concentrations, a fatigue crack is expected to initiate more likely from that area. Based on the information through the observation of various metals in Chapters 4 and 5, the phenomena of fatigue crack initiation are researched in this experiment.

Previous to this experimental work, two experiments were conducted. One was carried out for the Master's thesis by John M. Cushing Jr. referred to in 2.2 [Ref. 3]. Mr. Cushing found that the fatigue crack initiation was detected at the center of the weld crater or HAZ at start-up toe the of weld by a CSLM and a replica technique. This result was assured by the comparison between CSLM and SEM. He also discovered that the presence of micro-cracks before service does not necessarily mean a problem area.

The other experiment was done for the Master's thesis by Philippe Tannery in cooperation with the author to make sure that Mr. Cushing's results were correct. We used both a PVIM and a CSLM, which showed very good observation capabilities. The artificial defects such as notches, holes and scratches were made on some specimens to determine the influence of the defects and their stress concentration. Fatigue cracking did not always occur at

parts such as the center of a crater or HAZ at start-up toe of weld where Mr. Cushing found most likely fatigue cracks happened in his research. However, two welded specimens without artificial defects showed that the fatigue cracks initiated from the microcracks in the welds. These microcracks did or did not exist before testing. Consequently, early fatigue crack detection was found difficult. Because of lack of experimental data, the study was not conclusive. Mr. Tannery suggested that more number of experimental works would have proceeded better general conclusions.

As a succession to the work above, additional two experiments were planned.

First experiment (Fatigue Test I) is the extension of our research with Mr. Tannery. The specimens welded under different welding conditions and ones with different sizes were designed to investigate if those difference affect the above results.

There are four primary objectives of Fatigue test I in combination with the results obtained by Mr. Cushing and Mr. Tannery:

1. Find the microstructural features on weldments which will most likely lead to a fatigue fracture on low-carbon steels.
2. Find the microstructural features on weldments which suggest the amount of fatigue damage occurring later on low-carbon steels.
3. Develop a method for the early detection of fatigue crack initiations.

Second experimental work (Fatigue Test II) was suggested to investigate the effects of the material difference of the microstructural features which make a difference to the fatigue crack initiations and possibility to develop a new NDE for each material.

## 6.2 Specimen and Equipment

A CSLM is used to observe microstructural features and a PVIM is used primarily to observe relatively large cracks. A video recorder is used to keep track of the observation process and make a backup for a detailed investigation later and a video image printer is also used to print out the image on the monitor.

### **Tensile Testing Machine**

An electro-hydraulic MTS tensile testing machine was used to test the welded specimens in order to inspect fatigue crack initiation. The machine has a 100,000 pound load capacity. A tension-tension half sinusoidal loading with the operational range between maximum load and minimum load which is set to 10% value of the maximum load was used. The total number of cycles was counted by the counter drawer of the machine and loading was set to automatically stop when it reached the expected number of cycles. A stroke sensor was also set to stop the machine when the specimen separated.

### **Specimen**

There are two different experiments conducted in this study. The first one is a series of fatigue tests (Fatigue Test I) to study the microstructural features on weldments using low-carbon steels. Two different specimens in size and type of alloy shown in Figures 6.2.1 were used. The weld beads on the plates were made by GTAW (FT-1, 2 ,3 ,4 by automatic GTAW, FT-5, M-1, 2 by manual GTAW). A slit on the weldment of two specimens, FT-3, 4 was made by an electrical



discharge machined (EDM), as shown in Figure 6.2.2, to create artificial stress concentration on the middle of weldments.

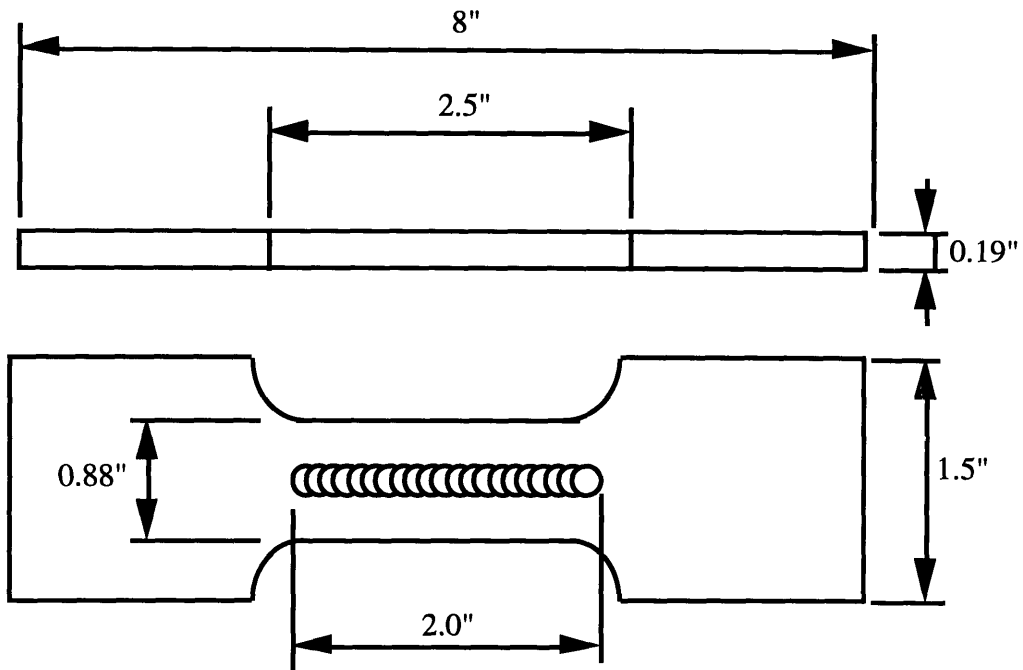
Other one is a different series of fatigue tests (Fatigue Test II) to study the effects of material differences to the microstructural features. The part of the specimens used for the observations in Chapters 4 and 5 were applied to these tests to inspect microstructural changes detected only by the set of a PVIM and a CSLM. The weld beads on the plates were made by GTAW. The materials of the specimens were low-carbon steels, stainless steels, aluminum alloys, and titanium alloys. Table 6.2.1 shows the details of the specimens and the welding conditions and Figure 6.2.3 shows the specimen for Fatigue Test II. The specification of materials used in this study are shown in Table 6.2.2.

Material	No.	Welding Processes	Welding Conditions	Qnet(J/mm)
Low-Carbon Steel	MT-3	GTAW	110Ax10.5Vx82mm/min	229.427
Stainless Steel (SUS304)	ST-3	GTAW	112Ax10.8Vx96mm/min	
Aluminum Alloy (A5083)	AT-2	GTAW	75Ax12.2Vx96mm/min	400.312
Aluminum Alloy (A5083)	AT-3	GTAW	112Ax12.1Vx96mm/min	529.9
Titanium (Ti-6Al-4V)	TT-2	GTAW	79Ax10.3Vx96mm/min	355.994

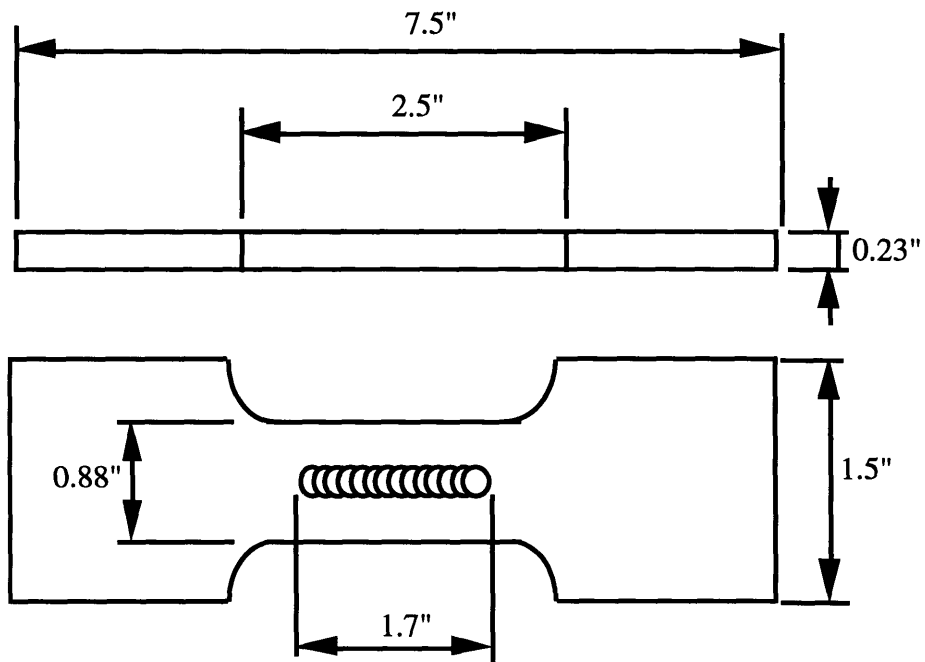
Table 6.2.1. Details of specimens for Fatigue Test II

Material	Unit	Low-Carbon Steel	Stainless Steel	Aluminum	Titanium
Type		1018 (H, C)	SUS304	A5083	Ti-6Al-4V
Modulus of Elasticity	$\times 10^6$ psi	29	29	10.2	16
Yield Strength, Min	psi	40,000, 69000	30,000	21,000	120,000
Ultimate Strength, Min	psi	69,000, 82000	80,000	42,000	130,000

Table 6.2.2. Specifications of materials

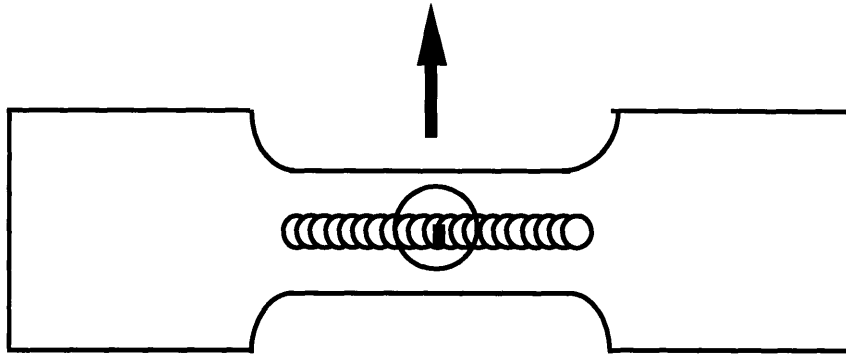
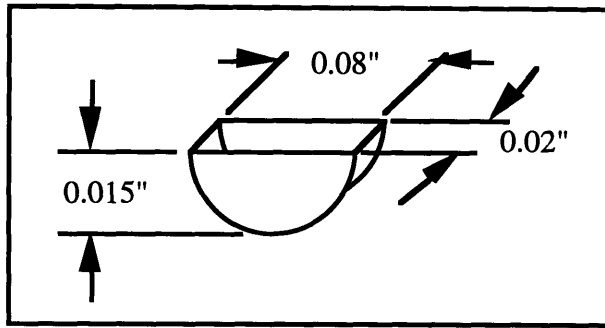


(Ultimate Tensile Strength: 82ksi, Cross Sectional Area: 0.167 in<sup>2</sup>, Polished Surface, FT-1, 2, 3, 4, 5)



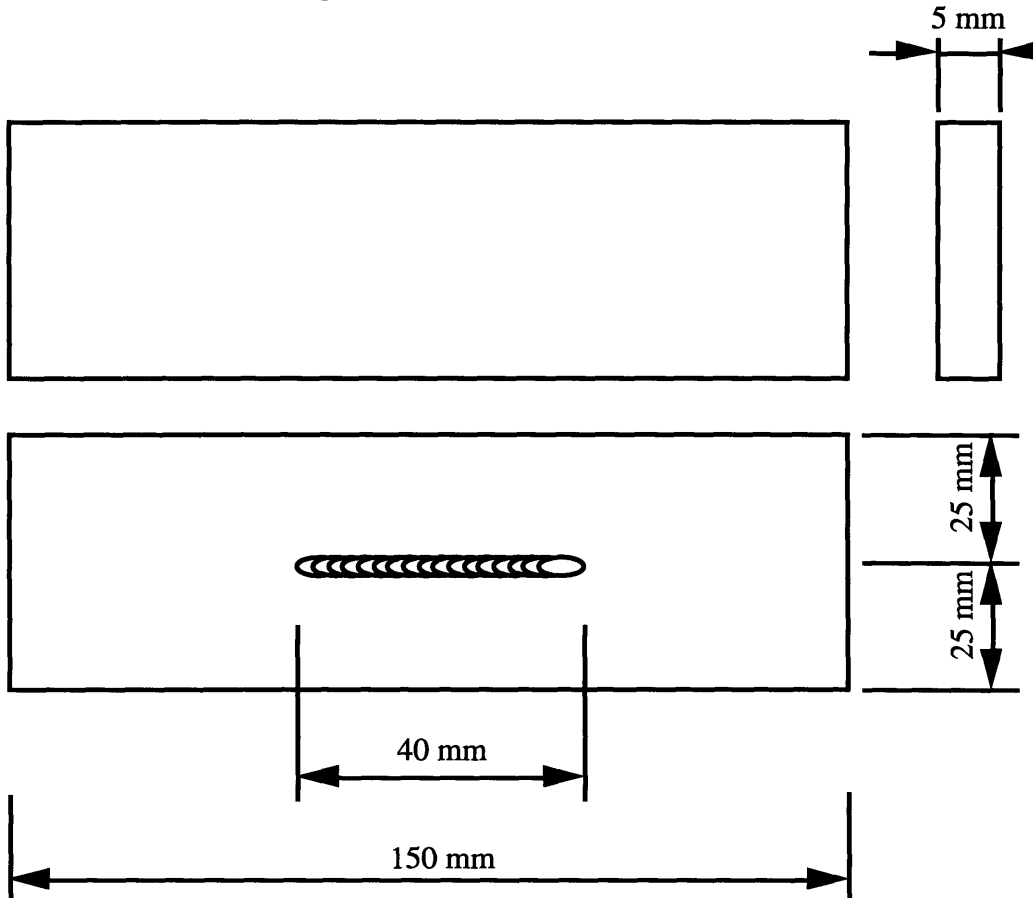
(Ultimate Tensile Strength: 69ksi, Cross Sectional Area: 0.167 in<sup>2</sup>, Polished Surface, M-1, 2)

Figure 6.2.1. Specimen for Fatigue Test I



(Ultimate Tensile Strength: 82ksi, Cross Sectional Area: 0.167 in<sup>2</sup>, Polished Surface, FT-3, 4)

Figure 6.2.2. A slit on a weld



(Cross Sectional Area: 0.389 in<sup>2</sup>, Normal Surface, MT-1, ST-3, AT-2, 3, TT-2)

Figure 6.2.2. Specimen for Fatigue Test II

## 6.3 Experimental Procedure

There are two different experiments conducted in this research. Each consists of two processes, a low-cycle high-stress fatigue test and an observation.

### 1. Fatigue Test I

Initially, tensile strength tests were conducted to make sure that the values from the mill sheet are correct. Two specimens for each size were tested.

#### **Fatigue Test**

The hydraulic pump and control cabinet were energized and allowed to run and warm up for 15 minutes before testing. Load set-point, load span and cycle frequency were calculated and set to 10% of the maximum load value, 90% of the maximum load value, and each calculated value in voltage per pound.

Each test piece was marked with lines on its surface for consistent mounting in the hydraulic chucks. It was mounted squarely in the upper chuck and locked, then in the lower chuck. The desired number of cycle to be stopped was set on the counter drawer each time the fatigue test was run. While operating a test, the machine was often stopped and the test piece was inspected for any change on the surface.

After a specific amount of cycles the test piece was removed and taken to the Welding Systems Laboratory to observe it using a PVIM and a CSLM.

## Observation

Each observation is made to see if any microstructural phenomenon happens on the surface of the specimen during a fatigue test using both a PVIM and a CSLM.

1. First, visually inspect the specimen to see if it has any large crack and oxide. This step helps to locate the large surface discontinuities which should not exist on carefully prepared specimens. Oxides often have their own colors which inform one of their existence.
2. Using a PVIM with a lens 250, make observations of the surface of the specimens for base-metal, HAZ, the edge of the weldment, and the center of the weldment to find the microstructural features which affect the fatigue crack and fracture and the oxides covering the surface. The name of locations is shown in Figure 4.3.1. Then those surface discontinuities are classified into the categories mentioned in 3.2. Through the whole process the video recorder is used to record all the information. The detailed procedures are the following:
  - a) Unlap the cover protecting the specimen and quickly scan it to avoid new oxide forming as indicated by the color.
  - b) Skim carefully all over the specimen to see the color and thickness of oxides and find special microstructural features of the specimen. If any, take a picture and describe it in the observation sheet.
  - c) Describe general microstructural features of the specimen in the sheet and take pictures.
3. Using a CSLM with lenses of 10X, 20X, 40X, and 100X, make observations of the surface of the specimen for base-metal, HAZ, the edge of the weldment, and the center of the weldment to find the microstructural features which

affect the fatigue crack and fracture. Then those surface discontinuities are classified into the categories mentioned in 3.2. The detailed procedures are the following:

- a) Skim carefully all over the specimen to find special microstructural features of the specimen. If any, take a picture and describe it in the observation sheet. Use a scanning feature of the CSLM if necessary.
- b) If any surface discontinuity is found, measure its height, depth, width, length and inspect its shape. And take a picture and describe it in the sheet. Use a scanning feature of the CSLM if necessary.
- b) Describe general microstructural features of the specimen in the sheet and take pictures. Use a scanning feature of the CSLM if necessary.

## 2. Fatigue Test II

One low-carbon steel, one stainless steel, two aluminum alloys, and one titanium alloy were inspected. The procedures are the same as described in Fatigue test I except test parameters. This is also the combination of fatigue test and observation.

# Chapter 7: Experimental Results and Discussions for Fatigue Experiment

## 7.1 Fatigue Test I

On specimens, FT-1 and 2 welded by the automatic GTAW, no low-cycle, high-stress fatigue crack initiated. Additional experiments were conducted using specimens FT-3 and 4 with a slit in the weldment. However, the specimens, M-1, 2, and FT-5 welded manually showed fatigue crack initiations on the weldments as happened in the experiments by Mr. Cushing and Mr. Tannery. Table 7.1 1 summarizes the experimental results of the above specimens. These results show that manually welded specimens more likely initiate fatigue cracks than automatically welded ones, even more than specimens with artificially produced slit, i. e. the roughness of the surface of manually welded structures is the primary cause of fatigue fracture.

	FT-1	FT-2	FT-3 slit	FT-4 slit	FT-5	M-1	M-2
YTS (kpsi)	69	69	69	69	69	40	40
UTS (kpsi)	82	82	82	82	82	69	69
Sectional Area (sqin)	0.167	0.167	0.167	0.167	0.167	0.202	0.202
Applied Stress (kpsi)	67	67	67	67	67	45	45
Crack Initiation (cycles)	No	No	No	No	22,000	3,100	500
Location of Crack Initiation					crater	crater	crater

Table 7.1.1. Summarized results of Fatigue Test I

Table 7.1.2 summarizes the locations where fatigue fracture initiated on the specimens including the ones tested by Lt. Cushing and Lt. Tannery. The specimens counted in this statistics are limited to the ones with longitudinal weld without artificial defects such as notches, arc strikes, and scratches.

	Number	Percentage (%)
Weld Crater	5	50
Start-up Toe (HAZ)	4	40
Start-up Toe (Weld)		0
HAZ		0
Weld Metal (Edge)		0
Weld Metal (Center)	1	10
Total	10	100

Table 7.1.2. Locations of fatigue crack initiation

The results show that the areas where fatigue crack most likely occurs are weld craters and weld start-up toes in the heat affected zone. This is consistent with the published reports on this subject [Ref. 9 and 10].

Through this experiment, the following features were observed:

1. Only one crack caused by fatigue tended to grow, while others stopped growing or did not grow at all.
2. Generally, the specimen which had more micro cracks (vertical discontinuity type) seemed more likely to cause fatigue cracks. However, the relation is merely qualitative, not quantitative, i. e. quantity of microcracks does not indicate the likeliness of fatigue crack initiation.
3. Although other surface discontinuities such as persistent slip bands and grain boundaries are also reported [Ref. 15] to be the initiation sites of fatigue cracks, all specimens initiated cracks either from weld craters or start-up toes except



one which did initiate from the center of a weldment. Therefore, we could not verify the above report.

4. Global plastic deformation due to high stress fatigue was often observed on the surface of specimens in the early stage of fatigue tests. Striations due to fatigue could not often be found until fatigue crack initiated. It shows the difficulty in finding the areas which may later be the fatigue crack initiation sites.
5. Local plastic deformation was observed around the areas on the artificially made surface discontinuities such as notches, scratches, and holes. Fatigue crack often initiated around these areas. However, we could not determine the effects of stress concentration caused by micro surface discontinuities produced through the welding processes.

All the testing data is shown in Table A-16 in Appendices.

Figures 7.1.1, 7.1.2, and 7.1.3 show the weld crater where a fatigue crack initiated around 500 cycles (M-2). Fatigue striations were not seen on the surface of the specimen. Other microcracks in the weldment did not change at all. Only fatigue crack newly formed in the weldment grew.

Figure 7.1.1 M-2  
(0 cycle)

42X	42X
42X	

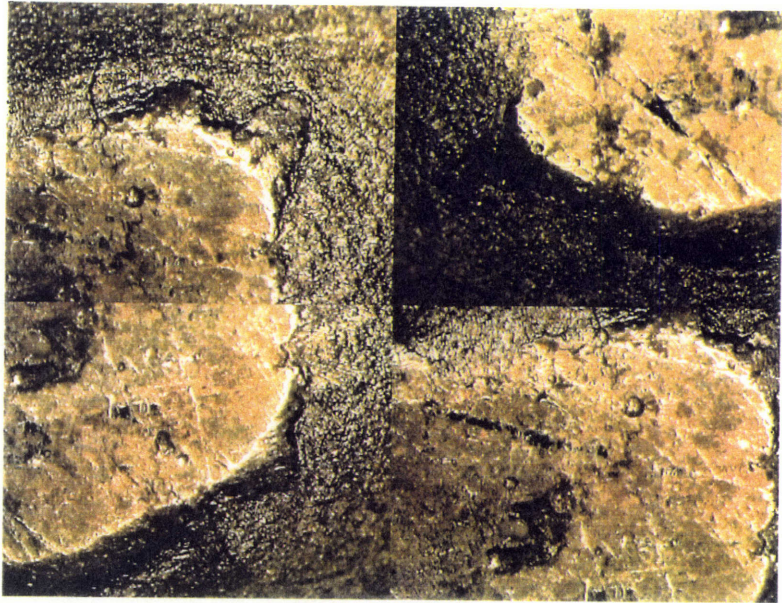
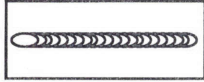


Figure 7.1.2 M-2  
(500 cycles)

42X	42X
42X	

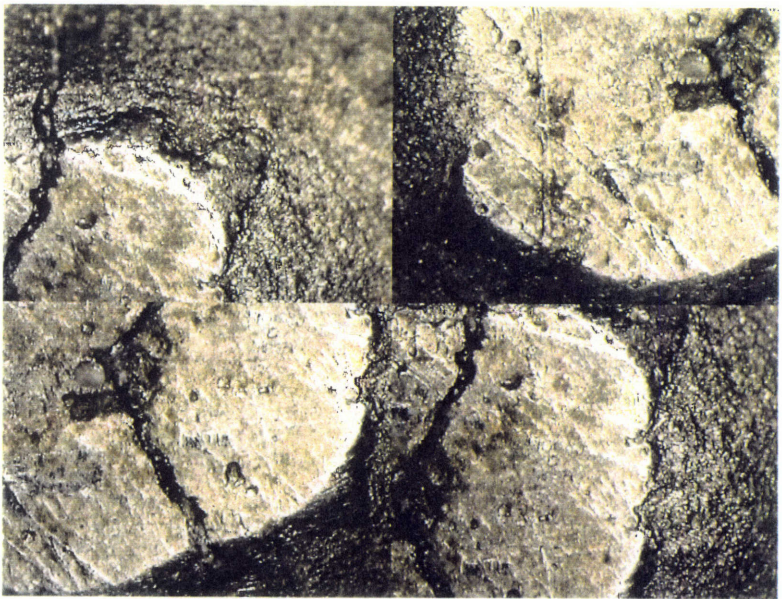
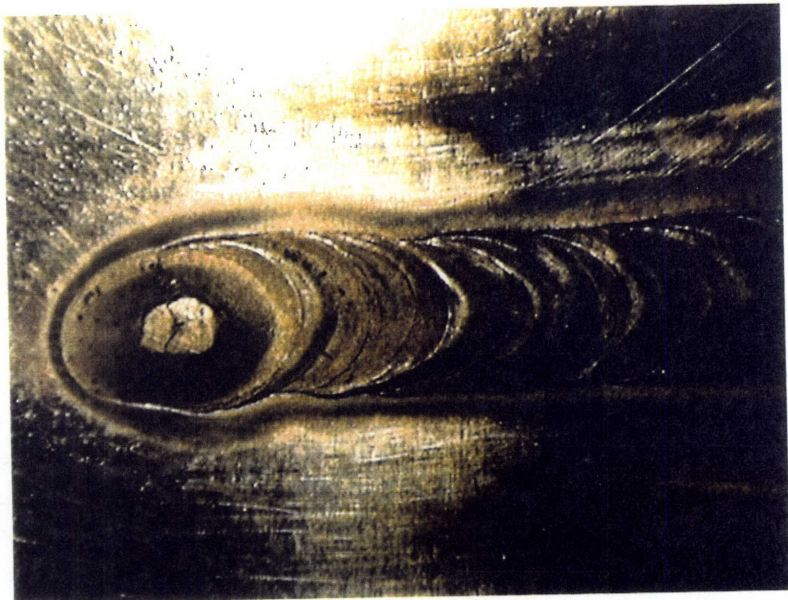
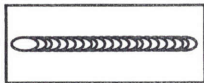


Figure 7.1.3 M-2  
(500 cycles)

6.5X
------



## 7.2 Fatigue Test II

Table 7.1 1 summarizes the experimental results of the Fatigue Test II. MT-3 and ST-3 did not show fatigue crack initiations, and no micro surface features showed any indication of fatigue crack. AT-2 and AT-3 broke around 3,450 and 470 cycles at weld craters due to low-cycle, high-stress fatigue. The surface of aluminum alloys were covered by thick oxide layers as discussed in Chapter 5. These layers prevented us from observing the specimens' surface of aluminum alloys. TT-2 had a fatigue fracture at 17,930 cycles in HAZ on the start-up toe .

All the testing data is shown in Table A-16 in Appendices.

	MT-3 Low-Carbon St	ST-3 Stainless St	AT-2 Al Alloy	AT-3 Al Alloy	TT-3 Ti Alloy
YTS (kpsi)	69	30	21	21	120
UTS (kpsi)	82	80	42	42	130
Sectional Area (sqin)	0.389	0.389	0.389	0.389	0.389
Welding Process	Automatic GTAW	Automatic GTAW	Automatic GTAW	Automatic GTAW	Automatic GTAW
Applied Stress (kpsi)	45~55	48~60	25~31	25~31	78~97
Crack Initiation (cycles)	No	No	3,450	470	17,930

Table 7.2.1. Summarized results of Fatigue Test II

### 7.2.1 Low-Carbon Steel

Low -carbon steel welded by automatic GTAW did not show fatigue crack initiation as we see in 7.1. Automatic GTAW makes smooth weld beads on the specimens, consequently they have less microcracks in weldments and less local stress concentration. Through the fatigue test, the micro surface discontinuities observed in 5.1 did not change at all. Figures 7.2.1 and 7.2.2 show two series of

pictures of micro surface discontinuities at 0, 13,000, and 23,000 cycles. These pictures show no changes of the discontinuities. Figure 7.2.3 shows another series of pictures at four locations, base metal, HAZ, edge of weld, and center of weld at 300, 23,000, and 40,000 cycles.

## 7.2.2 Stainless Steel

Stainless steel welded by automatic GTAW did not show fatigue crack initiation, also due to the same reason as M-3. Through the fatigue test, the micro surface discontinuities observed in 5.2 did not change at all. Figure 7.2.4 shows a series of pictures of micro surface discontinuities (inclusion) at 500, 14,000, and 24,000 cycles. These pictures show no changes of the discontinuities. Figure 7.2.5 shows another series of pictures of micro surface discontinuities at the crater at 500, 14,000, and 40,000 cycles. These pictures show no changes of the discontinuities. Figure 7.2.6 shows a series of pictures at four locations, base metal, HAZ, edge of weld, and center of weld at 0, 14,000, and 40,000 cycles.

## 7.2.3 Aluminum Alloy

Both aluminum alloy specimens failed at their craters due to fatigue with a 75% cyclic load of ultimate tensile strength. AT-2 and AT-3 failed around 470 cycles and 3,450 cycles respectively. These specimen were difficult to be observed by either a PVIM or a CSLM, because of thick oxide layers on the surface. However, the breaks of the oxide layers occurred and the surface of material itself could be seen through the breaks. Unfortunately, the height of oxide layers was too high to be well focused by a CSLM. There was a cone shape deep crater on both specimens and it became the source of stress concentration obviously.

The oxide layers on the crater did not touch the surface of material as shown in Figure 7.2.7. Therefore, it was difficult observing the surface of material and finding any micro surface discontinuity on it. Figure 7.2.8 shows a series of pictures of the craters of AT-2 at 0, 2,000, and 3,000 cycles. Figure 7.2.9 shows another series of pictures of micro surface discontinuities at 0, 2,000, and 3,450 cycles. These pictures show no changes of the discontinuities. Figure 7.2.10 shows a series of pictures at four locations, base metal, HAZ, edge of weld, and center of weld at 300, 2,000, and 3,450 cycles. Figure 7.2.11 shows the fatigue fracture of AT-2.

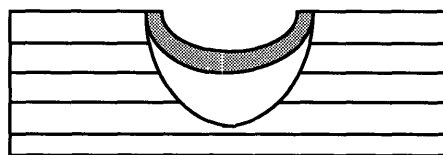


Figure 7.2.7. Section of crater

## 7.2.4 Titanium Alloy

Titanium alloy welded by automatic GTAW failed at its start-up toe around 17,930 cycles due to fatigue with 75% cyclic load of ultimate tensile strength. The weldment of titanium alloys show their large grains which are visible without using any microscope. The grain boundaries are often weaker than grains themselves. Therefore, crack initiation may occur on the boundaries. Although grain slips on the boundaries were observed through tensile test shown in Figure 7.2.15, they were not seen through the fatigue test. Figure 7.2.12 shows a series of pictures of the craters of TT-2 at 500, 9,000, and 17,930 cycles. Figure 7.2.13 shows another series of pictures of micro surface discontinuities at 0, 9,000, and 17,930 cycles. These pictures show no changes of

the discontinuities. Figure 7.2.14 shows a series of pictures at four locations, base metal, HAZ, edge of weld, and center of weld at 0, 6,000, and 14,000 cycles. Figure 7.2.16 shows the fatigue fracture of TT-2.

AT-2  
(3,450 cycles)  
6.5X

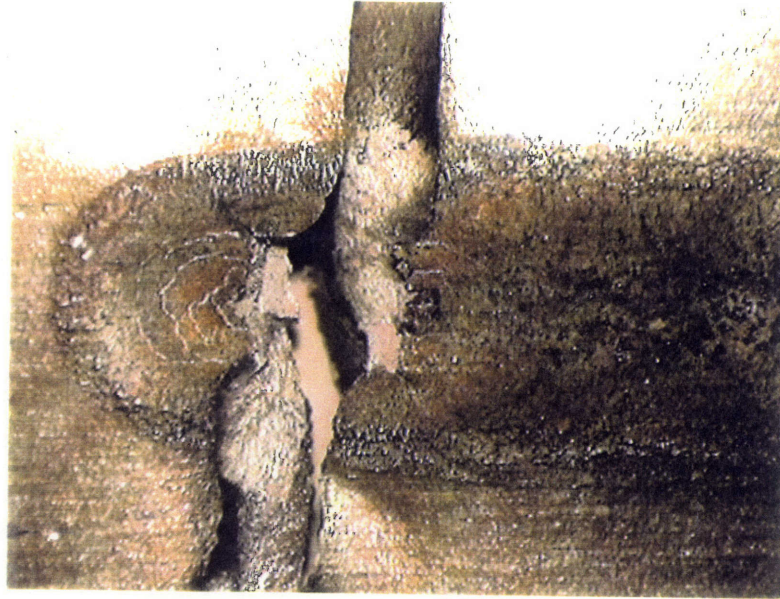
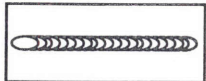


Figure 7.2.11. Fatigue fracture of AT-2

TT-2  
(17,930 cycles)  
6.5X

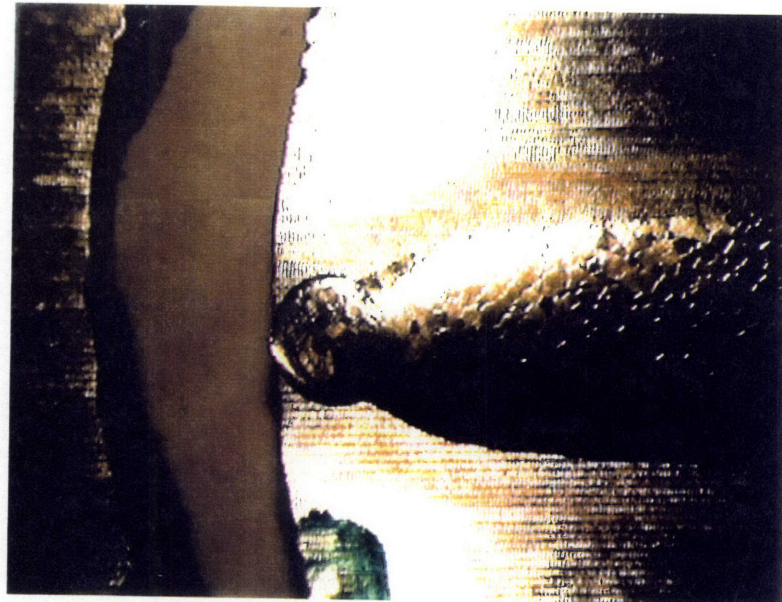
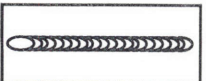
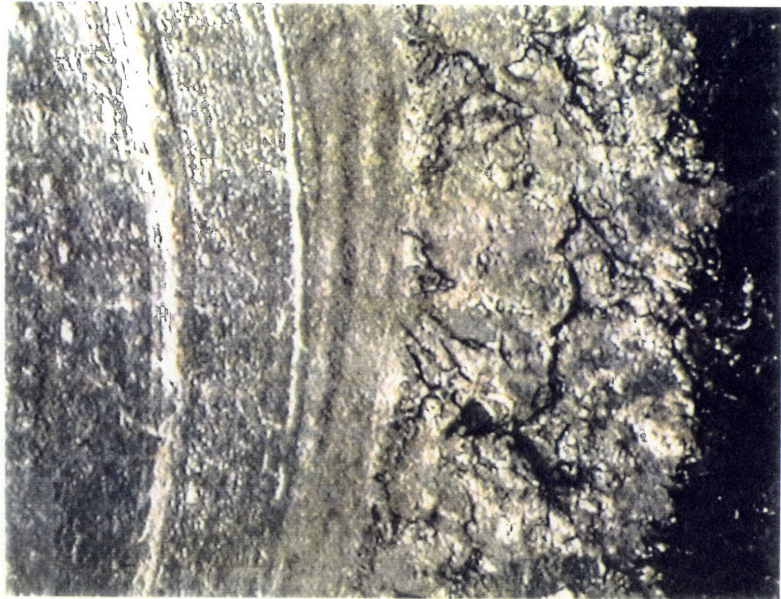
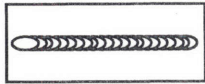


Figure 7.2.16. Fatigue fracture of TT-2

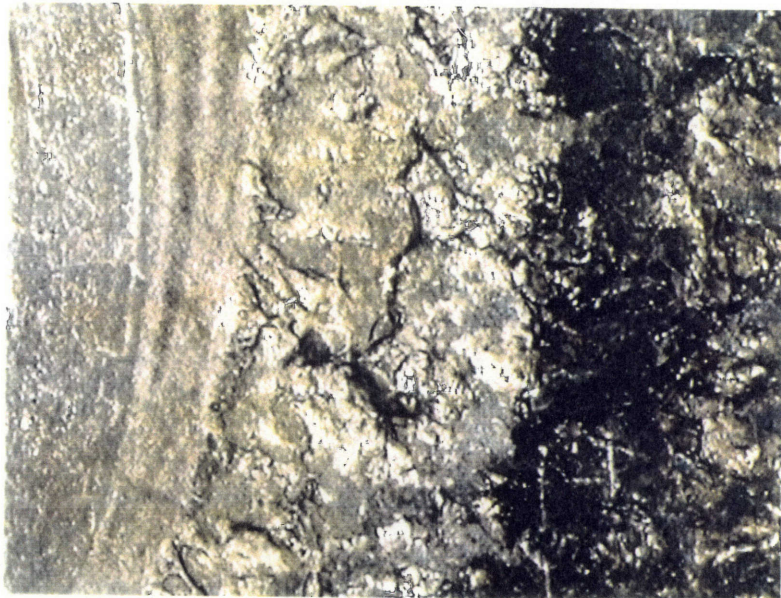
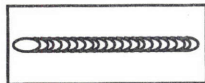
MT-3  
(0 cycle)

84X



MT-3  
(13,000 cycles)

84X



MT-3  
(23,000 cycles)

84X

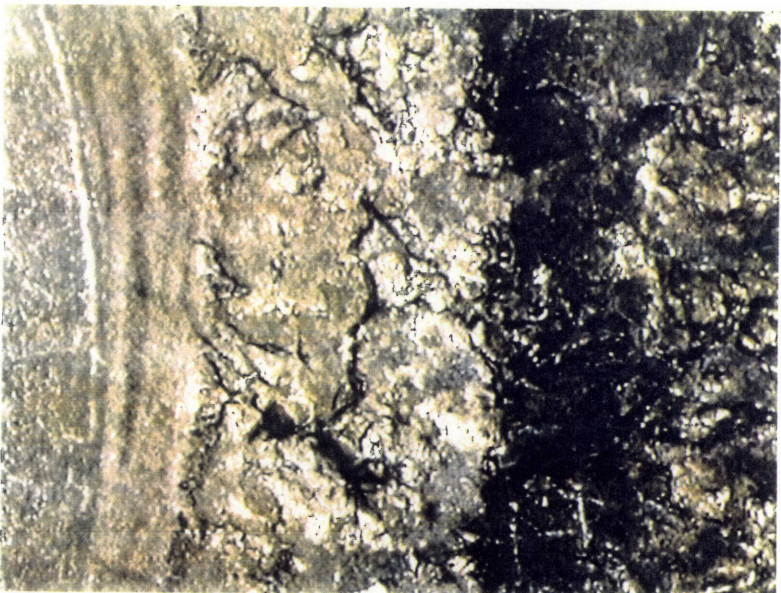
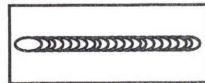


Figure 7.2.1. Surface discontinuity (Type V1) at start-up toe of MT-3

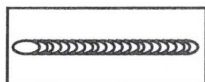
MT-3  
(0 cycle)

84X



MT-3  
(13,000 cycles)

84X



MT-3  
(23,000 cycles)

84X

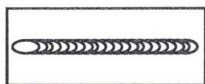
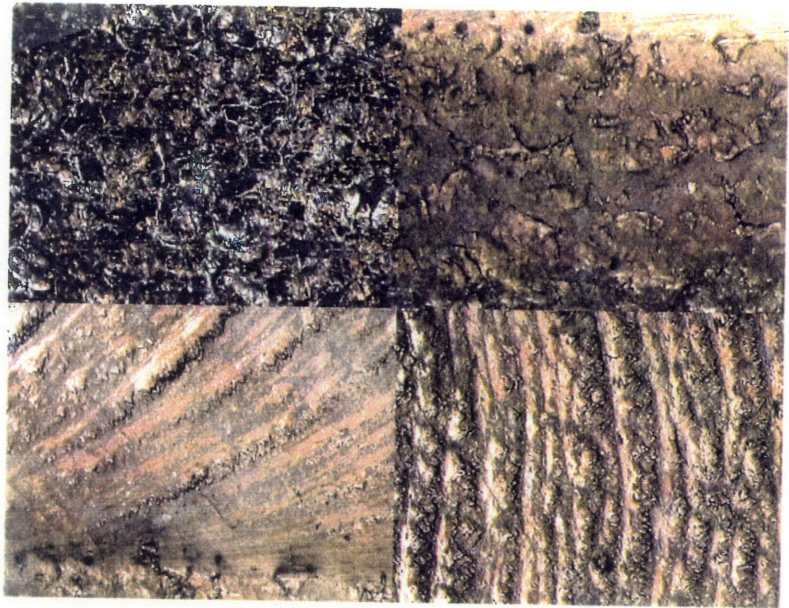
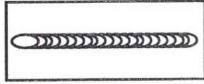


Figure 7.2.2. Surface discontinuity (inclusion) at weld edge of MT-3



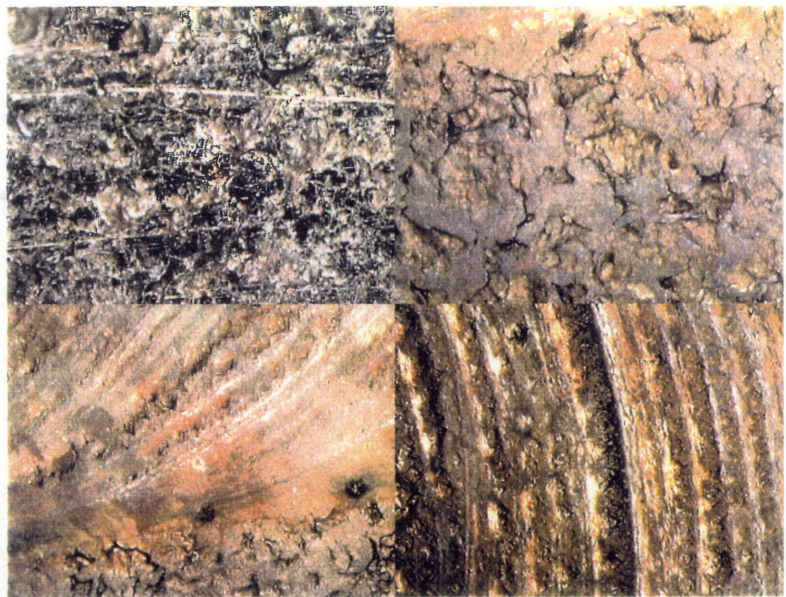
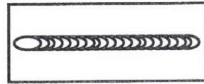
MT-3  
(300 cycle)

B.S. 42X	HAZ 42X
Edge 42X	Center 42X



MT-3  
(23,000 cycles)

B.S. 42X	HAZ 42X
Edge 42X	Center 42X



MT-3  
(40,000 cycles)

B.S. 42X	HAZ 42X
Edge 42X	Center 42X

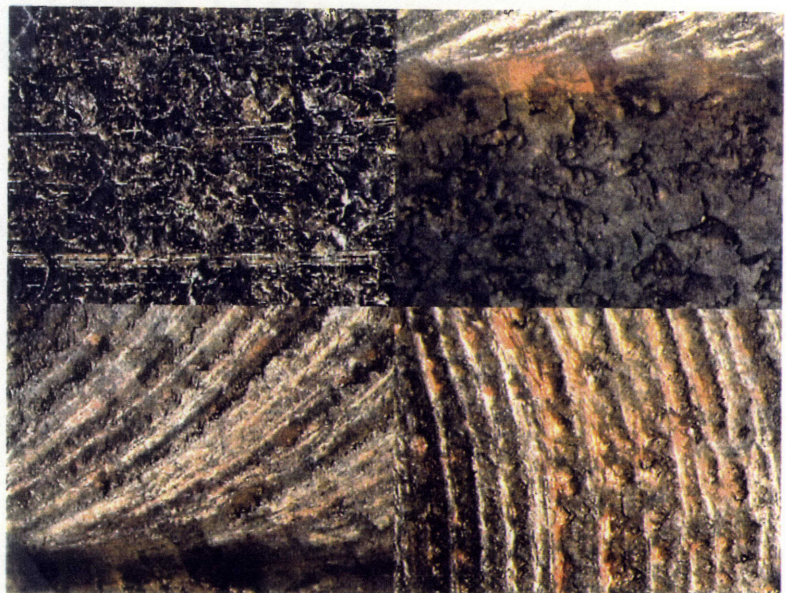
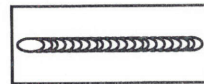
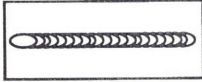


Figure 7.2.3. Surface features of MT-3

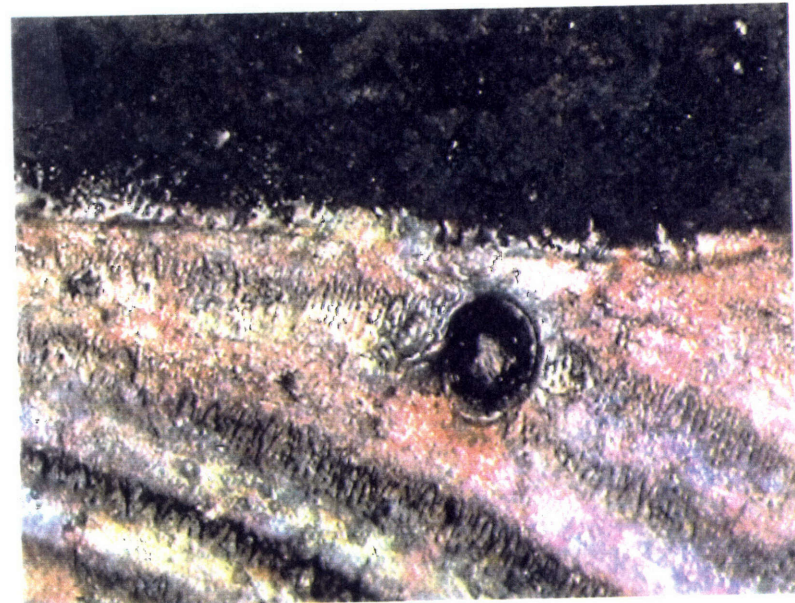
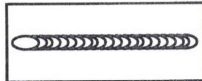
ST-3  
(500 cycle)

84X



ST-3  
(14,000 cycles)

84X



ST-3  
(24,000 cycles)

84X

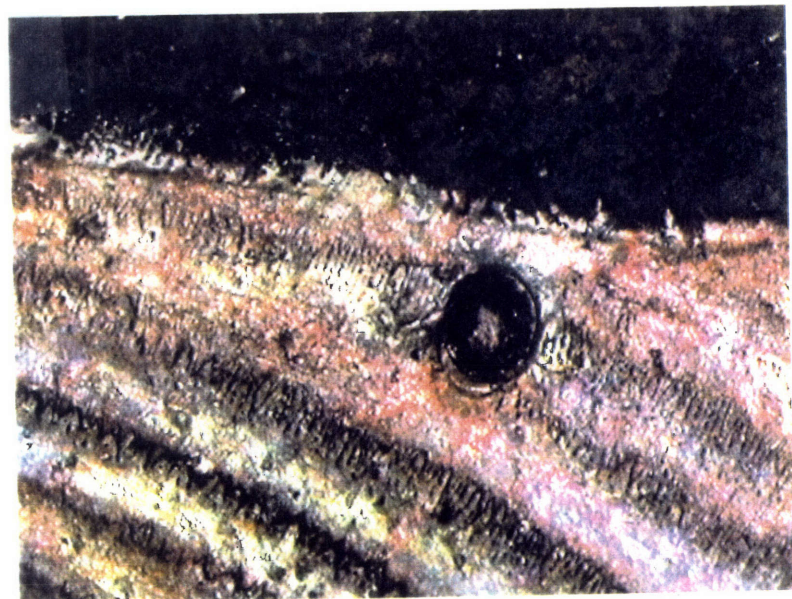
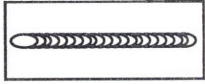


Figure 7.2.4. Surface discontinuity (inclusion) of ST-3

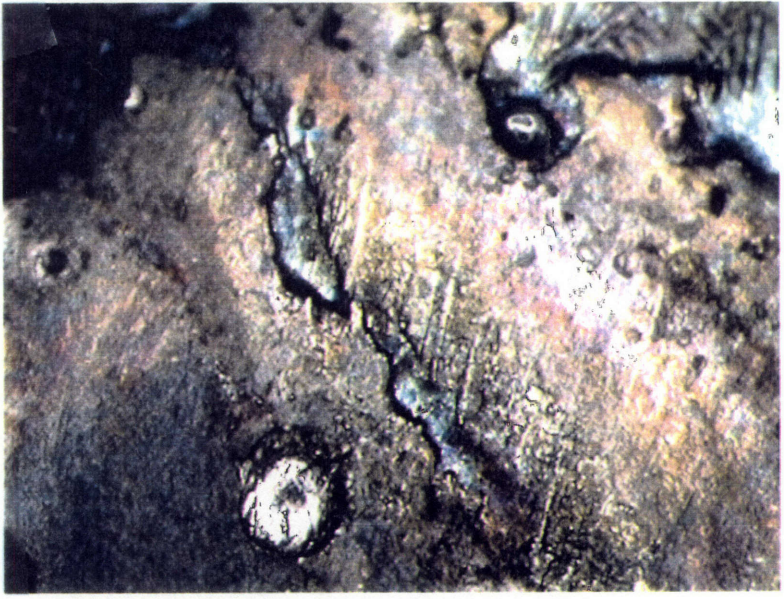
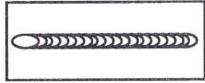
ST-3  
(500 cycle)

84X



ST-3  
(14,000 cycles)

84X



ST-3  
(40,000 cycles)

84X

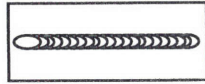
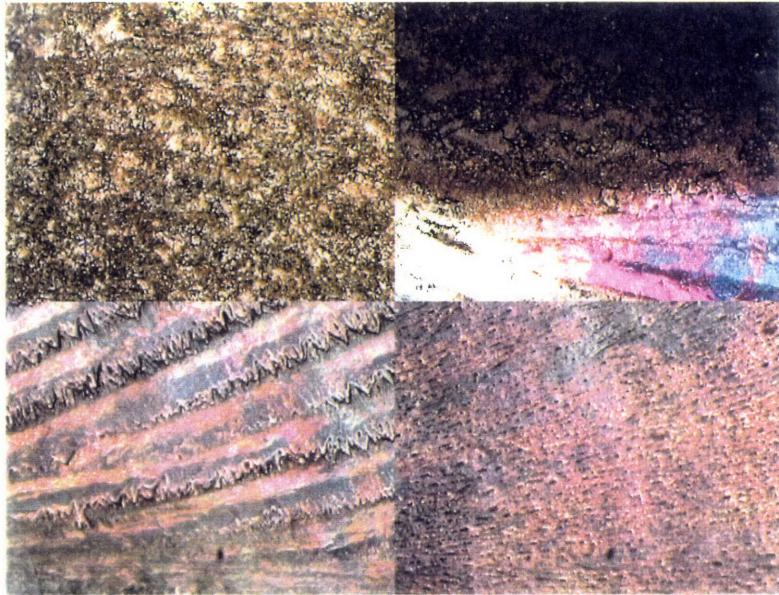
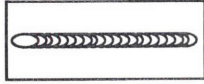


Figure 7.2.5. Surface discontinuity at crater of ST-3

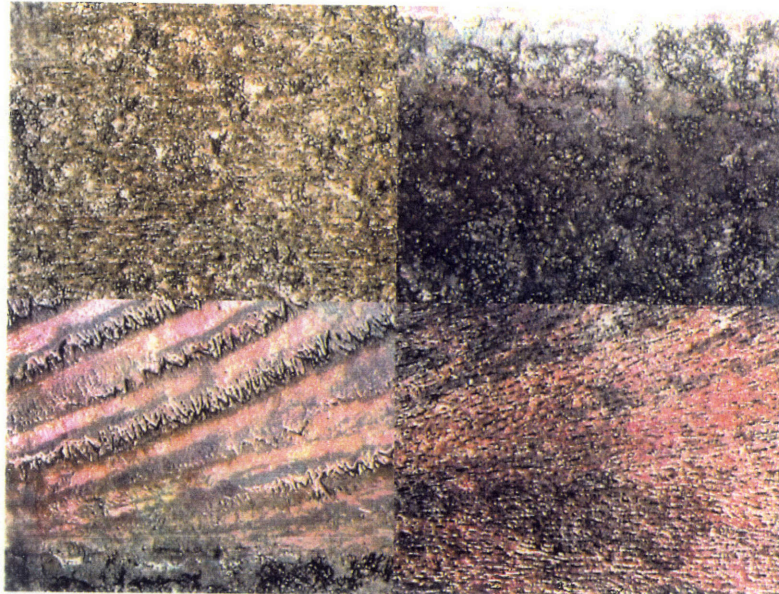
ST-3  
(0 cycle)

B.S. 42X	HAZ 42X
Edge 42X	Center 42X



ST-3  
(14,000 cycles)

B.S. 42X	HAZ 42X
Edge 42X	Center 42X



ST-3  
(40,000 cycles)

B.S. 42X	HAZ 42X
Edge 42X	Center 42X

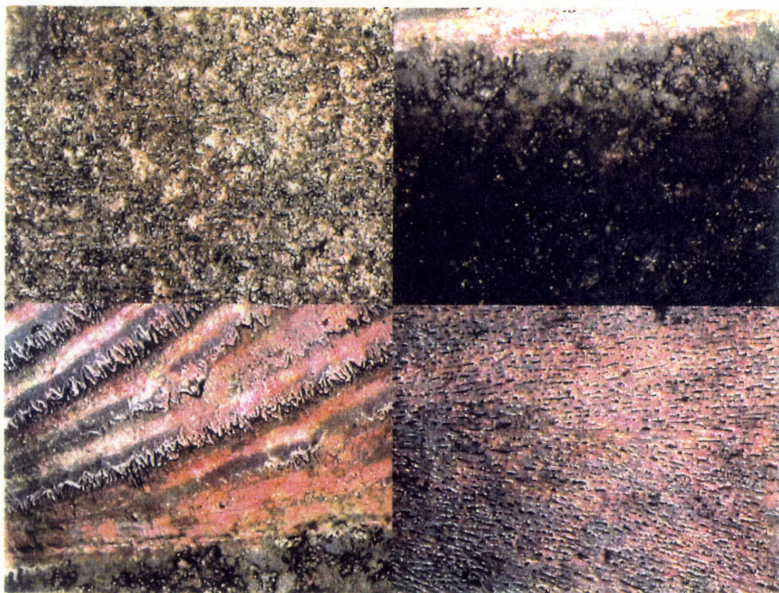
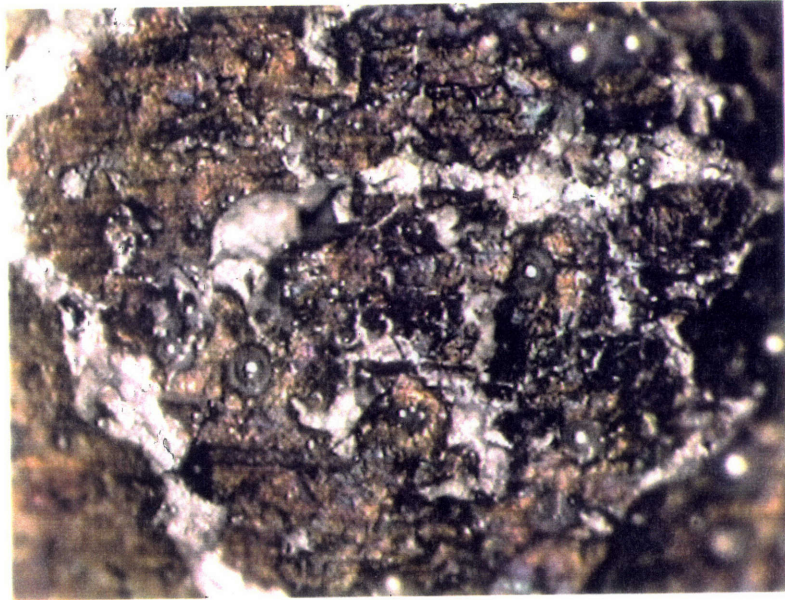
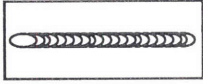


Figure 7.2.6. Surface features of ST-3

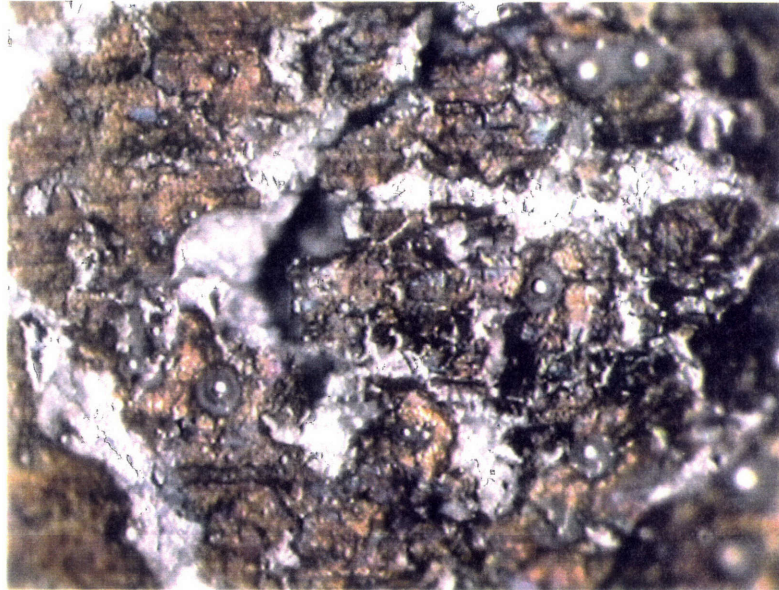
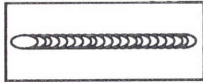
AT-2  
(0 cycle)

84X



AT-2  
(2,000 cycles)

84X



AT-2  
(3,000 cycles)

84X

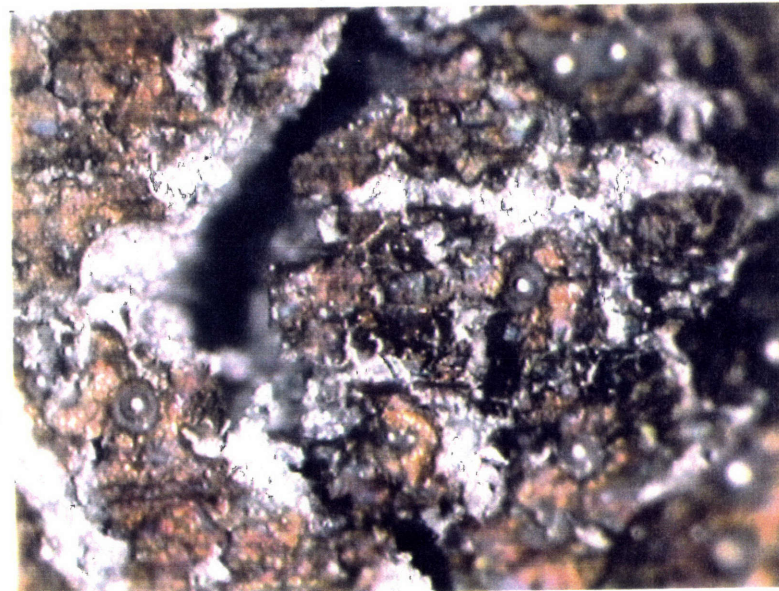
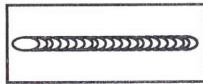
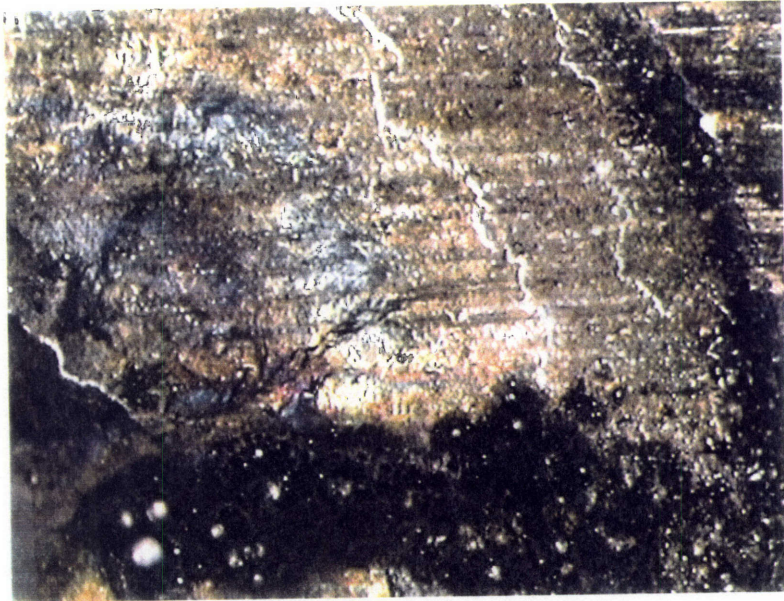
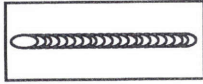


Figure 7.2.8. Surface discontinuity at crater of AT-2

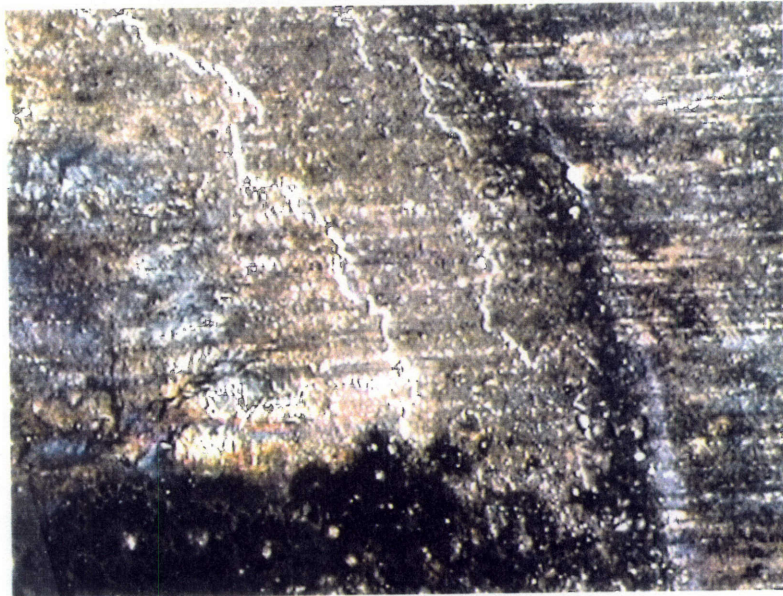
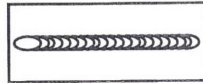
AT-2  
(0 cycle)

84X



AT-2  
(2,000 cycles)

84X



AT-2  
(3,450 cycles)

84X

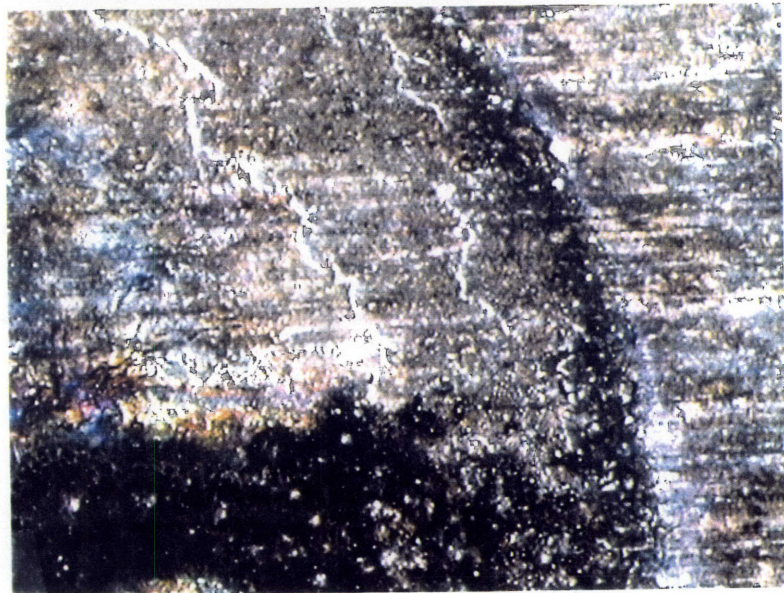
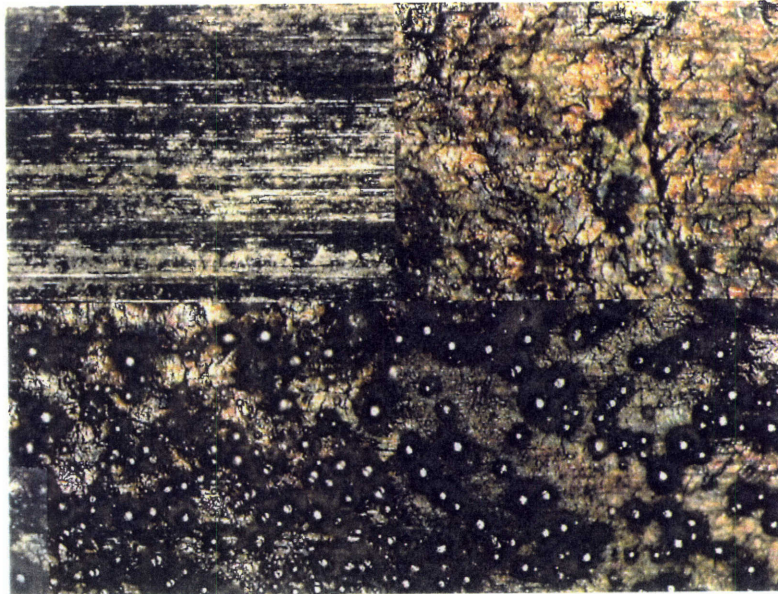
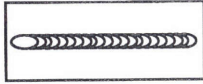


Figure 7.2.9. Surface discontinuity at start-up toe of AT-2

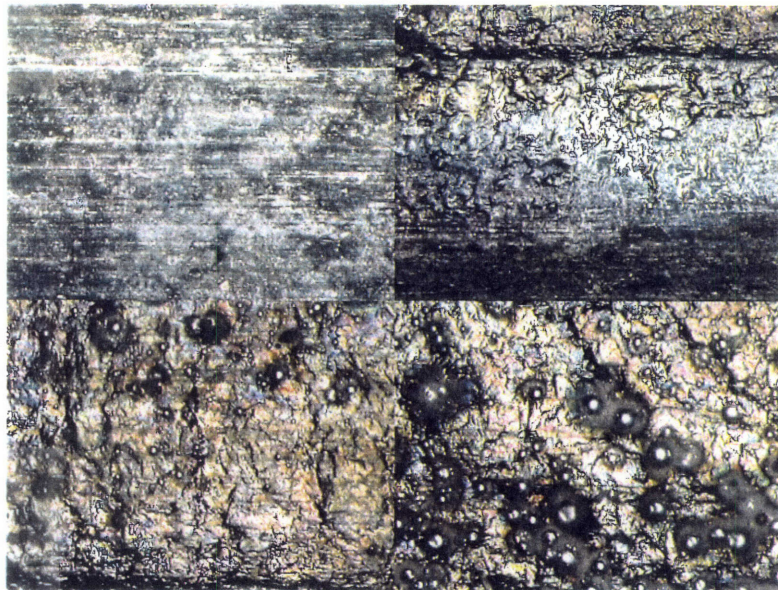
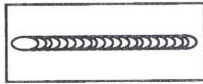
AT-2  
(300 cycle)

B.S. 42X	HAZ 42X
Edge 42X	Center 42X



AT-2  
(2,000 cycles)

B.S. 42X	HAZ 42X
Edge 42X	Center 42X



AT-2  
(3,450 cycles)

B.S. 42X	HAZ 42X
Edge 42X	Center 42X

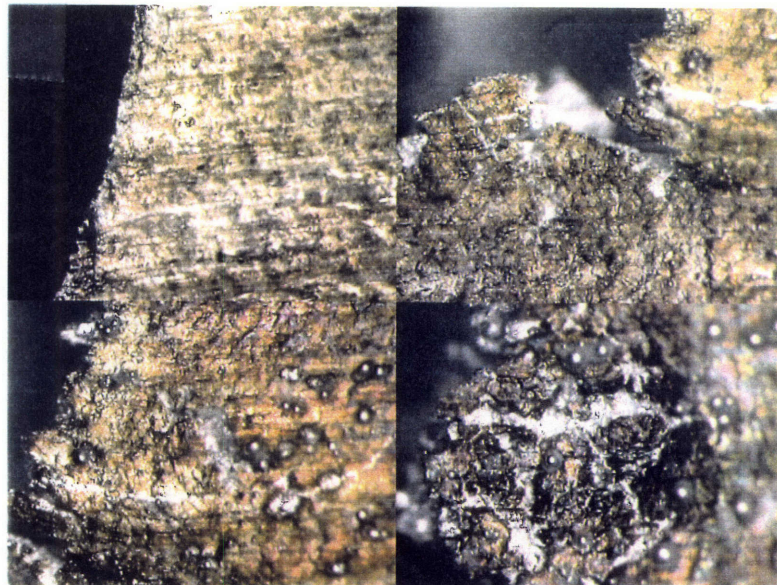
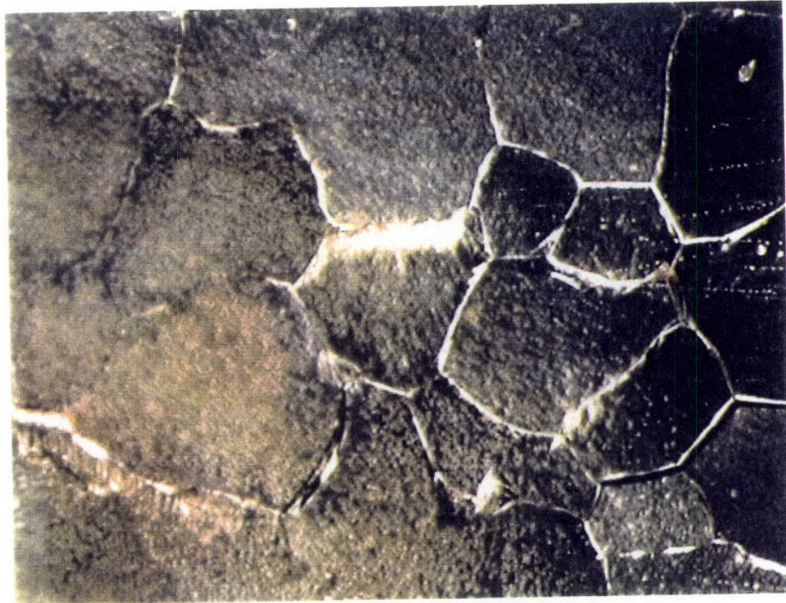
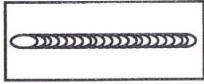


Figure 7.2.10. Surface features of AT-2

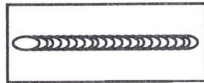
TT-2  
(500 cycle)

84X



TT-2  
(9,000 cycles)

84X



TT-2  
(17,930 cycles)

84X

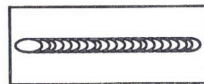
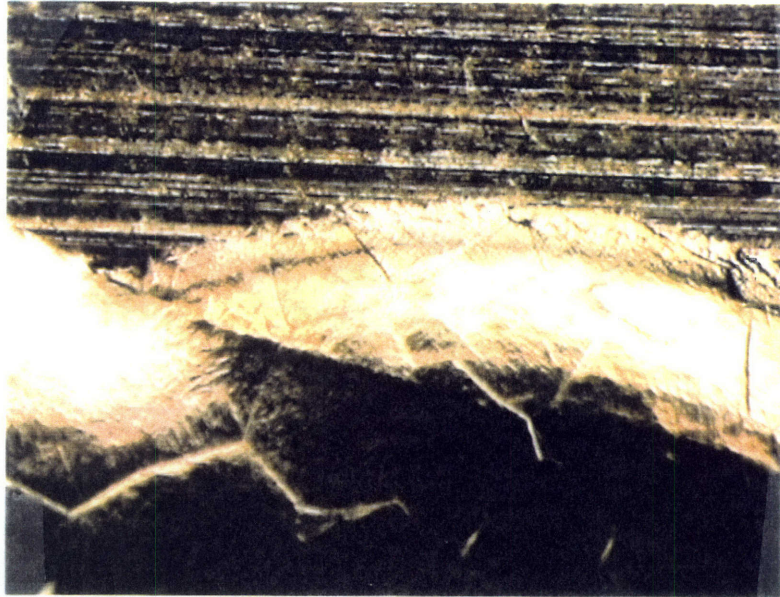
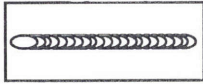


Figure 7.2.12. Surface discontinuity at crater of TT-2



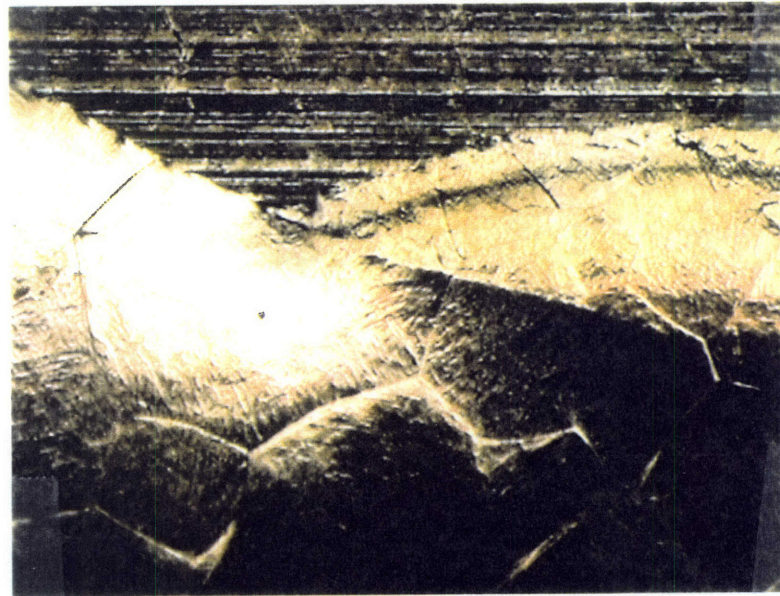
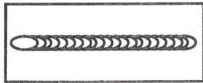
TT-2  
(0 cycle)

84X



TT-2  
(9,000 cycles)

84X



TT-2  
(17,930 cycles)

84X

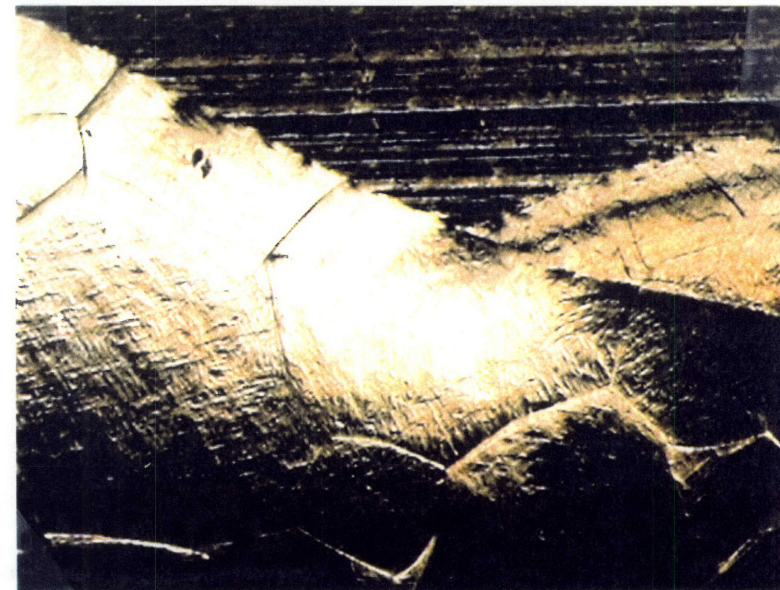
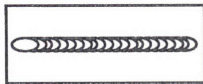
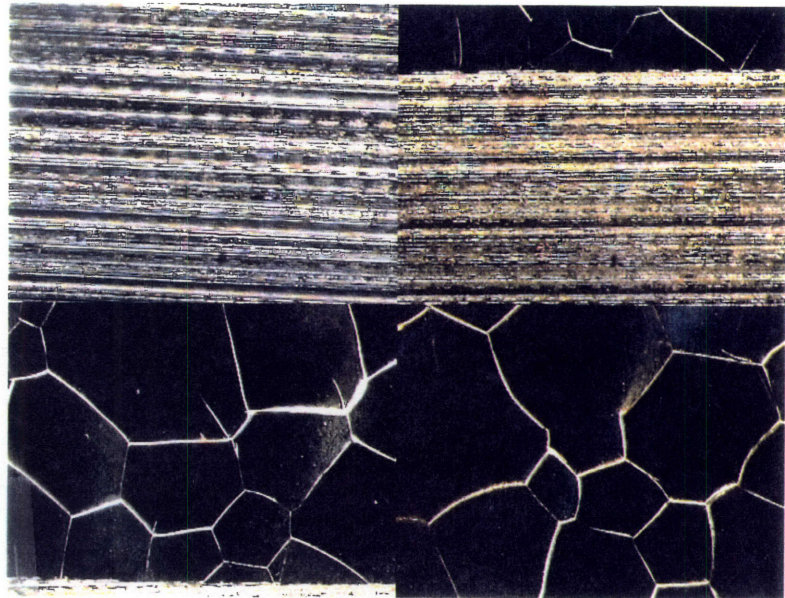
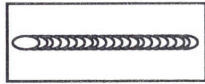


Figure 7.2.13. Surface discontinuity at weld edge of TT-2

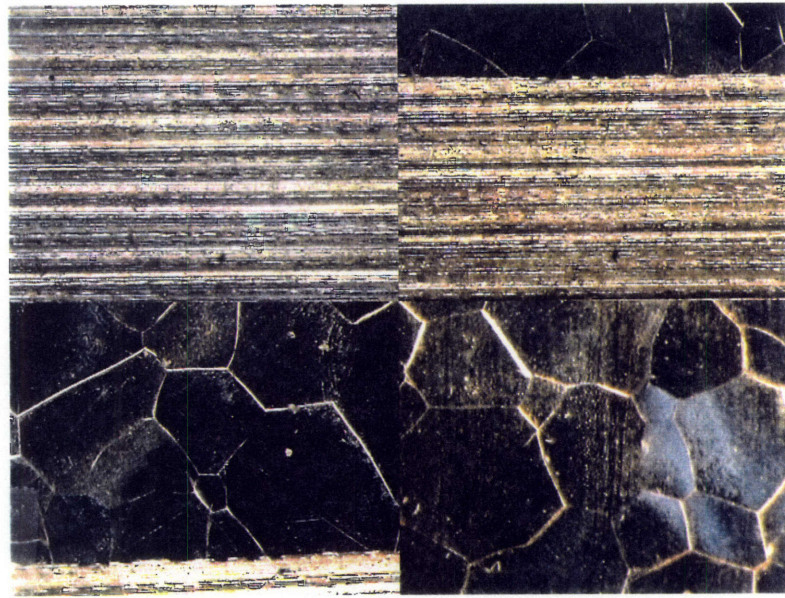
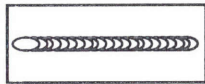
TT-2  
(0 cycle)

B.S. 42X	HAZ 42X
Edge 42X	Center 42X



TT-2  
(6,000 cycles)

B.S. 42X	HAZ 42X
Edge 42X	Center 42X



TT-2  
(14,000 cycles)

B.S. 42X	HAZ 42X
Edge 42X	Center 42X

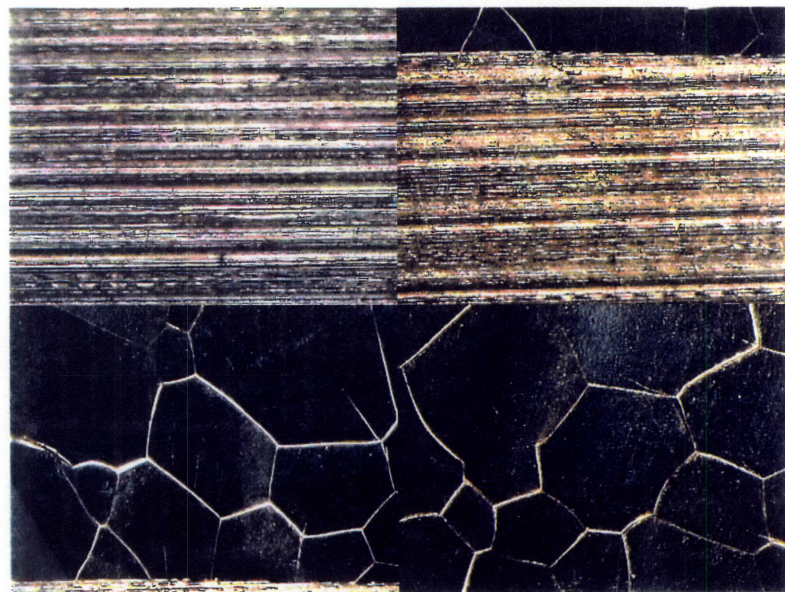


Figure 7.2.14. Surface features of TT-2

TT-1

84X

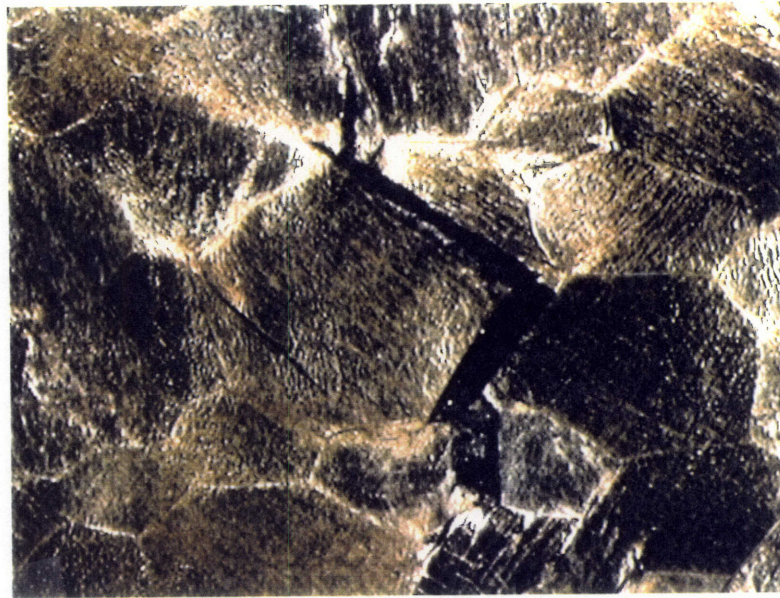
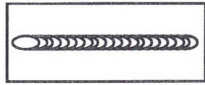


Figure 7.2.15. Grain slip after tensile strength test

# Chapter 8: Conclusions and Recommendations

## 8.1 Conclusions

There are several findings arrived at through the experimental work as follows:

- 1 The combination of a CSLM and a PVIM showed good observation capability. PVIM was useful to scan and find micro discontinuities all over the welded materials, while a CSLM was necessary to determine if the type of the discontinuity was horizontal or vertical, i. e. a shallow irregularity or a crack and to measure the depth or the height of the discontinuities.
2. The surface of welds are not always clear, often covered by oxides and several different types of surface discontinuities and colored dark. In such cases, it is difficult to observe specimens by a CSLM, because the reflected laser illumination is not bright enough to observe them. Laser light cannot penetrate into deep cracks and thus it is impossible to see the bottom and to measure the depth.
3. General information about microstructural surface discontinuities of the welded materials was essential to observe the fatigue test specimens, because it helped to find cracks and the surface information often disappeared after a fatigue test.
4. Only one fatigue crack grew to failure after it became large enough to be able to recognize on the monitor using the PVIM for most of the specimens.
5. Microstructural surface discontinuities themselves do not grow except the ones in the area of weld crater. Instead, a crack newly created by fatigue grows.

6. Microstructural surface discontinuities seemed to affect the initiation of the fatigue cracks due to stress concentrations around them.
7. The types of materials did not make any difference on the result that the surface discontinuities created through the welding processes did not grow after fatigue tests.
8. It is difficult to detect and specify the microstructural features which may have some influence on fatigue crack initiations in the early stages, because it is unpredictable from which parts the crack initiates and often oxides cover the microstructural features of fatigue cracking.
9. The inspection using a CSLM and a PVIM is limited to observe only surfaces of weldments. In order to detect sub-surface discontinuities, another NDE method such as an ultrasonic testing and a radio graphic testing should also be used.

Although the findings above could be obtained through limited experimental works, it will be necessary to run many more experiments to allow a meaningful statistical treatment of the data.

## 8.2 Practical Use of Results

Many structures including bridges and ships in the world are facing the dangers of fatigue fracture during their long service life. The findings of this research can suggest a new NDE to enable us to maintain and prevent such structures from failing due to fatigue.

Observe the surface of the weldments of the structures and find cracks while the structures are in service using a PVIM. If the cracks cannot be distinguished from other surface discontinuities, use replica techniques and a CSLM to identify cracks. After a certain period of time, observe the same cracks. If one of them has grown, it can be an initiation of fatigue crack growth. Therefore, repair or stress reduction of the area is necessary to prevent the structure from failing. There are two possible ways of repair. One is re-welding and it is only temporarily useful, since the same part contains enough stress to have another fatigue crack form again in the future. The other method is reinforcing the structure to reduce stresses in the area which showed the fatigue crack initiation. This method is more recommended, because it can remove the fear of having future fatigue fractures from the same area permanently. Because fatigue fractures of welded structures tend to fail from their welded parts, the parts should be inspected. This means that proper line inspection along welds can prevent most of the dangers of having future fatigue fracture. Line process is easily automated and this whole process to detect fatigue cracks can be automated in the future.

### 8.3 Recommendations

It is strongly recommended that more experiments be run to assure the findings obtained in this research. The findings may depend on the experimental conditions such as welding processes used to have a bead on plate, size of beads or specimens, or fatigue loading conditions.

The following possibilities can be considered to extend this research.

1. To verify the effects of material types to our findings, all the specimens used for the surface observation can be inspected by fatigue test,
2. To establish practical uses, use currently used specimens in industries,
3. Remove the oxides covering the surface of the specimens, conduct the same experiments, and compare the results.

# References



- [1] Masubuchi, K., Analysis of Welded Structures, Pergamon Press, 1980
- [2] Paris, P., "Fatigue Crack Growth," the Text used for the Workshop in Fracture Mechanics, August 16-28, 1964 held at Denver Research Institute sponsored by Universal Technology Corporation, Dayton, Ohio
- [3] Cushing, J. M., Jr., "Weld Surface Microstructure as an Indication of Fatigue Life for Marine Structures," Master's thesis, M.I.T., May 1992
- [4] Tannery, P., "Early Detection of Fatigue Damage in a Weldment by Use of a Laser Microscope and a Portable Video Microscope," Master's thesis, M.I.T., May 1993
- [5] Olsen, E., "Initiation and Growth of Microcracks in High Strength Steel Butt Welds," Engineer's thesis, M.I.T., May 1993
- [6] Douglas, S. A., "Mechanisms of Forming Intergranular Microcracks and Microscopic Surface Discontinuities in Welds," Engineer's thesis, M.I.T., May 1992
- [7] Kammer, P. A., Masubuchi, K., and Monroe, R. E., "Cracking in High Strength Steel Weldments," A Critical Review, DMIC Report 197, Defence Metals Information Center, Battelle Memorial Institute, Columbus, Ohio, Feb. 1964
- [8] Wood, W. A., "Recent observations on fatigue fracture in metals," ASTM STP 237, (1958) pp. 110-121
- [9] Liaw, P. K., Yang, C. Y., and Palusamy, S., "Fatigue Crack Initiation: Detection Methods and Micromechanisms," Welding Research Council Progress Reports, Vol. XLVI, No. 9/10, Sept/Oct 1991
- [10] McClintock, F. A., and Argon, A. S., Mechanical Behavior of Materials, Addison-Wesley Publishing Company, Inc., Reading MA, 1966
- [11] David Broek, Elementary Engineering Fracture Mechanics, Kluwer Academic Publishers, 1986

- [12] Awamura, D., Ode, T., and Yonezawa, M., "Scanning Color Laser Microscope," Proceedings of the International Society for Optical Engineering, Vol. 921, 1988, pp. 388-394
- [13] Almar-Naess, A., editor, Fatigue Handbook - Offshore Steel Structures, Tapir, 1985
- [14] Nakamura, T., "Observation of Discontinuities in Welding," Special Project, M.I.T., August 1992
- [15] Liaw, P. K., Yang, C. Y., and Palusamy, S., "Fatigue Crack Initiation: Detection Methods and Micromechanisms," Welding Research Council Progress Reports, Vol. XLVI, No. 9/10, Sept/Oct 1991
- [16] Paris, P. C., "The Growth of Fatigue Cracks due to variations in Load," Ph.D. Thesis, Lehigh University 1962
- [17] Paris, P. C., Gomez, M. P. and Anderson, W. E., "A Rational Analytic Theory of Fatigue," The Trend in Engineering, 13, 1961, pp9-14

# Appendices

A-1 Observation Data

A-2 Fatigue Test Data

# Appendix

## Table A-2

### Observation Data

<b>MT-1</b>									
<b>Micro Surface Discontinuities</b>					<b>Grains</b>			<b>Oxides</b>	
	Type	Density	Size(um)	Shape	Density	Size (um)	Shape	Color	Thickness
<b>HAZ</b>	1	(same as base metal)		No			narrow band	brown	very thin layer
	2								
<b>Edge</b>	1	very few		random	few #1	50-80	all over	brown	very thin layer
	2	very few							
<b>Center</b>	1	all over		random	few #1	20~	all over	brown	very thin layer
	2	all over			(N.A.S. due to ripples)				
<b>other</b>	1	all over		random	few #1	40~	all over	brown	very thin layer
	2	all over							
	3	all over							
<b>MT-2</b>									
<b>Micro Surface Discontinuities</b>					<b>Grains</b>			<b>Oxides</b>	
	Type	Density	Size(um)	Shape	Density	Size (um)	Shape	Color	Thickness
<b>HAZ</b>	1	(same as base metal)		No			narrow band	brown	thin layer
	2								
<b>Edge</b>	1			random	some #3	80-220	all over	grey	thicker
	2	ripples							
<b>Center</b>	1			random	few #2	40-60	all over	grey	thicker
	2	ripples							
<b>other</b>	1	all over			few #2	50?	all over	grey	thicker
	2	all over							
	3								
<b>MT-3</b>									
<b>Micro Surface Discontinuities</b>					<b>Grains</b>			<b>Oxides</b>	
	Type	Density	Size(um)	Shape	Density	Size (um)	Shape	Color	Thickness
<b>HAZ</b>	1	(N.A.S. due to oxides)		No			narrow band	brown	thicker layer
	2								
<b>Edge</b>	1			random	many #4	80-200	all over	grey	thicker
	2	ripples							
<b>Center</b>	1			random	few #2	40~	all over	grey	thicker
	2	ripples							
<b>other</b>	1				few #2	40~	all over	grey	thicker
	2								
	3								

<b>MLI-1</b>											
<b>Micro Surface Discontinuities</b>				<b>Grains</b>				<b>Oxides</b>			
	Type	Density	Size(um)	Shape	Density	Size (um)	Shape	Color	Thickness		
<b>HAZ</b>	1	part of GB continuous from Edge 1	many #2	~25	round	all over	~2	0.3mm band	grey	thin layer	
	2							0.1mm band	black+7 colors	thick	
	3							0.3mm band			
<b>Edge</b>	1	GB+H.C.		10~25x150	normal		13~30x40~200	all over	grey	not thick	
	2				SGB		2~3				
<b>Center</b>	1	cracks like GB (H.C.+C.C.)	like normal GB	15~30	SGB	all over #3	3~5	all over	grey	not thick	
	2										
<b>other</b>	1	cracks like GB (H.C.+C.C.)		15~30	round/oval	all over #3	3~5/3x10				
	2										
<b>MLI-2</b>											
<b>Micro Surface Discontinuities</b>				<b>Grains</b>				<b>Oxides</b>			
	Type	Density	Size(um)	Shape	Density	Size (um)	Shape	Color	Thickness		
<b>HAZ</b>	1	GB		10~20	round	all over	2~4	0.3mm band	grey	very thin layer	
	2							1.0mm band	black+7 colors	thick	
	3										
<b>Edge</b>	1	GB like crack (round/oval)		10~20x~30	round	all over	2~4	0.2mm band	grey	thin	
	2							0.5mm band	black	thick	
<b>Center</b>	1	cracks like GB		15~40	round/normal		5~8/~15	all over	black	thick	
	2										
<b>other</b>	1	cracks like GB (round)		D30~40							
	2										
<b>MLI-3</b>											
<b>Micro Surface Discontinuities</b>				<b>Grains</b>				<b>Oxides</b>			
	Type	Density	Size(um)	Shape	Density	Size (um)	Shape	Color	Thickness		
<b>HAZ</b>	1	GB like crack (H.C.)		10~25	round	all over	2~4	0.3mm band	grey	very thin layer	
	2							1.0mm band	black	very thick	
	3										
<b>Edge</b>	1	GB like crack (round/oval)		15~40/100max	round	many	3~7	0.3mm band	grey	thin	
	2							0.5mm band	black	very thick	
<b>Center</b>	1	cracks like GB		50~80	round		5~8	all over	black	very thick	
	2	(N.A.S.M. due to oxide)							black	very thick	
<b>other</b>	1	cracks like GB		~40	round		4~8				
	2	(N.A.S.M. due to oxide)									

<b>ML2-1</b>									
<b>Micro Surface Discontinuities</b>					<b>Grains</b>			<b>Oxides</b>	
Type	Density	Size(um)	Shape	Density	Size (um)	Shape	Color	Thickness	
<b>HAZ</b>		(N.A.S)		(N.A.S)					
1									
2									
<b>Edge</b>									
1	GB, H.C.+C.C.	pass through SG	15-40/40x100	pass through SG		normal	many #4	15-40	thick
2	GB, H.C.+C.C.	pass through SG				oval	many #4	max 40-100	thin
3	SG					SCGB (round)	many #4	5-7	thin
<b>Center</b>									
1	SGB					SGB (round/oval)	many #4/some #1	~3/10x3	thick
2	GB+C.C.	pass through SG				GB (normal)	#2	15-40	
1	SGB					SGB (round)	all over #5	3-5	
2	GB+C.C.					GB (normal)	all over #1	15-40	
<b>other</b>									
1									some clear parts on weld metals  grey   very thin
2									
<b>ME-2</b>									
<b>Micro Surface Discontinuities</b>					<b>Grains</b>			<b>Oxides</b>	
Type	Density	Size(um)	Shape	Density	Size (um)	Shape	Color	Thickness	
<b>HAZ</b>									
1	GB continuous from Edge					GB continuous from Edge			thick
2						(N.A.S.M. due to oxide)	black		
<b>Edge</b>									
1	GB (normal/oval)	15-40/40x200				normal/oval	all over #5	15-40/40x200	thick
2						SGB (normal)	some #4	3-5	
3									
<b>Center</b>									
1	SGB					SGB (round/oval)	70%/20%	3-5/1.5x3max	thick
2	GB+C.C.+H.C.					structure (round)	10%	~10	
3						SGB (round/oval)	70%/30%	3-5/3x1.5	
<b>Others</b>									
1	GB+C.C.+H.C.								some clear parts on weld metals  grey   very thin
<b>ML2-3</b>									
<b>Micro Surface Discontinuities</b>					<b>Grains</b>			<b>Oxides</b>	
Type	Density	Size(um)	Shape	Density	Size (um)	Shape	Color	Thickness	
<b>HAZ</b>									
1	GB continuous from Edge								thick
2	(N.A.S.M. due to oxide)						black		
<b>Edge</b>									
1	GB	all over	10x10/60x300	all over		SGB (round)	20%	~3/	thin
2									
3									
<b>Center</b>									
1	GB+C.C.+H.C.					round/oval	10%	3-5/2.5x3max	very thin
2						structure (round)		~15	
<b>other</b>									
1	GB+C.C.+H.C.					SGB (round/oval)		5-7/	
2									

**ME-1**

Micro Surface Discontinuities			Grains			Oxides		
Type	Density	Size(um)	Shape	Density	Size (um)	Shape	Color	Thickness
<b>HAZ</b>	1 H2	every 10um	~15	normal	some, #2	band	brown	very thin layer
	2 GB+H.C.			normal	some, #2	band	black	thick layer
<b>Edge</b>	1 GB, continuous from HAZ			round	all over 60%	band	brown	very thin layer
	2 H2 from HAZ			oval	30%			
	3 H3, H.C.	many	<50	large structure	10%			
<b>Center</b>	1 H3, C.C.	all over	~20	round	all over	band	brown	very thin layer
	2 H1, H2, C.C.			oval	30%			
	3 H3, H.C.			large structure	10%			
	4			round	all over			

**ME-2**

Micro Surface Discontinuities			Grains			Oxides		
Type	Density	Size(um)	Shape	Density	Size (um)	Shape	Color	Thickness
<b>HAZ</b>	1 H2+H.C.	Some along HAZ	~10	normal	some, #3	band	brown	very thin layer
	2 GB+H.C.			normal	some, #3	wider band	black	thick layer
<b>Edge</b>	1 GB, continuous from HAZ+H.C.			round	all over 15%	narrower band	brown	thin layer
	2 H2, H.C.	every 30um	<120	oval	80%			
	3 H3, H.C.	many		large structure	5%			
<b>Center</b>	1 H3, C.C.	all over		GB round	all over			
	2 H1, H2, C.C.	some						
	3 H3, H.C.	many						
	4							

**ME-3**

Micro Surface Discontinuities			Grains			Oxides		
Type	Density	Size(um)	Shape	Density	Size (um)	Shape	Color	Thickness
<b>HAZ</b>	1 H2	every 40um	<35	normal	some, #3	band	brown	very thin layer
	2 GB,+H.C.			normal	some, #2	wider band	black	thicker layer
<b>Edge</b>	1 GB, from HAZ	every 40um	<150	dendrite	15%	narrowest band	brown	not thin layer
	2 (N.A.S.M. due to oxide)			normal	80%			
	3			large structure	5%			
<b>Center</b>	1 H3, C.C.	all over	50	round	some			
	2 H1, H2, C.C.							
	3 H3, H.C.							
	4							



<b>ST-1</b>									
<b>Micro Surface Discontinuities</b>				<b>Grains</b>			<b>Oxides</b>		
	Type	Density	Size(um)	Shape	Density	Size (um)	Shape	Color	Thickness
<b>HAZ</b>	1 V3.1	Many	~300	No			0.3mm band	dark violet	thin
	2						0.4mm band	dark green+blue	thin
	3						0.1mm band	light grey	thin
	4						0.3mm band	white green	thicker
<b>Edge</b>	1 V1	few	~300	No			along ripples	violet	thin
	2 ripple						along ripples	black	thick
<b>Center</b>	1 V3.1		10~30	No			along ripples	violet	thin
	2 ripple						along ripples	black	thick
<b>ST-2</b>									
<b>Micro Surface Discontinuities</b>				<b>Grains</b>			<b>Oxides</b>		
	Type	Density	Size(um)	Shape	Density	Size (um)	Shape	Color	Thickness
<b>HAZ</b>	1 H1, H2, H3	many	20~70 ~100	No			1.0mm band	brown	thin
	2 V3.1						0.5mm band	dark violet	thicker
	3						0.8mm band	blue	thick
	4						0.3mm band	green	thin
	5						0.3mm band	violet	thin
	6						0.3mm band	black	thick
<b>Edge</b>	1 H1, H2	very few many	25 10~30	No			along ipples	violet	thin
	2 V3.1								
	3 ripple								
<b>Center</b>	1 H1, H2	very few all over (many)	10~30 105~110	No			along ipples	violet	thin
	2 GB3								
	3 ripple								
<b>ST-3</b>									
<b>Micro Surface Discontinuities</b>				<b>Grains</b>			<b>Oxides</b>		
	Type	Density	Size(um)	Shape	Density	Size (um)	Shape	Color	Thickness
<b>HAZ</b>	1 H1, H2	few	150	No			2.8mm band	green+violet	thin
	2 ripple						2.1mm band	blue	thin
	3						0.8mm band	green	thin
	4						1.1mm band	black	thick
<b>Edge</b>	1 ripple			No			along ripples	violet	thin
	1 ripple (melted craters)						along ripples	violet	thin
<b>Center</b>	1			No					
<b>Other</b>	1								

**SLI-1**

Micro Surface Discontinuities			Grains		Oxides			
Type	Density	Size(um)	Shape	Density	Size (um)	Shape	Color	Thickness
<b>HAZ</b>	1	(N.A.S)		(N.A.S)		0.2mm band	black	thick
	2	(N.A.S)		(N.A.S)		1.0mm band	blue+brown	thin
<b>Edge</b>	1	(N.A.S)		(N.A.S)		all over	green+grey	thin
	2	(N.A.S)		(N.A.S)		spots	brown	thick
	3	(N.A.S)		(N.A.S)		all over	green+grey	thin
<b>Center</b>	1	(N.A.S)		(N.A.S)		narrow band along ripples	black	thick
	2	(N.A.S)		(N.A.S)				
<b>other</b>	1	(N.A.S)		(N.A.S)				
	2	(N.A.S)		(N.A.S)				

**SLI-2**

Micro Surface Discontinuities			Grains		Oxides			
Type	Density	Size(um)	Shape	Density	Size (um)	Shape	Color	Thickness
<b>HAZ</b>	1	(N.A.S)		(N.A.S)		0.2mm band	black	thick
	2	(N.A.S)		(N.A.S)		1.0mm band	orange	thin
<b>Edge</b>	1	(N.A.S)		(N.A.S)		all over	grey	thin
	2	(N.A.S)		(N.A.S)		spots	green+yellow+red	thick
	3	(N.A.S)		(N.A.S)		all over	black	thick
<b>Center</b>	1	(N.A.S)		(N.A.S)				
	2	(N.A.S)		(N.A.S)				
<b>other</b>	1	(N.A.S)		(N.A.S)				
	2	(N.A.S)		(N.A.S)				

**SLI-3**

Micro Surface Discontinuities			Grains		Oxides			
Type	Density	Size(um)	Shape	Density	Size (um)	Shape	Color	Thickness
<b>HAZ</b>	1	(N.A.S)		(N.A.S)		0.3mm band	black	thick
	2	(N.A.S)		(N.A.S)		1.0mm band	orange	very thin
<b>Edge</b>	1	(N.A.S)		(N.A.S)		all over	grey	thick
	2	(N.A.S)		(N.A.S)		spots	green+yellow+red	very thick
	3	(N.A.S)		(N.A.S)		all over	black	very thick
<b>Center</b>	1	(N.A.S)		(N.A.S)				
	2	(N.A.S)		(N.A.S)				
<b>other</b>	1	(N.A.S)		(N.A.S)				
	2	(N.A.S)		(N.A.S)				

**SL2-1**

		Micro Surface Discontinuities			Grains			Oxides		
		Type	Density	Size(um)	Shape	Density	Size (um)	Shape	Color	Thickness
HAZ	1		(N.A.S.)			(N.A.S.)		0.2mm band	black	thicker
	2									
	3									
Edge	1	H3	all over	~D30	all over	all over #2	10	all over	brown	thin
	2	H2	every 20um	150		all over	~3			
Center	1	GB			SGB (dendrite)	all over	2x15	all over	brown	thin
	2				round		~3			
other	1	H2		25	round	all over	3-5	along ripples	black	thick
	2	GB			round	some planes	~9			

**SL2-2**

		Micro Surface Discontinuities			Grains			Oxides		
		Type	Density	Size(um)	Shape	Density	Size (um)	Shape	Color	Thickness
HAZ	1		(N.A.S.)			(N.A.S.)		0.2mm band	black	thick
	2							1.0mm band	blue+brown	thin
	3							all over	light blue	thin
Edge	1	V3.1, V3.2, GB		D10				all over	brown	thin
	2	H2-V3.1	every 10um	300	SGB (round?)	all over #2	~3			
Center	1	GB			SGB (dendrite)	all over	2x6	all over	brown	thin
	2				SGB (round)		~3			
other	1	GB		800	SGB (round)	all over	2-4	all over	brown	thin
	2	H2-C	every 100um							

**SL2-3**

		Micro Surface Discontinuities			Grains			Oxides		
		Type	Density	Size(um)	Shape	Density	Size (um)	Shape	Color	Thickness
HAZ	1		(same as base metal)					0.3mm band	black	very thick
	2							narrow band	blue	thick
	3									
Edge	1	V3.1-H2	every 10um	<300				0.2mm band	brown	thick
	2									
Center	1	GB	all over		round	all over	3x5	all over	brown	thin
	2				oval	all over	3x9			
other	1	GB	all over	<300	round	all over	3-5	0.5mm band	black	thick
	2	H2-V3.1	every 30um							

<b>SE-1</b>									
<b>Micro Surface Discontinuities</b>					<b>Grains</b>			<b>Oxides</b>	
Type	Density	Size(um)	Shape	Density	Size (um)	Shape	Color	Thickness	
	(same as base metal)		(same as base metal)						
<b>HAZ</b>	1								
	2								
<b>Edge</b>	1	GB2		all over	5	SG (round)			
	2	V3.2		many					
	3								
<b>Center</b>	1	GB formation							
	2	ripples							
<b>Others</b>	1	GB							
	2	ripples							

<b>SE-2</b>									
<b>Micro Surface Discontinuities</b>					<b>Grains</b>			<b>Oxides</b>	
Type	Density	Size(um)	Shape	Density	Size (um)	Shape	Color	Thickness	
	(same as base metal)								
<b>HAZ</b>	1	GB formation							
	2	(same as base metal)							
<b>Edge</b>	1	GB2		many	?	round			
	2	V3.2		some					
	3								
<b>Center</b>	1	GB		all over		oval			
	2								
<b>Others</b>	1	GB		all over		round			
	2								

<b>SE-3</b>									
<b>Micro Surface Discontinuities</b>					<b>Grains</b>			<b>Oxides</b>	
Type	Density	Size(um)	Shape	Density	Size (um)	Shape	Color	Thickness	
	(continuous from Edge)								
<b>HAZ</b>	1	GB formation							
	2								
<b>Edge</b>	1	V3.2		many		?			
	2	V1		many					
	3								
<b>Center</b>	1	GB		all over		oval/round			
	2	ripples							
<b>Others</b>	1	GB		all over		SG (round)			
	2	ripples							

AT-1N										
Micro Surface Discontinuities			Grains			Oxides				
	Type	Density	Size(um)	Shape	Density	Size (um)	Shape	Color	Thickness	
HAZ	1	(same as base metal)		No	(same as base metal)		(same as base metal)	(same as base metal)		
Edge	1			normal	everywhere	2-10	all over	light brown/matalic color	thin layer	
	2						spots	black with white center	very thick	
Center	1	(Vertical discontinuities like mountains)		No			all over	light brown/matalic color	thin layer	
	2						spots	black with white center	very thick	
AT-2N										
Micro Surface Discontinuities			Grains			Oxides				
	Type	Density	Size(um)	Shape	Density	Size (um)	Shape	Color	Thickness	
HAZ	1	(same as base metal)		No			(same as base metal)	(same as base metal)		
Edge	1	(rough surface)		No			all over	light brown/matalic color	thin layer	
	2						less spots	black with white center	very thick	
Center	1	(rough surface)		No			all over	light brown/matalic color	thin layer	
	2						dense spots	black with white center	very thick	
Others	1							(spot size is smaller than 1N)		
AT-2										
Micro Surface Discontinuities			Grains			Oxides				
	Type	Density	Size(um)	Shape	Density	Size (um)	Shape	Color	Thickness	
HAZ	1	(same as base metal)		No			(same as base metal)	(same as base metal)		
Edge	1			No			all over	light brown/matalic color	thin layer	
	2						less spots	black with white center	very thick	
Center	1	Vertical discontinuities like mountains	few	No			all over	light brown/matalic color	thin layer	
	2		every 17um				dense spots	black with white center	very thick	
Others	1							(spot size is between 1N and 2N)		
AT-3										
Micro Surface Discontinuities			Grains			Oxides				
	Type	Density	Size(um)	Shape	Density	Size (um)	Shape	Color	Thickness	
HAZ	1	(same as base metal)		No			(same as base metal)	(same as base metal)		
Edge	1	Vertical discontinuities like mountains	many	No			all over	light blue	very thin	
	2		every 17um				dense spots	black with white center	thin	
Center	1	Vertical discontinuities like mountains	few	No			all over	dark grey	very thick	
	2		every 3um				dense spots	black with white center	thin	
							all over	dark grey	very thick	

<b>ALI-1</b>											
<b>Micro Surface Discontinuities</b>				<b>Grains</b>				<b>Oxides</b>			
	Type	Density	Size(um)	Shape	Density	Size (um)	Shape	Color	Thickness		
<b>HAZ</b>	1	(N.A.S. due to oxides)		(N.A.S. due to oxides)			(same as base metal)				
	2										
<b>Edge</b>	1	(N.A.S. due to oxides)		(N.A.S. due to oxides)							
	2										
<b>Center</b>	1	(N.A.S. due to oxides)		(N.A.S. due to oxides)							
	2										
<b>Others</b>	1	thick oxides	all over weld metal	peeled off black & white (all over)		-2	all over weld metal along ripples	black	thick		
	2			(round/oval)				black	very thick		
	3										
<b>ALI-2</b>											
<b>Micro Surface Discontinuities</b>				<b>Grains</b>				<b>Oxides</b>			
	Type	Density	Size(um)	Shape	Density	Size (um)	Shape	Color	Thickness		
<b>HAZ</b>	1	(N.A.S. due to oxides)		(N.A.S. due to oxides)			(same as base metal)				
	2										
<b>Edge</b>	1	(N.A.S. due to oxides)		(N.A.S. due to oxides)							
	2										
<b>Center</b>	1	(N.A.S. due to oxides)		(N.A.S. due to oxides)							
	2										
<b>Others</b>	1	very thick oxides	all over weld metal	peeled off black & white (all over)		-2	all over weld metal	black	thick		
	2	GB like discontinuities		(round/oval)			0.05mm spots	green/orange/brown	very thick		
	3						oxides peeled off	metal color			
<b>ALI-3</b>											
<b>Micro Surface Discontinuities</b>				<b>Grains</b>				<b>Oxides</b>			
	Type	Density	Size(um)	Shape	Density	Size (um)	Shape	Color	Thickness		
<b>HAZ</b>	1	(N.A.S. due to oxides)		(N.A.S. due to oxides)			(same as base metal)				
	2										
<b>Edge</b>	1	(N.A.S. due to oxides)		(N.A.S. due to oxides)							
	2										
<b>Center</b>	1	(N.A.S. due to oxides)		(N.A.S. due to oxides)							
	2										
<b>Others</b>	1	much thicker oxides	all over weld metal	peeled off black & white (all over)		-2-4	all over weld metal	black	thick		
	2	GB like discontinuities		(round/oval)			0.05mm spots	pink/brown	very thick		
	3						oxides peeled off	metal color			

<b>AL2-1</b>											
<b>Micro Surface Discontinuities</b>				<b>Grains</b>				<b>Oxides</b>			
	Type	Density	Size(um)	Shape	Density	Size (um)	Shape	Color	Thickness		
<b>HAZ</b>	1	(same as base metal)		(N.A.S. due to oxides)	(N.A.S. due to oxides)		(same as base metal)				
	2										
<b>Edge</b>	1	(N.A.S. due to oxides)			(N.A.S. due to oxides)		0.2mm band along/inside ripples	black	thick		
	2							black	thick		
	3							black	thick		
<b>Center</b>	1	(N.A.S. due to oxides)			(N.A.S. due to oxides)		0.2mm band along/inside ripples	black	thick		
	2							black	thick		
<b>Others</b>	1	thick oxides	all over weld metal				some parts	black	thick		
	2	GB of oxides/base metal are seen on some parts	~D0.1		all over #1		~D0.1 spots	blue+orange	thin		
<b>AL2-2</b>											
<b>Micro Surface Discontinuities</b>				<b>Grains</b>				<b>Oxides</b>			
	Type	Density	Size(um)	Shape	Density	Size (um)	Shape	Color	Thickness		
<b>HAZ</b>	1	(same as base metal)		(N.A.S. due to oxides)	(N.A.S. due to oxides)		thin layer	blue	very thin		
	2										
<b>Edge</b>	1	(N.A.S. due to oxides)			(N.A.S. due to oxides)		very narrow band along fusion line	black	thick		
	2						along ripples	black	thick		
	3						large spots	black	thick		
<b>Center</b>	1	(N.A.S. due to oxides)			(N.A.S. due to oxides)		spots	blue+orange	thin (more than 1)		
	2										
<b>Others</b>	1	rough surface (thick oxides)	all over weld metal		?? (black & white)	~2	all over	dark grey	thick		
	2										
<b>AL2-3</b>											
<b>Micro Surface Discontinuities</b>				<b>Grains</b>				<b>Oxides</b>			
	Type	Density	Size(um)	Shape	Density	Size (um)	Shape	Color	Thickness		
<b>HAZ</b>	1	(same as base metal)		(N.A.S. due to oxides)	(N.A.S. due to oxides)		(same as base metal)				
	2										
<b>Edge</b>	1	(N.A.S. due to oxides)			(N.A.S. due to oxides)		very narrow band along fusion line	black	thick		
	2						all over spots	black	very thick		
	3						spots	green+orange			
<b>Center</b>	1	(N.A.S. due to oxides)			(N.A.S. due to oxides)		very narrow band along fusion line	black	thick		
	2						all over spots	black	very thick		
<b>Others</b>	1	rough surface (thick oxides)	all over weld metal		black & white	~2	black	green+orange			
	2										

**AE-1**

Micro Surface Discontinuities			Grains			Oxides		
Type	Density	Size(um)	Shape	Density	Size (um)	Shape	Color	Thickness
HAZ	1	no cracks, no GB				all over	black	thick
	2							
Edge	1					all over	black	thick
	2							
	3							
Center	1					spots	black	thick
	2							
Others	1	oxid grains or cracks ?		all over weld metal	~2	normal	grey/brown	thick
	2							

**AE-2**

Micro Surface Discontinuities			Grains			Oxides		
Type	Density	Size(um)	Shape	Density	Size (um)	Shape	Color	Thickness
HAZ	1	no cracks, no GB				all over	black	thick
	2							
Edge	1					all over	black	thick
	2							
	3							
Center	1					spots	black	thick
	2							
Others	1	oxid grains or cracks ?		all over weld metal	~2	normal	grey/brown	thick
	2							

**AE-3**

Micro Surface Discontinuities			Grains			Oxides		
Type	Density	Size(um)	Shape	Density	Size (um)	Shape	Color	Thickness
HAZ	1	no cracks, no GB				all over	black	thick
	2							
Edge	1					all over (more)	black	thick
	2							
	3							
Center	1					all over	grey	thick
	2							
Others	1	oxid grains or cracks ?		all over weld metal	3	normal	black	thick
	2							



**TT-1**

		Micro Surface Discontinuities			Grains			Oxides		
	Type	Density	Size(um)	Shape	Density	Size (um)	Shape	Color	Thickness	
<b>HAZ</b>	1 GB	closer to edge, bigger sizes	1.75 high	GB(normal)	all over	10-400		(same as base metal)		
	2 VI									
<b>Edge</b>	1 GB			GB(normal) SCGB(normal)	all over all over	200-500	layers on all over GB's	yellow	thin	
	2 SCGB									
	3									
<b>Center</b>	1 GB			GB(normal) SCGB(normal)	all over all over	200-350	layers on all over GB's	yellow	thin	
	2 SCGB									
	3									
	4									

**TT-2**

		Micro Surface Discontinuities			Grains			Oxides		
	Type	Density	Size(um)	Shape	Density	Size (um)	Shape	Color	Thickness	
<b>HAZ</b>	1 GB	closer to edge, bigger sizes		GB(normal)	all over	1200-400		(same as base metal)		
	2									
<b>Edge</b>	1 GB			GB(normal)	all over	200-650	layers on all over GB's	yellow	thin	
	2									
	3									
<b>Center</b>	1 GB			GB(normal) SCGB(normal)	all over all over	200-600 D30-50	layers on all over GB's	yellow	thin	
	2 SCGB									
	3									
	4									

**TT-3**

		Micro Surface Discontinuities			Grains			Oxides		
	Type	Density	Size(um)	Shape	Density	Size (um)	Shape	Color	Thickness	
<b>HAZ</b>	1 GB	closer to edge, bigger sizes		GB(normal)	all over	~800	layers on all over GB's	violet+blue	thin	
	2									
<b>Edge</b>	1 GB			GB(normal)	all over	~800	layers on all over GB's	violet+blue	thin	
	2									
	3									
<b>Center</b>	1 GB			GB(normal) dendrite	all over all over		layers on all over GB's	violet+blue	thin	
	2 SCGB									
	3									
	4									

**TL2-1**

		Micro Surface Discontinuities			Grains			Oxides		
		Type	Density	Size(um)	Shape	Density	Size (um)	Shape	Color	Thickness
<b>HAZ</b>	1	GB only (no cracks)			normal (next to Edge)	all over #3	15-25	0.5mm band	brown	very thin
	2	GB only (no cracks)			normal (next to HAZ)	all over #5	20-30	all over	brown	very thin
<b>Edge</b>	1	GB only (no cracks)			normal	all over #5	30-150	narrow center band	black	thin
	2	GB only (no cracks)						spots	black	thin
	3	GB only (no cracks)						all over	brown	very thin
<b>Center</b>	1	GB only (no cracks)		(0.4um high)			500 max	narrow center band	black	thin
	2	GB only (no cracks)						spots	black	thin
	3	GB only (no cracks)						all over	black	thin
	4	GB only (no cracks)						spots	black	thin

**TL2-2**

		Micro Surface Discontinuities			Grains			Oxides		
		Type	Density	Size(um)	Shape	Density	Size (um)	Shape	Color	Thickness
<b>HAZ</b>	1	GB only (no cracks)			normal	all over #3	15-25	all over	brown	thin
	2	(N.A.S. clearly)						0.2mm band	black	thick
<b>Edge</b>	1	GB only (no cracks)			normal (next to HAZ)	all over #3	30-50	all over	brown	very thin
	2	GB only (no cracks)					50-200	narrow center band	black	thin
	3	GB only (no cracks)								
<b>Center</b>	1	GB only (no cracks, transverse)		100x400	transverse	all over	100x400	all over	brown	very thin
	2	GB only (no cracks)			round		70-500	narrow center band	black	thin
	3	GB only (no cracks)						band	black	medium
	4	GB only (no cracks)								

**TL2-3**

		Micro Surface Discontinuities			Grains			Oxides		
		Type	Density	Size(um)	Shape	Density	Size (um)	Shape	Color	Thickness
<b>HAZ</b>	1	(N.A.S.)				(N.A.S.)		0.5mm band	brown	thin
	2	(N.A.S.)						0.2mm band	black	thick
<b>Edge</b>	1	(N.A.S.)			normal (next to HAZ)		~70	0.2mm band	black	thick
	2	(N.A.S.)					~200	0.5mm band	brown	thin
	3	(N.A.S.)								
<b>Center</b>	1	(N.A.S.)			center		160max	0.1mm band	black	thin
	2	(N.A.S.)			transverse (next to center)		200x500	0.2mm band	light brown	very thin
	3	(N.A.S.)						1.0mm band	black	thick
	4	(N.A.S.)								

**TE-1**

		Micro Surface Discontinuities			Grains			Oxides		
		Type	Density	Size(um)	Shape	Density	Size (um)	Shape	Color	Thickness
<b>HAZ</b>	1	GB only			normal	all over #4	12-40	No		
	2						60x160max			
<b>Edge</b>	1	GB only (no cracks)			normal	all over		0.5mm band	black	thin
	2	some GB lines continuous from Edge			(transverse dir. is longer)			(along ripples)		
	3									
<b>Center</b>	1	GB only (no cracks)			normal	all over	60x160max	No		
	2									
<b>Others</b>	1				normal	all over	60x160max			
	2									

**TE-2**

		Micro Surface Discontinuities			Grains			Oxides		
		Type	Density	Size(um)	Shape	Density	Size (um)	Shape	Color	Thickness
<b>HAZ</b>	1	GB only (no cracks) continuous from Edge			normal	all over #4	10-30	0.8mm no oxide band		
	2							0.8-1.8mm band	light brown	very thin
<b>Edge</b>	1	GB only (no cracks)			normal	all over #4	30x100	all over	brown	thin
	2									
	3									
<b>Center</b>	1	GB only (no cracks)					70x100	all over	brown	thin
	2									
<b>Others</b>	1	(N.A.S. clearly)					60x160max	along ripples	burned black	not thin
	2									

**TE-3**

		Micro Surface Discontinuities			Grains			Oxides		
		Type	Density	Size(um)	Shape	Density	Size (um)	Shape	Color	Thickness
<b>HAZ</b>	1	GB only (no cracks) continuous from Edge			normal	all over #4	20-50	1.0mm no oxide band		
	2							0.8-1.8mm band	light brown	very thin
<b>Edge</b>	1	GB only (no cracks)				all over	60-100max	all over	brown	thin
	2							along ripples	black	not thin
	3									
<b>Center</b>	1	GB only (no cracks)					40x160max	all over	light brown	thin
	2	V4						(No black oxide)		
<b>Others</b>	1	(N.A.S. clearly)					-80	all over	brown	thin
	2							along ripples	black	not thin

# Appendix

Table A-2

Fatigue Test Data

Specimen	Cycles	Applied Stress	Comments	
<b>FT-1</b>	Low-Carbon Steel	0	67kpsi	
	YTS=69kpsi	5,000	67kpsi	No changes on micro surface discontinuities
	UTS=82kpsi	10,000	67kpsi	No changes on micro surface discontinuities
	Section=0.167sqin	15,000	67kpsi	No changes on micro surface discontinuities
	Automatic GTAW	20,000	67kpsi	No changes on micro surface discontinuities
		25,000	67kpsi	No changes on micro surface discontinuities
		30,000	67kpsi	No changes on micro surface discontinuities
		35,000	67kpsi	No changes on micro surface discontinuities
		40,000	67kpsi	No changes on micro surface discontinuities
		45,000	67kpsi	No changes on micro surface discontinuities
		50,000	67kpsi	No changes on micro surface discontinuities
		55,000	67kpsi	No changes on micro surface discontinuities
		60,000	67kpsi	No changes on micro surface discontinuities
		100,000		Stopped
<b>FT-2</b>	Low-Carbon Steel	0	67kpsi	
	YTS=69kpsi	5,000	67kpsi	No changes on micro surface discontinuities
	UTS=82kpsi	10,000	67kpsi	No changes on micro surface discontinuities
	Section=0.167sqin	15,000	67kpsi	No changes on micro surface discontinuities
	Automatic GTAW	20,000	67kpsi	No changes on micro surface discontinuities
		25,000	67kpsi	No changes on micro surface discontinuities
		30,000	67kpsi	No changes on micro surface discontinuities
		35,000	67kpsi	No changes on micro surface discontinuities
		40,000	67kpsi	No changes on micro surface discontinuities
		45,000	67kpsi	No changes on micro surface discontinuities
		50,000	67kpsi	No changes on micro surface discontinuities
		55,000	67kpsi	No changes on micro surface discontinuities
		60,000	67kpsi	No changes on micro surface discontinuities
		100,000		Stopped
<b>FT-3</b>	Low-Carbon Steel	0	67kpsi	
	YTS=69kpsi	2,000	67kpsi	No changes around a slit
	UTS=82kpsi	4,000	67kpsi	No changes around a slit
	Section=0.167sqin	6,000	67kpsi	No changes around a slit
	slit	8,000	67kpsi	No changes around a slit
	Automatic GTAW	10,000	67kpsi	No changes around a slit
		12,000	67kpsi	No changes around a slit
		14,000	67kpsi	No changes around a slit
		16,000	67kpsi	No changes around a slit
		18,000	67kpsi	No changes around a slit
		20,000	67kpsi	No changes around a slit
		23,000	67kpsi	No changes around a slit
		26,000	67kpsi	No changes around a slit
		40,000		Stopped



Specimen	Cycles	Applied Stress	Comments
<b>MT-3</b> Low-Carbon Steel	0	45kpsi	
YTS=69kpsi	300	45kpsi	No changes on micro surface discontinuities
UTS=82kpsi	2,000	45kpsi	No changes on micro surface discontinuities
Section=0.389sqin	5,000	45kpsi	No changes on micro surface discontinuities
Automatic GTAW	6,000	55kpsi	No changes on micro surface discontinuities
	8,000	55kpsi	No changes on micro surface discontinuities
	13,000	55kpsi	No changes on micro surface discontinuities
	23,000	55kpsi	No changes on micro surface discontinuities
	40,000		stopped
<b>ST-3</b> Stainless Steel	0	48kpsi	
YTS=30kpsi	500	48kpsi	No changes on micro surface discontinuities
UTS=80kpsi	2,000	48kpsi	No changes on micro surface discontinuities
Section=0.389sqin	5,000	60kpsi	No changes on micro surface discontinuities
Automatic GTAW	6,000	60kpsi	No changes on micro surface discontinuities
	9,000	60kpsi	No changes on micro surface discontinuities
	14,000	60kpsi	No changes on micro surface discontinuities
	24,000	60kpsi	No changes on micro surface discontinuities
	40,000		stopped
<b>AT-2</b> Aluminum Alloy	0	25kpsi	
YTS=21kpsi	470		Failure occurred
UTS=42kpsi			
Section=0.389sqin			
Automatic GTAW			
<b>AT-3</b> Aluminum Alloy	0	25kpsi	
YTS=21kpsi	300	31kpsi	Could not see well. Holes at crater became bigger
UTS=42kpsi	2,000	31kpsi	Could not see well. Holes at crater became bigger
Section=0.389sqin	3,000	31kpsi	Could not see well. Holes at crater became bigger
Automatic GTAW	3,450		Failure occurred
<b>TT-2</b> Titanium Alloy	0	78kpsi	
YTS=21kpsi	500	78kpsi	Could not see well due to oxides
UTS=42kpsi	2,000	78kpsi	Oxides peeled off on B.M, HAZ, W.M.
Section=0.389sqin	5,000	97kpsi	Oxides peeled off
Automatic GTAW	6000	97kpsi	Micro surface discontinuities never changed
	9,000	97kpsi	Oxides peeled off
	14,000	97kpsi	Micro surface discontinuities never changed
	17,930		Failure occurred